NORTHWESTERN UNIVERSITY

Using the [*SWI*$^+$] Prion to Study Protein Misfolding, Aggregation, and Amyloid Formation

A DISSERTATION

SUBMITTED TO THE GRADUATE SCHOOL
IN PARTIAL FULFILLMENT OF THE REQUIREMENTS

for the degree

DOCTOR OF PHILOSOPHY

Field of Northwestern University Interdepartmental Neuroscience Program

By

Stephanie Valtierra

EVANSTON, ILLINOIS

September 2017

ABSTRACT

Using the [*SWI+*] Prion to Study Protein Misfolding, Aggregation, and Amyloid Formation

Stephanie Valtierra

Thesis Advisor: Liming Li

Saccharomyces cerevisiae contains several epigenetic elements known as yeast prions. Our laboratory discovered the yeast prion [*SWI+*], whose protein determinant is Swi1, a subunit of the SWI/SNF chromatin-remodeling complex. Formation of [*SWI+*] results in abolishment of multicellular features and a partial loss-of-function phenotype of non-glucose carbon source usage. Our laboratory previously showed that the first 38 amino acids of Swi1 propagate [*SWI+*]. We show here that a region as small as the first 32 amino acids of Swi1 (Swi1$_{1-32}$) aggregates and stably maintains and transmits [*SWI+*]. Regions smaller than Swi1$_{1-32}$ are either incapable of aggregation or unstably propagate [*SWI+*]. When fused to Sup35MC, the [*PSI+*] determinant lacking its prion domain (PrD), Swi1$_{1-31}$ and Swi1$_{1-32}$ can act as transferable PrDs. Thus, an NH$_2$-terminal region of ~30 amino acids of Swi1 contains all necessary information for *in vivo* prion formation, maintenance, and transmission. This PrD is unique in size and composition: it is glutamine-free, asparagine-rich, and the smallest defined to date. Our results broaden our understanding of what features allow a protein region to serve as a PrD.

In addition to our previous studies, our laboratory recently designed a novel reporter system that can faithfully report the prion status of Swi1. High-throughput screens were conducted to identify compounds that can inhibit or eliminate [*SWI+*] and obtained several promising hits. Using secondary assays, we confirmed prion loss after treatment with anti-[*SWI+*] compounds. Furthermore, we examined the ability of the selected compounds to eliminate other yeast prions – including [*PSI+*], [URE3], and [*MOT3+*] – and observed diverse curing abilities. Our results suggest that our novel reporter system is a useful method for finding potential anti-prion molecules and future work will aim to determine the mechanism of action of the compounds. Our studies will allow us to develop chemical probes for the study of prion biology and potentially result in the development of therapeutics for neurodegenerative diseases that are tightly associated to prion-like behaviors of various aggregation-prone proteins.

ACKNOWLEDGEMENTS

I would like to express my deepest gratitude to my thesis advisor, Dr. Liming Li for her support and patience throughout my research studies. Her guidance and mentorship were critical to my growth as a scientist. I could not have asked for a better advisor and mentor and I am extremely fortunate to have been a part of her laboratory. I would also like to thank current and past laboratory members, including Dustin Goncharoff, Luzivette Robles, Xudong Cheng, Anthony Kowal, and Emily Crow, who not only gave me critical feedback and support, but also made the laboratory an amazing place to work in. In particular, I would like to thank Dr. Zhiqiang Du for all his help and mentorship. This work would not have been possible without his help.

I would also like to thank my thesis committee, Adriana Ferreira, Richard Miller, Sarah Rice, and Robert Vassar, for their critical guidance and support. Special thanks to Dr. Shubhik DebBurman, who first opened my eyes to research and who has provided me with mentorship for over a decade.

Above all, I would like to thank my biggest cheerleaders – my family. I thank my siblings, Jennifer and Steven, as well my aunts, Marisol and Guadalupe, for their support throughout graduate school. Lastly, I would like to express my most sincere gratitude to my parents, who have worked tirelessly to help me achieve my dreams and who had faith in me even when I did not. I could not have done this without their unconditional love and support. This is for you mom and dad.

ABBREVIATIONS

5-FOA	5-fluoroorotic acid
AD	Alzheimer's disease
ALS	amyotrophic lateral sclerosis
BME	beta-mercaptoethanol
DIC	differential interference contrast
DMSO	dimethyl sulfoxide
ECL	peroxidase substrate for enhanced chemiluminescence
EDTA	Ethylenediaminetetraacetic acid
GdnHCl	guanidine hydrochloride
GFP	green fluorescent protein
GLFG	glycine-leucine-phenylalanine-glycine
HD	Huntington's disease
Hsp104^{DN}	Dominant negative mutant of Hsp104
kDa	kila-dalton
LiAc	lithium acetate
N	asparagine
NaCl	sodium chloride
NaOH	sodium hydroxide
N$_{30}$	poly-asparagine molecule of composed of 30 asparagines

N-YFP	N domain of Swi1 fused to YFP (First 327 amino acids of Swi1)
NQ-YFP	N and Q domains of Swi1 fused to YFP (First 524 amino acids of Swi1)
P	pelleted fraction in centrifugation assay containing aggregated protein
PEG	polyethylene glycol
PD	Parkinson's disease
PMCA	<u>P</u>rotein <u>M</u>isfolding <u>C</u>yclic <u>A</u>mplification
PrD	prion domain
PrP	prion protein
PrP^C	α-helix-rich cellular prion protein
PrP^{Sc}	β-sheet-rich misfolded infectious isoform of PrP
PVDF	polyvinylidene fluoride
Q	glutamine
Q$_{30}$	poly-glutamine molecule composed of 30 asparagines
Raf	raffinose
rpm	revolutions per minute
RT-PCR	reverse-transcription polymerase chain reaction
SC	Synthetic complete media
SC-HLU	Synthetic complete media lacking histidine, leucine and uracil
SDD-AGE	Semi-Denaturating Detergent Agarose Gel Electrophoresis
SDS	sodium dodecyl sulfate

SDS-PAGE	sodium dodecyl sulfate polyacrylamide gel electrophoresis
S	Supernatant fraction in centrifugation assay containing soluble protein
Sup35^N	Sup35 PrD in which all glutamines are replaced with asparagines
Sup35^Q	Sup35 PrD in which all asparagines are replaced with glutamines
Swi1N	Swi1 domain containing first 327 amino acids of Swi1
Swi1$_{TRUNC}$MC	Swi1 truncation mutant fused to MC domain of Sup35
Swi1$_{TRUNC}$YFP	Swi1 truncation mutant fused to YFP
T	Total fraction in centrifugation assay
TSE	Transmissible spongiform encephalopathy
USA	ureidosuccinate
x g	relative centrifugal force
YFP	yellow fluorescent protein
YPD	yeast extract peptone dextrose

TABLE OF CONTENTS

LIST OF FIGURES

LIST OF TABLES

CHAPTER ONE

Introduction

Prions, proteinaceous infectious particles, are the causative agents of a class of fatal mammalian neurodegenerative disorders known as transmissible spongiform encephalopathies (TSEs). Conversion of the host prion protein, PrP, from its native conformation, PrP^C, to a group of pathogenic and infectious conformations collectively known as PrP^{Sc} is now known to underlie the pathogenesis of TSEs (Fig 1 and (1, 2)). This protein-mediated self-perpetuating conversion results in the formation of protease-resistant amyloid and neuronal loss that are characteristic of TSEs (3).

The formation of highly ordered β-sheet-rich filamentous protein aggregates, or amyloids, is not unique to TSEs, as many mammalian neurodegenerative diseases are characterized by the misfolding of specific proteins that aggregate as amyloid fibrils (4). Recent evidence suggests that the prion concept, one in which normally folded proteins undergo conformational changes to misfolded conformations resulting in self-perpetuating oligomerization and disease progression, can be extended to other diseases, such as Alzheimer's disease (AD) (5-7), Parkinson's disease (PD) (8-10), Huntington's disease (HD) (11), and amyotrophic lateral sclerosis (ALS) (For reviews see (12-15)). Therefore, understanding the mechanisms that underlie protein aggregation and prion formation is fundamentally important.

Interestingly, the budding yeast *Saccharomyces cerevisiae* also contain several protein-based epigenetic elements, known as yeast prions, which like PrP propagate as altered conformations. Yeast prion formation results in the transmission of heritable phenotypes (16, 17). These proteins with diverse functions, including Sup35, Ure2, Rnq1, Swi1, Cyc8, Mot3, Mod5, Nup100, and Lsb2, are the protein determinants of the yeast prions [*PSI*$^+$] (18), [URE3] (19, 20), [*PIN*$^+$] (21, 22), [*SWI*$^+$] (23), [*OCT*$^+$] (24), [*MOT3*$^+$] (25), [*MOD*$^+$] (26), [*NUP100*$^+$] (27), and [*LSB*$^+$] (28), respectively (Table 1). Yeast prion proteins are typically characterized by an enrichment in glutamine (Q) and asparagine (N) and do not share a sequence similarity with PrP, however, like PrP, most yeast prions form amyloid aggregates (see Chapter two introduction for further information on yeast prion sequence features) (16, 29). Transformation of these purified amyloid aggregates or lysates from prion cells into naïve non-prion cells results in the transmission
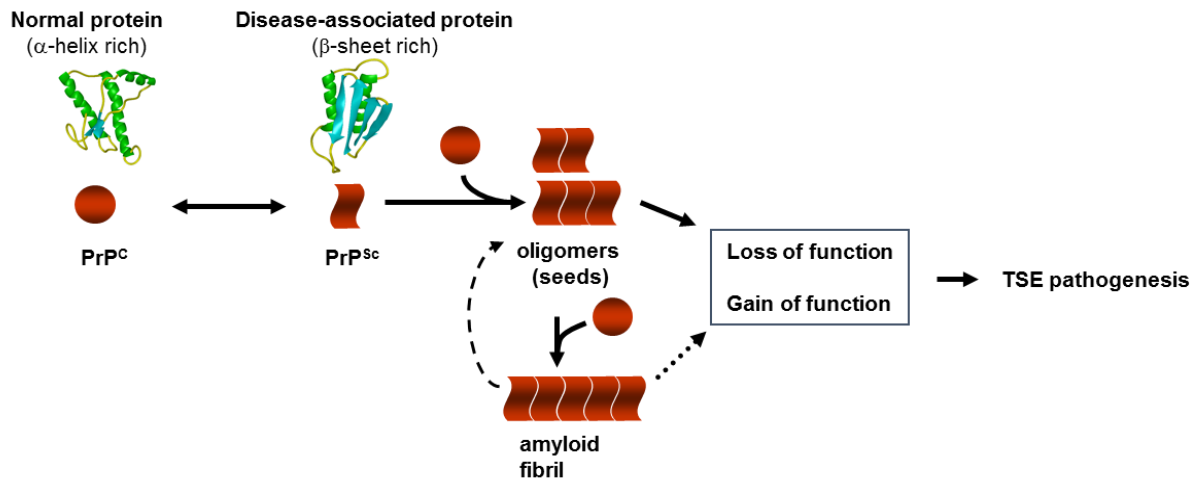
Figure 1. Schematic of prion replication cycle. PrP^C, an α-helix rich protein, can misfold into disease associated β-sheet rich conformations, collectively known as PrP^{Sc}. These misfolded conformations aggregate into oligomers and amyloid fibrils, which can be fragmented, providing seeds for new cycles of self-perpetuating conformational conversion.

Table 1. Prion proteins in *S. cerevisiae*

Prion	Protein Determinant	Native Function	Phenotype
[*PSI*+]	Sup35	Translation termination subunit	Nonsense suppression
[URE3]	Ure2	Negative regulator of nitrogen catabolism	Derepression of metabolic enzymes for poor nitrogen source
[*RNQ*+]/ [*PIN*+]	Rnq1	Unknown	Increase in prion induction of other prions
[*SWI*+]	Swi1	Subunit of SWI/SNF chromatin remodeling complex	Poor utilization of non-glucose nitrogen sources
[*OCT*+]	Cyc8	Transcriptional regulation	Derepression of Cyc8 targets
[*MOT3*+]	Mot3	Transcriptional repressor	Derepression of Mot3 targets, environmentally responsive modulator of multicellularity
[MOD+]	Mod5	Transfer RNA isopentenyl transferase	Increased resistance to antifungal agents
[*NUP100*+]	Nup100	Nucleoporin	Unknown, non-sense suppression phenotype using Sup35 reporter assay
[*LSB*+]	Lsb2	Negative regulator of actin nucleation-promoting factor activity	[*PSI*+] inducibility

of heritable phenotypes, demonstrating infectivity by these misfolded prion conformers (16, 25, 26, 30-34). A typical yeast prion protein also contains a region, termed prion domain (PrD), which is required for prion formation and propagation (35, 36). Detailed information on yeast PrDs can be found in Chapter 2.

Propagation of yeast prions requires the molecular chaperone Hsp104, a homohexameric AAA ATPase (22-26, 28, 29, 37-40). The role of Hsp104 in prion propagation is in the fragmentation of prion fibers, which results in an increased availability of prion seeds and in further prion propagation (39, 41). Inhibition or absence of Hsp104 results in the accumulation of prion aggregates, composed of longer SDS-resistant polymers. The increased size of the polymers causes retention in the mother cell during cells division resulting in prion loss (42-44). Treatment of millimolar levels of guanidine hydrochloride (GdnHCl), which inactivates Hsp104, or expression of a dominant negative mutant of Hsp104 eliminates yeast prions (21, 23-25, 37, 42, 45-49). Further studies have revealed a critical role for several cellular factors, including Hsp70-Ssa1, J-proteins Sis1 and Ydj1, and the nucleotide exchange factor Sse1 in the maintenance of yeast prions (16, 50-58).

[PSI+] and [URE3], the first yeast prions identified, were discovered in genetics screens as phenotypes that were transmitted in a dominant non-Mendelian manner (18, 19). [PSI+] was first described by Brian Cox in 1965 as a phenotype resulting from non-sense suppression (18). [URE3] was later described by Francois Lacroute as a genetic element that produced failure in nitrogen catabolite repression (19). Years later Reed Wickner would propose that these genetic elements were in fact prion-based and that [PSI+] and [URE3] were the prion forms of the proteins Sup35 and Ure2 (20). Wickner showed that [URE3] was cytoplasmically inherited, demonstrating that the phenotypes associated with [URE3] were not due to altered chromosomal gene sequences. Wickner also showed that maintenance of [URE3] required the integrity of the URE2 gene, suggesting the expression of the normal, wild-type protein was required for the maintenance of [URE3]. Furthermore, while ure2 mutations were recessive, [URE3] was dominant and therefore, all four products of meiosis expressed the [URE3] phenotype. Wickner further showed that overexpression of Ure2 resulted in the increase in the appearance of [URE3] (20).

Based on this collection of seminal work by Wickner and his colleagues, several criteria were established for the discovery of other yeast prions, including dominant cytoplasmic inheritance, the requirement for the requirement of the prion protein gene, the *de novo* appearance of the prion, which is increased by the overexpression of the prion protein, reversible curability, and infectivity, where the prion form of the protein is used to induced a prion phenotype in a non-prion cell (17).

Sup35, the protein determinant of the [*PSI*] prion, is a translational termination factor containing three domains – an amino-terminal prion domain that is glutamine/asparagine-rich and essential for [*PSI*] formation and propagation (N), a highly charged middle domain (M), and a C-terminal functional domain necessary for translational termination (C) (59). The prion state of Sup35 can be easily assessed in a strain containing the *ade1-14* allele with a premature stop codon in the ORF of *ADE1.* This strain also contains suppressor tRNAs which allow for read-through of the premature stop codon (37). In non-prion cells, [*psi*], functional Sup35 efficiently terminates translation at the premature stop codon, resulting in a lack of growth on media lacking adenine (-Ade) and red colonies on YPD media due to the blockage of the adenine biosynthesis pathway leading to accumulation of a red-pigmented precursor. In contrast, Sup35 is aggregated in [*PSI*] cells and its function of translation termination is compromised, resulting in the growth on -Ade media and pink/white colonies on YPD due to nonsense suppression (Fig 2). The high-molecular weight aggregates of Sup35 can be pelleted by high-speed centrifugation, making them distinguishable from the soluble Sup35 found in non-prion cells (41, 60).

[*PSI*] has distinct, self-perpetuating conformations, which are similar to mammalian prion strains. These distinct conformations, termed variants, have distinct phenotypic and biochemical characteristics (16, 51, 61). Yeast prion variants were first described for [*PSI*], where weak and strong isolates of the prion were isolated in the same yeast strain (62). The variants are characterized by differences in color phenotype on YPD, which are a result of differences in the levels of Sup35 aggregation and thus differences in translational termination efficiency (Fig 3A and 3B). Differences can also be seen in the stability of distinct [*PSI*] variants, as well as in aggregate structure and polymer size (Fig 3A, 3C, and 3D) (30, 31, 44, 62-66).
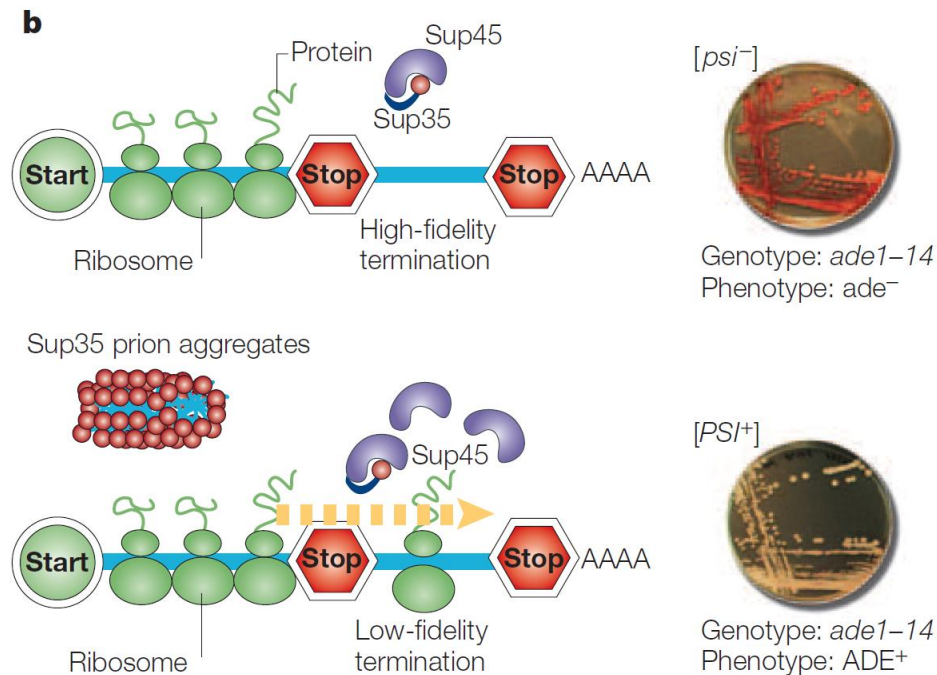
Figure 2. Reporter system for [*PSI+*] detection. The prion state of Sup35, a subunit of the translation termination factor and the protein determinant of [*PSI+*], can be easily assessed in a strain containing the *ade1-14* allele with a premature stop codon in the ORF of *ADE1*. In non-prion cells, [*psi*], functional Sup35 forms a heterodimer with Sup45 and efficiently terminates translation at the premature stop codon, resulting in a lack of growth on media lacking adenine (-Ade) and red colonies on YPD media due to the blockage of the adenine biosynthesis pathway leading to pigment accumulation. In contrast, Sup35 is aggregated in [*PSI+*] cells and its function of translation termination is compromised, resulting in the growth on -Ade media and pink/white colonies on YPD due to nonsense suppression. This reporter thus allows for an easy visual detection of prion status with prion loss resulting in red colony color. Figure adapted from J. Shorter and S. Lindquist *Nature Reviews Genetics* (2005).
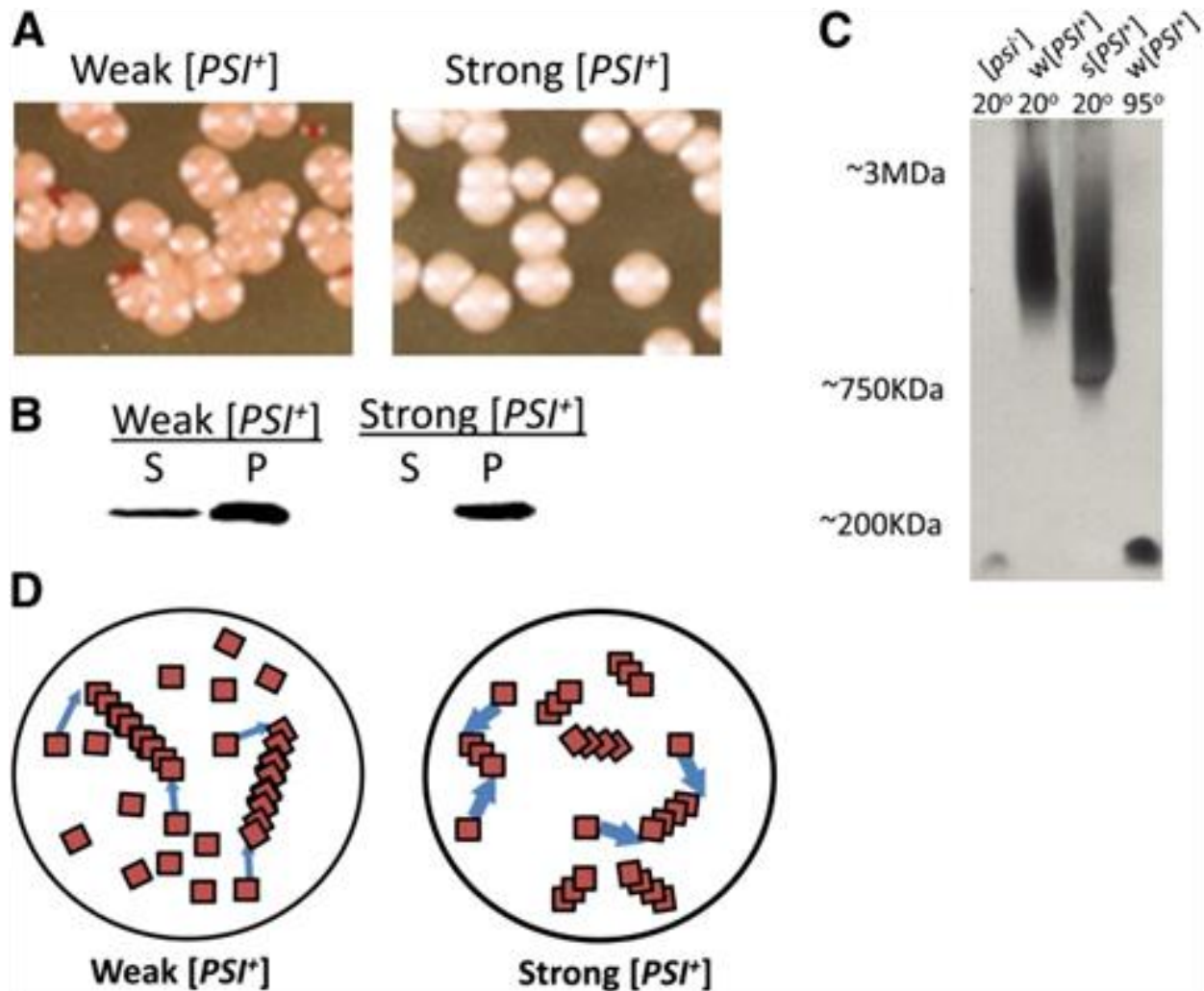
Figure 3. [*PSI*⁺] exists in multiple variants with different phenotypes and biochemical properties. A. Different variants can be distinguished by their color on YPD. While strong [*PSI*⁺] is white, the weak [*PSI*⁺] is pink and gives rise to red colonies more frequently than strong [*PSI*⁺]. B. [*PSI*⁺] variants also differ in the amounts of aggregated versus soluble protein in the prion cells. When lysates from different stains can be separated by high-speed centrifugation into the pellet (P) or soluble (S) fraction, more soluble protein can be found in the weak [*PSI*⁺] variant. C. Differences in the size of SDS-resistant polymers can be determine by semidenaturing agarose gel electrophoresis (SDD-AGE). Cell lysates were treated with 2% SDS at various temperatures. Sup35 runs as monomers in both the [*psi*⁻] cells and the boiled samples. Weak variants are differentiated by the increased size of polymers in weak versus strong [*PSI*⁺] variants. D. Weak [*PSI*⁺] variants are characterized by fewer larger aggregated, which is in contrast to the many small aggregates that are observed in strong [*PSI*⁺] variants. The large aggregates provide fewer ends through which Sup35 can be captured, thus resulting in more soluble protein and decreased non-sense suppression. Figure adapted from S.W. Liebman and Y.O. Chernoff, *Genetics* (2012).

Interestingly, [*PSI*] can be eliminated by treatment of millimolar concentration of GdnHCl supplemented in the medium, which inhibits the molecular chaperone Hsp104, and by overexpression of Hsp104 (37, 45).

Ure2, a regulator of nitrogen catabolism, is the protein determinant of [URE3] (20). In non-prion cells, Ure2 is soluble and binds and represses Gln3 and Gat1, transcriptional activators of genes involved in nitrogen metabolism. This binding, however, is dependent on good nitrogen sources. In [URE3] cells, Ure2 is aggregated and is not bound to Gln3 and Gat1, allowing for their translocation to the nucleus and subsequent activation of transcription of genes, including *DAL5*. *DAL5*, encodes a membrane transporter required for the uptake of poor nitrogen sources, such as allantoate and succinate. Therefore, [URE3] cells are able to take up poor nitrogen sources, such as ureidosuccinate (USA), even in the presence of rich nitrogen sources (20). Like [*PSI*], [URE3] can also exists as multiple variants displaying distinct phenotypes (67).

[*RNQ*], also known as [*PIN*], for [*PSI*] inducible, was the third yeast prion identified (21, 22, 68). The protein determinant of [*RNQ*] is Rnq1, a non-essential protein of unknown function whose high Q/N content was used to identify it as a prion protein candidate. The aggregation of Rnq1 is associated with a gain of function, as it can facilitate the *de novo* appearance of other yeast prions, such as [*PSI*] (22, 68),[URE3] (69) and [*SWI*] (70). Distinct prion variants have also been described for [*RNQ*] and these variants can be differentiated by different aggregation patterns and the efficiency with which they enhance the *de novo* appearance of [*PSI*] (69, 71-73).

[*SWI*] was the fourth prion identified (23) and is the major focus of this thesis. More detailed information on this prion will be presented later in this introduction.

Cyc8, part of the evolutionarily conserved Cyc8-Tup1 global transcriptional repressor complex, is the protein determinant of [*OCT*] (24). Cyc8/Tup1 controls gene expression of more than 7% of yeast genes, including *CYC7*, *RNR3*, *FLO1*, *ANB1* and *SUC2* (74). Cyc8 was predicted to be a prion protein based on its ability to induce *de novo* [*PSI*] formation when overexpressed and its unusually high Q/N content, two factors that were also observed for other prion proteins (68). Transient overexpression of the Q-rich region of Cyc8 was found to induce *cyc8* mutant phenotypes, including growth on media with lactate

as a sole carbon source and increased flocculation. [*OCT*⁺] phenotypes were dominant, cytoplasmically inherited, dependent on Hsp104, and dependent on continued expression of Cyc8 protein. Moreover, Cyc8 was found to be aggregated in [*OCT*⁺] cells and the prion-induced inactivation of the protein was found to be associated with derepression of five Cyc8-repressed genes, demonstrating a partial loss of function of Cyc8 in [*OCT*⁺] cells (24).

[*MOT3*⁺] was discovered as part of a bioinformatic screen which used the PrDs of verified prion proteins were used to search for novel prion candidates in yeast (25) (For more detailed information in prion domains, see Chapter two introduction). Mot3, the protein determinant of [*MOT3*⁺] is a transcription factor that represses anaerobic genes, including *DAN1*, during aerobic growth. Alberti et al. showed that several prion candidates formed SDS-resistant cytoplasmic aggregates, bound Thioflavin T, indicative of amyloid formation, and conferred heritable changes in phenotypes using a Sup35 reporter assay (25). A novel Mot3 reporter – *dan1::URA3,* in which URA3 was under the control of the *DAN1* promoter, was created to investigate prion properties of one prion candidate - Mot3. Mot3 represses *DAN1*, therefore, the use of this reporter allows for the positive selection of [*MOT3*⁺] by selecting for Ura⁺ cells. Over-expression of the Mot3 PrD resulted in the transmission of a dominant phenotype of growth on media lacking uracil. This phenotype was associated with the formation of SDS-resistant aggregates and was eliminated by treatment with GdnHCl or *HSP104* deletion. The final evidence demonstrating prion-based transmission of heritable phenotypes was the ability to induce [*MOT3*⁺] in non-prion cells by transformation of *in vitro* produced amyloid fibers to non-prion cells (25). More recent research showed that [*MOT3*⁺] promoted multicellularity in yeast, through the derepression of Mot3 target *FLO11* (47). The formation and elimination of [*MOT3*⁺] was found to be environmentally regulated, suggesting that prions have important roles in regulation of multicellularity (47).

[*MOD*+] is the prion form of the protein Mod5, a tRNA isopentenyltransferase which lacks Q/N-rich domains. Mod5 was shown to form amyloid fibers that could both accelerate the aggregation of soluble Mod5 and of soluble Sup35, indicating that despite the lack of a Q/N rich domain, Mod5 was able to cross-seed Sup35 (26). Double knockout of Mod5 and Trm1, which encodes tRNA methyltransferase, shows

sensitivity to 5-fluorouracil, therefore, Suzuki et al. used a Δ*trm1* strain to screen for 5-fluorouracil sensitive isolates. Several isolates displayed GdnHCl-curable sensitivity to 5-fluorouracil. While deletion of *HSP104* reversed the observed sensitivity, Hsp104 over-expression partially reversed sensitivity to 5-fluorouracil, demonstrating that like other yeast prions, [*MOD*+] was propagated in an Hsp104-dependent manner. Suzuki et al. further showed that Mod5 underwent conformational changes, as it was found to be largely in the pellet fraction in a centrifugation assay, formed cytoplasmic aggregates, and formed SDS-resistant aggregates in [*MOD*+] cells but not in [*mod*-] cells (26). [*MOD*+] was shown to be dominant by both mating and through cytoduction, an assay involving cytoplasmic transfer in the absence of nuclear fusion. Conversion of Mod5 was shown to have important physiological consequences, namely a decrease in tRNA modification and increases in sterol synthesis. Moreover, [*MOD*+] cells showed increased resistance to nocodazole, a microtubule inhibitor and acquired resistance to anti-fungal agents. Lastly, it was demonstrated that selective pressure by antifungal agents increased the *de novo* appearance of [*MOD*+], suggesting that prionization of Mod5 may allow yeast to adapt to harmful environments, once again demonstrating important biological roles of yeast prions.

Nup100, a Q/N rich nucleoporin with glycine-leucine-phenylalanine-glycine (GLFG) repeats, is the protein determinant of [*NUP100*+] (27). Work by Alberti et al. initially demonstrated that Nup100 formed cytoplasmic foci, SDS-resistant aggregates, as well as amyloid fibers *in vitro*. Low basal activity of Nup100 PrD in a Sup35 assay, however, did not allow for further examination of the proteins prion activity (25). Recent work by Halfmann et al. demonstrated that Nup100 did in fact form a prion (27). Multiple regions of Nup100 were examined for their ability to aggregate and it was found that these Q/N-rich regions aggregated in an Hsp104 and [*RNQ*+]-dependent manner. Interestingly, aggregates formed upon over-expression of Nup100[201-400] were found to sequester endogenous GLFG nucleoporins. Analysis of Nup100f, a region containing amino acids 300-400, which had the highest similarity to other yeast prions, also formed amyloid under physiological conditions. Reduction of Q/N-richness or disruption of GLFG repeats resulted in a severe delay in the formation of amyloid (with some exceptions), suggesting that the GLFG repeats contribute significantly to Nup100's ability to form amyloid. Moreover, using a Sup35 reporter assay,

Nup100f was shown to propagate [*PSI+*]-like phenotypes, demonstrating that in addition to being a driver of amyloid formation, GFLG repeats drive prion formation (27).

Lsb2, also known as Pin3, is the protein determinant of the metastable prion [*LSB+*] (28). Lsb2 is a Q/N-rich protein that was previously shown to promote *de novo* formation of [*PSI+*] (68, 75). Lsb2 levels were found to be increased by heat stress, which in turn was associated with an increase in [*PSI+*] formation. [*LSB+*] cells were also found to contain heritable Lsb2 aggregates, the abundance of which was increased in ubiquitination-defective mutants of Lsb2. Moreover, ubiquitination of Lsb2 was found to impair its prion-inducing ability, suggesting that prion formation by Lsb2 was a ubiquitin dependent process (75). The [*PSI+*]-inducibility phenotype generated after Lsb2 overproduction was dependent on both the continued presence of the *LSB2* gene and Hsp104. Rnq1 was found to be soluble in [*LSB+*] cells, demonstrating that the [*PSI+*]-inducibility phenotype was not attributable to [*RNQ+*]. The binding to Las17 and actin were found to be important for aggregation and prion formation, as an Las17 mutant deficient in binding to both was found to block the formation of detergent-resistant Lsb2 aggregates and [*LSB+*]. Importantly, it was demonstrated that [*LSB+*] was stress-induced, suggesting that Lsb2 may also have a biological role in stress sensing and in the induction of other prions, whose presence may afford a competitive advantage to yeast (28).

The major focus of this thesis is [*SWI+*], whose protein determinant is the protein Swi1. Swi1, like Cyc8, Lsb2, and Ure2, was initially identified as a protein whose overexpression facilitated *de novo* formation of [*PSI+*] (68) and was identified as a prion candidate due to its high Q/N content (23, 76). Swi1 is a subunit of the SWI/SNF chromatin remodeling complex, which regulates approximately 6% of gene expression in yeast, including *SUC2* and *FLO1* (77). Our laboratory demonstrated that Swi1 could be become a prion, [*SWI+*], which was dominantly and cytoplasmically inherited (23). Swi1 was shown to form aggregates in [*SWI+*], but not [*swi-*] cells (Fig 4A). Moreover, cells harboring [*SWI+*] exhibit a partial loss-of-function phenotype of poor growth in non-glucose (e.g. raffinose) media, a phenotype similar to that observed in SWI/SNF null mutants (Fig 4B and (23)) and a complete loss of multicellular features (Fig 5 and (78)).
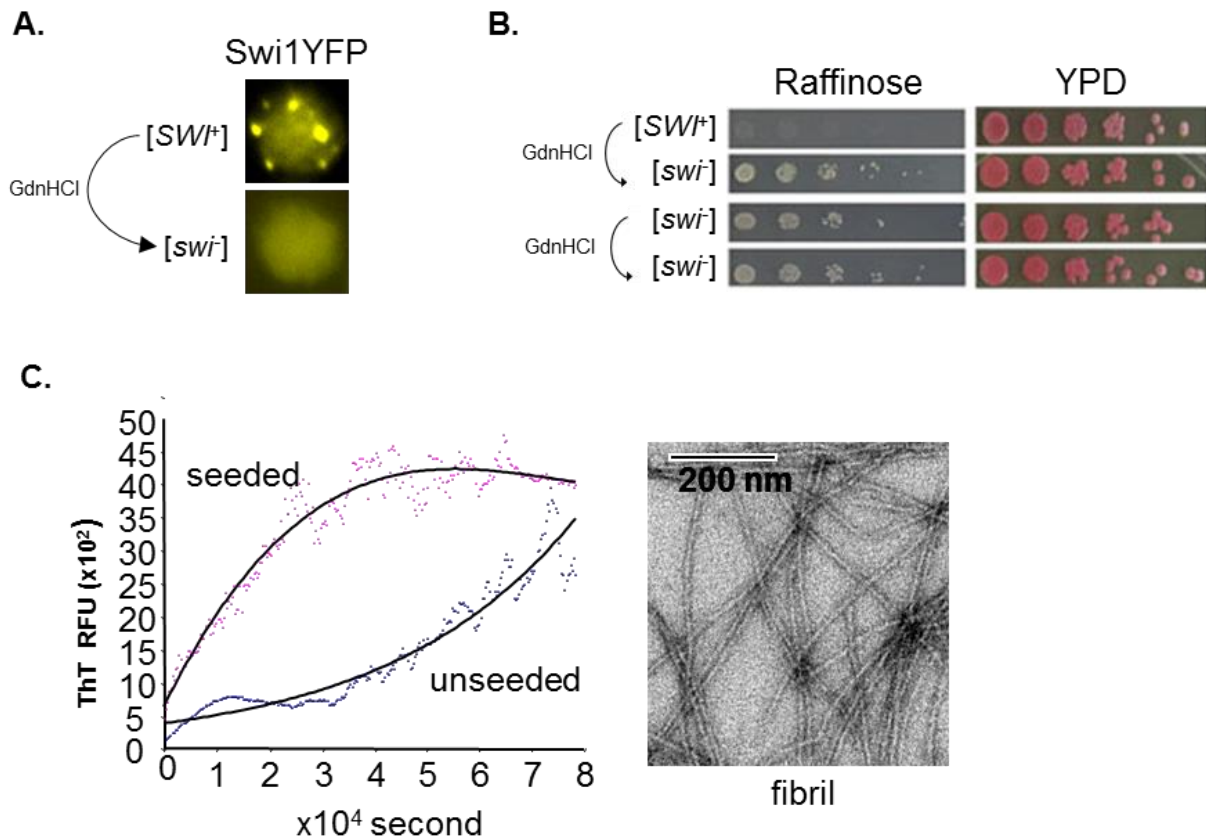
Figure 4. [*SWI⁺*]-related phenotypes. A. Aggregation of Swi1-YFP was assessed by fluorescence microscopy. Swi1-YFP is aggregated in [*SWI⁺*] cells and is diffuse in GdnHCl treated cells. B. [*SWI⁺*] cells exhibit a partial loss-of-function phenotype of poor growth in non-glucose (e.g. raffinose media). Treatment with GdnHCl restored cell growth to levels similar to those of [*swi⁻*] cells. C. Purified Swi1N monomers (2.5 µM) were assembled into amyloid fibers in the presence or absence of preformed Swi1N seeds (left). In vitro formed Swi1N fibrils were viewed by electron microscope. Figures adapted from Du *et al.*, *Mol Cell Bio* (2010).

The maintenance of [*SWI*[+]] was dependent on Hsp104, as inhibition of the chaperone by treatment with 5 mM GdnHCl, eliminated [*SWI*[+]]. Interestingly, while inactivation of Hsp104 eliminated [*SWI*[+]], overexpression of Hsp104 did not (23). Later work by Hines et al demonstrated that [*SWI*[+]] was highly sensitive to alterations in the Hsp70 chaperone system, including the Hsp70 Ssa, J-protein co-chaperones Sis1 and Yjd1, as well as the nucleotide exchange factors Sse1/2 (58). Specifically, [*SWI*[+]] is dependent on Ydj1 and Sis1 for propagation and was found to sensitive to their overexpression. Interestingly, deletion of *SSE1* or overexpression of either Sse1 or Sse2 was also found to cure [*SWI*[+]] in the 74D-684 strain but not the BY strain (58, 79).

Importantly, loss of Swi1 production caused [*SWI*[+]] elimination, confirming Swi1 as the protein determinant of [*SWI*[+]] (23). Furthermore, [*SWI*[+]] was shown to be "infectious", as cytoduction, cytoplasmic mixing in the absence of nuclear fusion, results in transmission of [*SWI*[+]] to non-prion cells (23). Additional work from our laboratory showed that prion behavior was sole attributable the N-rich region of Swi1, Swi1N, containing the first 327 amino acids of the protein. Swi1N was shown to form infectious amyloid fibers (Fig 4C) and Swi1 mutants lacking this domain did not exhibit prion behavior (23). The Q-rich middle region of Swi1 was neither sufficient for aggregation in [*SWI*[+]] cells nor essential for Swi1 function. This region, however, was found to modify Swi1 aggregation patterns (33). Swi1 function was attributable to the C-terminus. Further studies in our laboratory have aimed to define the minimal region of Swi1 that can aggregate, maintain and propagate [*SWI*[+]] (See Chapter two).

Recent studies in our laboratory have demonstrated an important role for Swi1 and [*SWI*[+]] in regulation of flocculin gene expression and multicellularity in yeast (78). *S. cerevisiae* can reversibly switch from a unicellular form to distinct multicellular forms and features associated with multicellularity, including flocculation, biofilm formation, pseudohyphal formation, and invasive growth can be assessed in yeast (80, 81). These features are regulated by flocculins, cell wall proteins that are encoded by *FLO* genes, including *FLO1* (82, 83). Du et al. reported that Swi1 was required for *FLO1* gene expression, as adhesive growth, flocculation and pseudohyphal formation were absent in both *swi1Δ* and [*SWI*[+]] BY4741 cells (Fig 5A, 5B, and 5C). Using novel reporter systems (*FLO1pr-URA3* or *FLO11pr-URA3*), in which the uracil ORF was
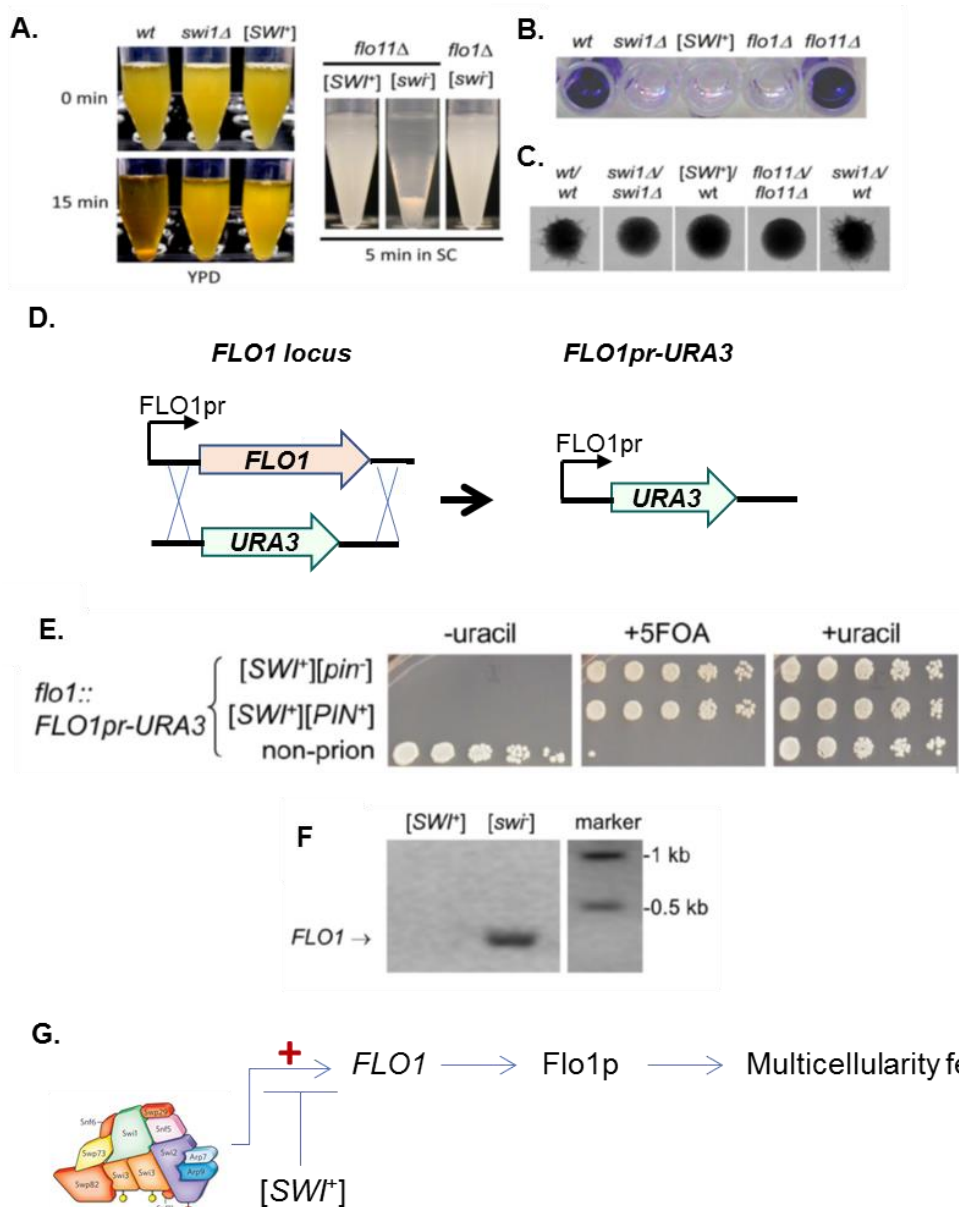
Figure 5. [*SWI⁺*] tightly regulates *FLO1* expression. A. Stationary-phase cells were tested for flocculation in YPD, which was absent in both *swi1Δ* and [*SWI⁺*] cells (left) and found to be dependent on *flo1*, but not *flo11* (right). B. Another multicellularity feature, adhesion to plastic surfaces was eliminated in both *swi1Δ* and [*SWI⁺*] cells and was dependent on *flo1*, but not *flo11*. C. Pseudohyphal growth was eliminated in *swi1Δ* and [*SWI⁺*] cells and was dependent on *flo11*. D. Diagram showing gene replacement strategy of *FLO1* with *URA3* ORF, resulting in a *URA3* gene under the control of the *FLO1* promoter. E. [*SWI⁺*] or [*swi⁻*] cells containing *FLO1pr-URA3* reporter were spotted on media lacking uracil, 5-FOA, and on media containing uracil. F. RT-PCR was used to detect expression of FLO1 in [*SWI⁺*] and [*swi⁻*] cells. G. Diagram summarizing effect of Swi1 and [*SWI⁺*] on multicellularity in yeast. Swi1 is required for expression of the *FLO1* gene, which encodes the Flo1 protein. Flo1 is required for multicellular growth in yeast. [*SWI⁺*] eliminates FLO1 gene expression and thus multicellularity in yeast. Figure adapted from Du et al., *Cell Reports* 2015.

placed under the control of the *FLO1* or *FLO11* promoters (Fig 5D), Du et al. demonstrated that *FLO1* and *FLO11* were not transcribed in *swi1Δ* and [*SWI⁺*] cells, suggesting that abolishment of multicellularity was due to transcriptional inactivation of *FLO* gene expression (Fig 5E and 5F). Du et al. further showed that the lack of *FLO* gene expression and absence of multicellularity was attributable not only to prion-mediated inactivation of Swi1 in [*SWI⁺*] cells, but also the functional sequestration and conformational inactivation of other *FLO* gene upregulators, including Mss11, Sap30, and Msn1 (78). These studies demonstrate that [*SWI⁺*] tightly regulates *FLO* genes and underscore the role of prions in the regulation of important biological pathways in yeast.

Work from our laboratory also demonstrated that the presence of [*SWI⁺*] enhances the appearance of two other prions, [*PSI⁺*] and [*PIN⁺*]. Du et al. showed that a single yeast cell could harbor three prions [*PSI⁺*], [*PIN⁺*], and [*SWI⁺*] and that [*SWI⁺*] was destabilized when all three prions are present in the same cell. Moreover, [*SWI⁺*] was found to be a stronger inducer of [*PIN⁺*] than [*PSI⁺*], a difference that was attributed to a higher sequence homology between Rnq1 and Swi1, which would allow for more efficient cross-seeding and prion conversion (70). Interestingly, spontaneous *de novo* formation of [*SWI⁺*] is promoted by pre-existing [*PSI⁺*] or [*PIN⁺*]. Moreover, aggregates formed by Swi1 in the presence of a pre-existing prion initially colocalized with Sup35 or Rnq1 aggregates, demonstrating that cross-seeding by Sup35 or Rnq1 is a major mechanism in promoting Swi1 aggregation and [*SWI⁺*] formation. Recently, Nizhnikov *et al* demonstrated that the interaction of [*SWI⁺*] and [*PIN⁺*] causes inactivation of *SUP45* gene that leads to transmission of heritable phenotypes of nonsense suppression in strains bearing a deleted or modified Sup35 N-terminal domain (84). These studies indicate that protein-protein interactions are important and complex mechanisms underlying prion formation in yeast, all of which have important implications in diverse biological pathways.

Yeast prion studies have elucidated a major role for prion in the regulation of multiple biological pathways. Significant insight into the mechanisms underlying prion formation, maintenance and propagation has come from studies in *S. cerevisiae*. This thesis aims to elucidate the sequence features that are required for prion formation, maintenance and propagation (Chapter 2). Furthermore, given the

similarities between yeast and mammalian prions, and the previous success in the use of yeast in screening for anti-prion compounds, we used a novel reporter system to uncover novel anti-prion compounds (Chapter 3). These studies may lead to the identification of anti-prion compounds that can be used as therapies for prion disease, but also importantly, these compounds can be used as probes for the elucidation of factors that contribute to prion and amyloid formation.

CHAPTER TWO

Small regions of Swi1 confer prion formation, maintenance and transmission

Introduction

While there are many proteins that form amyloid, only a few are able to form transmissible amyloids. Yeast prion proteins, which form transmissible amyloids, serve as excellent models to study the determinants underlying amyloid and prion formation, maintenance and transmission. As discussed in previous chapters, several prion proteins have been discovered in *S. cerevisiae*, each of which propagate as self-templating misfolded conformers (29). Studies of these fungal proteins have shed light on the importance of domains, termed prion domains (PrDs), which are usually dispensable for normal protein function, but are essential and sufficient for prion formation and propagation (Table 2 and (16, 85, 86)).

Initial characterization of prion domains initially focused in the two well-studied prion proteins Sup35 and Ure2 (59, 87-89). Sup35 is known to possess an oligopeptide repeat domain with a consensus sequence that bears a significant resemblance to the octapeptide repeat found in PrP. The sequence has been shown to be important as deletion of some or all of the repeats destabilizes or eliminates [*PSI*⁺] and various point mutations also affect propagation of [*PSI*⁺] (90-94). These repeats, however, are not present in all yeast prion proteins, indicating that while important for aggregation and prion formation of Sup35, these sequences are not required for prion formation in general.

Interestingly, when the primary sequence of Sup35 and Ure2 was scrambled, the both PrDs retained the ability to form prions, suggesting that the amino acid composition of PrDs was responsible for prion formation (95, 96). Furthermore, deletion analysis of the scrambled Ure2 PrD demonstrated that no single segment was absolutely required for prion formation. Combined, the data demonstrating the importance of the oligopeptide repeat domain of Sup35 and the data on the shuffled domains suggest that length and composition of these regions is more important than the primary sequence of the proteins (95).

Most PrDs have been found to be biased in their amino acid compositions, as they are enriched in glutamine and asparagine residues (85). However, some proteins that are not enriched in glutamine or

Table 2. Prion domains of verified prion proteins in *S. cerevisiae*

Prion protein	Prion domain	PrD Characteristics	Reference
Sup35	1-123	Q/N/G/Y-rich, imperfect PQGGYQQ-YN repeat	(59)
Ure2	1-89	Q/N-rich	(87)
Rnq1	153-405	Q/N/G/S-rich	(21)
Swi1	~1-32	N-rich, Q-free	this thesis
Cyc8	465-966	Q/A-rich	(24)
Mot3	1-295	Q/N/H-rich	(25)
Nup100	201-400	Q/N-rich, GLFG repeats	(27)
Lsb2	124-183	Q/N-rich	(28)

asparagine can also switch to altered conformations and confer prion-like patterns of inheritance (26, 97, 98). Bioinformatic and mutational analysis has revealed that charged resides and prolines are strongly under-represented among prion forming domains relative to the yeast proteome (94, 99-101). The prevalence of glutamine and asparagine and the underrepresentation of charged residues and prolines was not surprising as both glutamine and asparagine residues are known to stabilize amyloids. Conversely, prolines, known β-sheet breakers, would be predicted to be absent from these regions (25).

Using the compositional determinants of known prion proteins, a number of novel prions were identified. Investigations into the PrD of all verified prion proteins have shown most share several characteristics: enrichment in Q/N-residues, intrinsic disorderedness, modularity and transferability, ability to form amyloid-based aggregates, necessity of this domain for prion formation (102).

Several algorithms have been created to predict aggregation and/or prion propensity of proteins, including BETASCAN (103), STITCHER (104), Zyggregator (105), Zipper DB (106), Tango (107), SALSA (108), PASTA (109), pWaltz (110), PAPA (36), PLAAC (111) , PrionW (112), and pRANK (113). While some of these algorithms have been successful in identifying amyloidogenic proteins, it has proved more difficult to predict aggregation or prion formation of Q/N-rich proteins.

Algorithms like PLAAC and PrionW use parameters, including compositional similarity to known PrDs to identify proteins with prion activity (25, 111, 112). Using this approach, Alberti et al. identified 100 yeast prion domains with the highest similarity to four known yeast prions (25). Interestingly, 18 of the 100 proteins showed prion-like activity and one protein, Mot3 was determined to be a novel prion protein, suggesting that compositional similarity to known yeast PrDs allows for efficient identification of novel prion protein candidates.

Another algorithm, *p*rion *a*ggregation *p*rediction *a*lgorithm (PAPA), calculates a protein's prion propensity based on the prion propensity score of each amino acid. Using PAPA, Toombs et al. were able to find proteins with high predicted prion propensity and predicted disorderedness, which was found to correlate well with observed prion propensity (36, 99). Toombs et al. concluded that while non-Q/N amyloid proteins are characterized by short, highly amyloidogenic segments, yeast PrDs are characterized by longer

segments containing disorder promoting, moderately aggregation prone amino acids. In contrast, using pWaltz, Sabate et al. concluded that specific, short amyloid-prone sequences that occur within intrinsically disordered Q/N-rich regions determines a protein's prion behavior (110). Recently, Afsar Minhas et al. showed, however, that the success of pWaltz was a result of the scoring matrices to capture amino acid composition, again demonstrating the importance of amino acid composition in PrDs, against demonstrating the importance of amino acid composition for prion behavior (113). While significant progress has been made in designing prion prediction algorithms, several challenges still remain, including the limited data set of known prion proteins, therefore, more insight of the requirements of PrDs is still required.

Additional work has also attempted to elucidate the structure of the prion and non-prion states of proteins. Several groups, including our laboratory, have established that amyloid fibrils can be assembled *in vitro* from recombinant PrDs and that these fibrils can induce a [*PRION*+] state upon transforming non-prion cells, confirming the importance of the prion domain in prionogenesis (25, 30-33, 114). Due to the filamentous nature of these PrDs the use of traditional approaches, like X-ray crystallography and solution NMR, are less suitable for the investigation of prion structures. Several groups have used other approaches, including solid-state NMR (115-119), H/D exchange (65), electron paramagnetic resonance (31, 120), circular dichroism (121, 122), X-ray diffraction (123), and fluorophore labeling (63) and data suggests that the PrDs of Sup35, Ure2, and Rnq1 are all in a β-sheet rich conformation. Using the data obtained from these approaches, specific models have been proposed for the structure of prions including parallel in-register β-sheets (35) and a β-helix model for the structure of Sup35 (63). Investigations into the structure of other verified PrDs, including Swi1 is still lacking.

It has been shown that extracellular environments can modulate the frequency of *de novo* formation and loss of yeast prions, demonstrating the important role of the prion-mediated inheritance in adaptation (124-127). Elucidating the determinants of prion formation will shed light on our understanding of how prions are formed and propagated *in vivo*.

Investigation into Swi1's PrD has focused on the NH2-terminal region of Swi1 due to its high glutamine/asparagine content. It was shown that deletion of the first 327 amino acids (Swi1 1-327 or Swi1N)
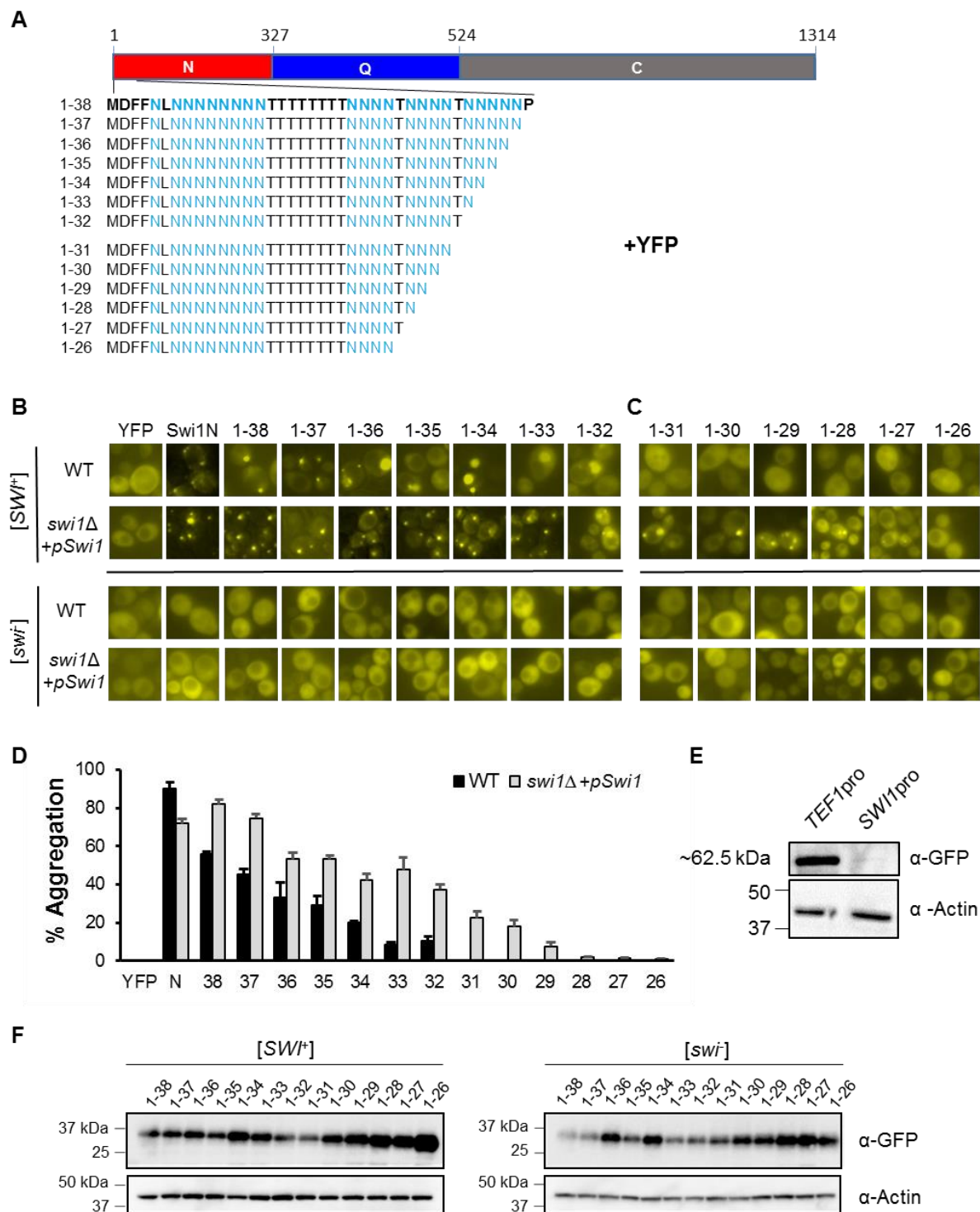
at the chromosomal *SWI1* locus resulted in [*SWI+*] loss (33). Additionally, transformation of fibrils made from recombinant Swi1N protein resulted in *de novo* formation of [*SWI+*] in naïve non-prion cells, demonstrating that the Swi1 PrD lies within the Swi1N region and amyloid is the structural basis of [*SWI+*] (33). Further deletion analysis of Swi1N showed that a region consisting of the first 38 amino acids of Swi1, which is rich in asparagine but lacking glutamine, could propagate the prion fold of [*SWI+*] in the absence of full-length Swi1 (128). Still to be determined is whether smaller regions of Swi1 can propagate [*SWI+*] and promote *de novo* prion formation, and thus constitute the minimal Swi1 PrD.

To this end, the ability of small truncation mutants ranging from $Swi1_{1-26}$ to $Swi1_{1-37}$ to propagate [*SWI+*] was examined. The minimal length of Swi1 NH_2-terminal regions required for [*SWI+*] propagation was determined to vary at different Swi1 expression levels. Under our examined conditions, a region as small as the first 32 amino acid residues ($Swi1_{1-32}$) is sufficient to stably support [*SWI+*] propagation. While $Swi1_{1-31}$ is not able to stably propagate [*SWI+*], it can confer [*PSI+*]-like prion phenotypes when fused to Sup35's MC region, establishing that this small region can serve as a transferable PrD.

Results

Minimal region of Swi1 required for [*SWI+*] propagation is dependent on Swi1 levels.

A small region consisting of the first 38 amino acids of Swi1 fused with YFP ($Swi1_{1-38}YFP$) was previously shown by our laboratory to be able to decorate [*SWI+*] aggregates (128). $Swi1_{1-38}YFP$ was also shown to maintain an aggregated prion conformation in the absence of Swi1 and to transmit the prion conformation to endogenous Swi1 (128). However, truncation to the first 32 amino acids resulted in a significant loss of aggregation (128). To examine whether regions between 32-38 amino acids were able to form Swi1 prion aggregates in [*SWI+*] cells and were capable of prion transmission, corresponding truncation mutants were constructed and fused to a C-terminal YFP reporter (Fig 6A). These truncation mutants ($Swi1_{Trunc}YFP$) were expressed in [*SWI+*] and [*swi-*] cells of either wild-type (WT) BY4741, or *swi1*Δ BY4741 cells expressing full-length Swi1 from a plasmid, *p416TEFSwi1* (*pSwi1*) (Fig 6B). All proteins were expressed at expected sizes (Fig 6F). A size-dependent decrease in the aggregation frequency was observed in both WT and *swi1Δ/pSwi1* [*SWI+*] cells: as Swi1 was increasingly truncated it became less

A

1 327 524 1314

N Q C

1-38 **MDFF**NLNNNNNNNNTTTTTTTTTNNNNTNNNNTNNNNNP
1-37 MDFFNLNNNNNNNNTTTTTTTTTNNNNTNNNNTNNNNN
1-36 MDFFNLNNNNNNNNTTTTTTTTTNNNNTNNNNTNNNN
1-35 MDFFNLNNNNNNNNTTTTTTTTTNNNNTNNNNTNNN
1-34 MDFFNLNNNNNNNNTTTTTTTTTNNNNTNNNNTNN
1-33 MDFFNLNNNNNNNNTTTTTTTTTNNNNTNNNNTN
1-32 MDFFNLNNNNNNNNTTTTTTTTTNNNNTNNNNT

1-31 MDFFNLNNNNNNNNTTTTTTTTTNNNNTNNNN
1-30 MDFFNLNNNNNNNNTTTTTTTTTNNNNTNNN
1-29 MDFFNLNNNNNNNNTTTTTTTTTNNNNTNN
1-28 MDFFNLNNNNNNNNTTTTTTTTTNNNNTN
1-27 MDFFNLNNNNNNNNTTTTTTTTTNNNNT
1-26 MDFFNLNNNNNNNNTTTTTTTTTNNNN

+YFP

B **C**

D **E**

F

(Figure legend on next page)

Figure 6. Minimal region of Swi1 required for [*SWI+*] propagation is dependent on Swi1 levels. (A) Diagram illustrating Swi1 and its truncation mutants used in this study. The amino-acid sequences of the truncation mutants are shown. Asparagine residues are highlighted in blue. (B) Fluorescence microscopy using YFP fusions of Swi1$_{1-38}$ to Swi1$_{1-32}$. Swi1N and Swi1$_{1-38}$, which were previously shown to propagate [*SWI+*], were used as positive controls, and YFP was used as negative control. Truncation mutants were expressed in WT and *swi1Δ/pSwi1* cells in both [*SWI+*] (top) and [*swi–*] (bottom) backgrounds. Three individual transformants were imaged for each truncation mutant and representative images are shown. (C) Additional fluorescence microscopy using YFP-fusions of Swi1$_{1-31}$ to $_{1-26}$. Experiments were done as described in B. (D) Percent of cells containing aggregates in WT [*SWI+*] and *swi1Δ/pSwi1* [*SWI+*] cells imaged in B and C. Aggregation was averaged for three individual transformants. Bars indicate standard error. (E) Western blot showing YFP-tagged Swi1-NYFP expressed from the *TEF1* promoter and *SWI1* promoter in WT BY4741 [*swi–*] cells. Blots were probed with an anti-GFP antibody and anti-actin antibody for a loading control. (F) Western blot showing YFP-tagged Swi1 truncation mutants expressed at expected sizes in WT BY4741 [*SWI+*] (left) and [*swi–*] cells (right). Blots were then stripped and re-probed with an anti-actin antibody for a loading control (bottom).

aggregated (Fig 6B and 6D). Interestingly, the minimal region required for aggregation differed depending on full-length Swi1 proteins levels. In WT [*SWI+*] cells, which express Swi1 from the endogenous chromosomal Swi1 promoter, only 5-10% of [*SWI+*] cells expressing Swi1$_{1-32}$YFP contained aggregation. In contrast, in *swi1Δ/pSwi1* [*SWI+*] cells, which express Swi1 at higher levels from the *TEF1* promoter (Fig 6E and (33)), ~40% of cells contained Swi1$_{1-32}$YFP aggregates (Fig 6B and 6D). This result encouraged us to construct a set of additional truncation mutants ranging from Swi1$_{1-26}$ to Swi1$_{1-31}$ (Fig 6A). Similar experiments were carried and it was determined that while further deletion to Swi1$_{1-31}$YFP resulted in a complete loss of aggregation in WT [*SWI+*] cells, significant aggregation of Swi1$_{1-31}$YFP was observed in *swi1Δ/pSwi1* [*SWI+*] cells, and detectable aggregation could be seen in cells expressing Swi1$_{1-28}$YFP (Fig 6C and 6D). All truncation mutants exhibited diffuse fluorescence in [*swi*] cells, suggesting that over-expression of Swi1 truncation mutants *per se* did not result in aggregation (Fig 6B and 6C, bottom). Taken together, these results show that the increase of Swi1 protein levels promotes prion-like aggregation of smaller NH$_2$-terminal regions of Swi1.

Swi1$_{1-32}$ stably maintains [*SWI+*] in the absence of full-length Swi1.

We next asked if the aggregatable small regions of Swi1 could maintain an aggregated prion conformation in the absence of full-length Swi1. To this end, *swi1Δ/pSwi1/pSwi1$_{Trunc}$YFP* [*SWI+*] cells were grown in medium supplemented with 5-fluoroorotic acid (5-FOA) to counter-select against *pSwi1*, eliminating the source of full-length Swi1 (Fig 7A). If Swi1 truncation mutants maintained [*SWI+*], the appearance of fluorescent foci is expected. In contrast, if Swi1 truncation mutants did not maintain [*SWI+*], a diffuse YFP fluorescence would be observed. In both cases, if full-length Swi1 was eliminated, a transition from a Raf$^±$ to Raf$^-$ phenotype is expected due to the loss of Swi1 function. In agreement with our previous report (128), cells of *swi1Δ/Swi1$_{1-38}$YFP* and *swi1Δ/Swi1N-YFP* background maintained the [*SWI+*] conformation in the absence of Swi1 (Fig 7B). Moreover, regions as small as Swi1$_{1-30}$ maintained the [*SWI+*] conformation in the absence of *pSwi1*. However, changes in the stability of [*SWI+*] in cells expressing smaller truncations in the absence of Swi1 were observed. Only 4% of 5-FOA treated (-*pSwi1*) Swi1$_{1-30}$YFP colonies examined maintained aggregation and [*SWI+*] was frequently lost upon passaging. 5-FOA treated

A
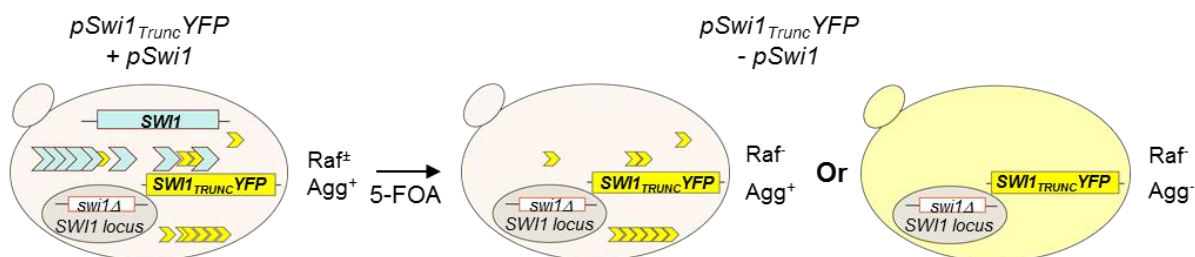
B
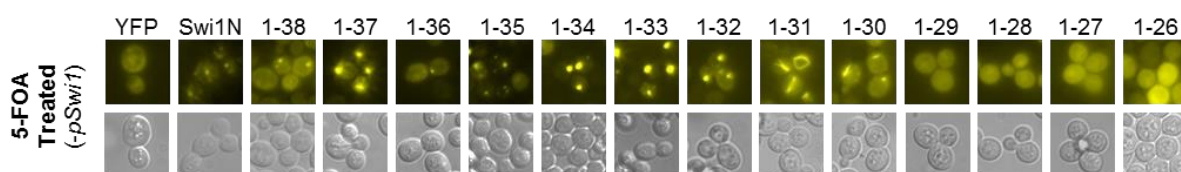
C
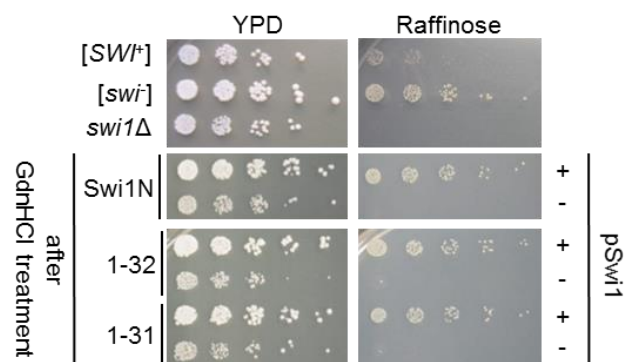
D
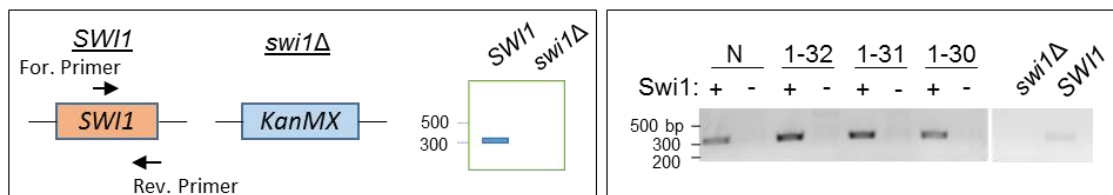
(Figure legend on next page)

Figure 7. Swi1$_{1-32}$ stably maintains [*SWI*$^+$] in the absence of full-length Swi1. (A) A schematic of the experimental design. *swi1Δ*/*pSwi1*/*pSwi1$_{TRUNC}$YFP* [*SWI*$^+$] cells were treated with 5-FOA to counter-select against *pSwi1*. After loss of full-length Swi1 (*pSwi1*), *swi1Δ*/*pSwi1$_{TRUNC}$YFP* cells that maintain [*SWI*$^+$] are expected to have Swi1 aggregates (middle), while cells that have not maintained [*SWI*$^+$] are expected to lack aggregation (right). Both cell types will have Raf$^-$ phenotype if full-length Swi1 is eliminated. (B) Fluorescence microscopy using YFP-fusion proteins of Swi1 truncation mutants. Negative (YFP) and positive (Swi1N and Swi1$_{1-38}$) controls for Swi1 aggregation are also shown. A minimum of six individual colonies from each truncation mutant were imaged and representative images are shown. (C) Loss of full-length Swi1 (*pSwi1*) in *swi1Δ*/*pSwi1$_{TRUNC}$YFP* cells treated with 5 mM GdnHCl was confirmed by assessing growth phenotype on media containing raffinose as the sole carbon source. Log-phase cells were serially diluted and spotted onto rich media (YPD) or raffinose media (raffinose). WT, [*SWI*$^+$], and *swi1Δ* are included as controls. (D) Diagram showing experimental design of RT-PCR to detect the presence or absence of *SWI1* gene in the examined strains (left). RT-PCR was performed with Swi1 specific primers. *swi1Δ*/*pSwi1*/*pSwi1$_{TRUNC}$YFP* [*SWI*$^+$] cells (+) contain *SWI1* transcript while 5-FOA treated cells do not contain *SWI1* transcript (-). [*swi*$^-$] and *swi1Δ* controls are included (right).

Swi1$_{1-31}$YFP and Swi1$_{1-32}$YFP cells maintained aggregation in 14% and 80% of colonies examined, respectively. Interestingly, in the absence of full-length Swi1, a change in the morphology of the aggregates was observed upon shortening of the expressed fragment length. While cells containing Swi1$_{1-38}$YFP to Swi1$_{1-32}$YFP had aggregates whose morphology was exclusively dot-shaped in nature, cells containing Swi1$_{1-31}$YFP and Swi1$_{1-30}$YFP not only contained the dot-like aggregates, but also contained ring-like aggregates in [*SWI$^+$*] cells lacking Swi1 (Fig 7B). These results demonstrate that while smaller regions of Swi1 can maintain [*SWI$^+$*] in the absence of the full-length Swi1, Swi1$_{1-32}$ is the smallest domain able to do so stably under our examined conditions.

To confirm that the treatment of 5-FOA had indeed resulted in the loss of *pSwi1*, the raffinose phenotype of cells before and after treatment with 5-FOA was assessed. In agreement with our laboratory's published results, WT [*SWI$^+$*] cells, which express Swi1 endogenously, displayed a phenotype of reduced growth on media using raffinose, a non-glucose sugar, as the sole carbon source (Raf$^±$), whereas *swi1Δ* cells, which do not express Swi1, had no growth on raffinose media (Raf$^-$) (Fig 7C) (23). While *swi1Δ/pSwi1$_{Trunc}$YFP* [*SWI$^+$*] cells expressing *pSwi1* (+*pSwi1*) exhibited a Raf$^±$ phenotype, the 5-FOA treated cells (-*pSwi1*) displayed a Raf$^-$ phenotype suggesting that the *pSwi1* plasmid was indeed lost as a result of 5-FOA treatment. Next, cells were treated with 5 mM guanidine hydrochloride (GdnHCl), a chemical known to inhibit prion propagation by inactivating the molecular chaperone Hsp104, a disaggregase that is required for [*SWI$^+$*] propagation (23). After treatment with GdnHCl, the growth of *swi1Δ/pSwi1/pSwi1$_{Trunc}$YFP* cells on raffinose media was restored to levels comparable to those of [*swi$^-$*] cells (Fig 7C). In contrast, after GdnHCl treatment, *swi1Δ/pSwi1$_{Trunc}$YFP* cells still maintained the Raf$^-$ phenotype, confirming that these cells had in fact lost full-length Swi1.The loss of *pSwi1* for the 5-FOA treated cells was further confirmed by a reverse-transcription PCR (RT-PCR) experiment using primers specific for the C-terminal region of Swi1. A ~300 bp band representative of the targeted region of Swi1 was observed in the *swi1Δ/pSwi1/pSwi1$_{Trunc}$YFP* samples, while this band was absent in the 5-FOA treated cells, confirming that *pSwi1* was in fact lost (Fig 7D).

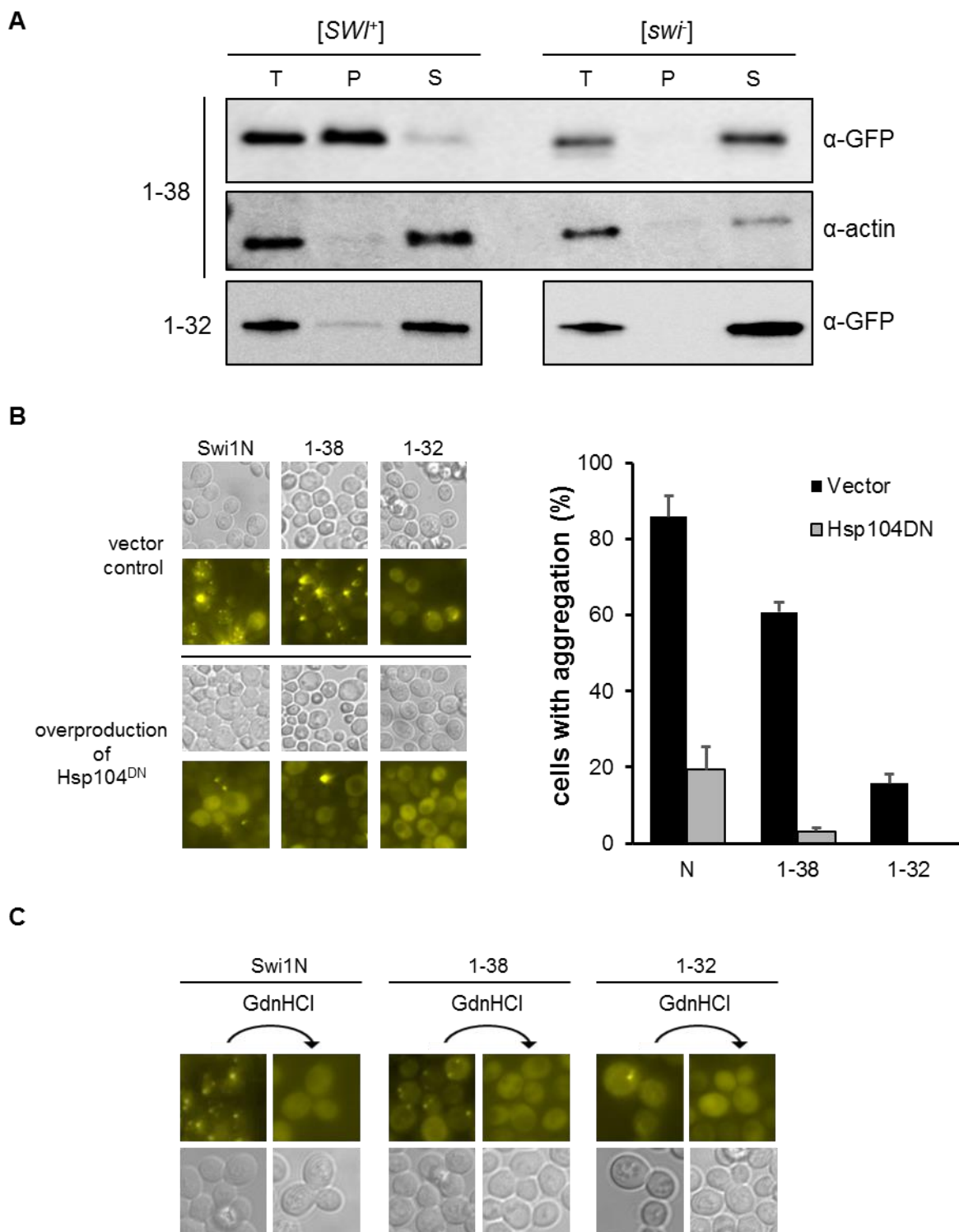**Insoluble protein aggregates are formed by truncated Swi1.**

To complement our microscopic analysis, the solubility of Swi1$_{1-32}$YFP and Swi1$_{1-38}$YFP was examined by a centrifugation assay (Fig 8A). Lysates from [*SWI+*] and [*swi*] cells of *swi1Δ*/pSwi1$_{1-32}$YFP or *swi1Δ*/pSwi1$_{1-38}$YFP background but lacking endogenous Swi1 were separated by centrifugation at 20,000 x g and resolved by SDS-PAGE. Western blot analysis revealed that Swi1$_{1-38}$YFP protein was found mostly in the pelleted, insoluble fraction in [*SWI+*] cells. Analysis also revealed that a fraction of Swi1$_{1-32}$YFP protein was found in the pelleted insoluble fraction of [*SWI+*] cells. In contrast, Swi1$_{1-32}$YFP or Swi1$_{1-38}$YFP proteins were found entirely in the soluble, supernatant fraction in [*swi*] cells. As a control, actin was only found in the total and supernatant fractions (Fig 8A). This result demonstrates that Swi1$_{1-32}$YFP and Swi1$_{1-38}$YFP can maintain the [*SWI+*] fold in the form of insoluble aggregates in [*SWI+*] cells without full-length Swi1.

Functional Hsp104 is required for maintaining the prion conformation of truncated Swi1.

Most yeast prions examined to date, including [*SWI+*], require the function of Hsp104 for their propagation. A treatment of millimolar levels of GdnHCl, which inactivates Hsp104, or expression of a dominant negative mutant of Hsp104 eliminates these hsp104-dependent prions (21, 23, 24, 37, 45-47). To test if the truncated Swi1 prions also require Hsp104 function for propagation, [*SWI+*] cells of *swi1Δ*/pSwi1N-YFP, *swi1Δ*/pSwi1$_{1-38}$YFP or *swi1Δ*/pSwi1$_{1-32}$YFP background were transformed with a dominant negative variant of Hsp104, Hsp104^{DN}, which has been shown to cure other amyloid yeast prions (24, 37, 42, 47, 60). We found that the YFP-fusion aggregation decreased dramatically for Swi1N and Swi1$_{1-38}$ after overproduction of Hsp104^{DN} compared to vector controls (Fig 8B). We also found that Swi1$_{1-32}$ aggregation was completely gone in cells transformed with Hsp104^{DN} as opposed to the persistent aggregation in cells transformed with a vector control. Similar results were obtained after serially passaging cells on medium containing 5 mM GdnHCl (Fig 8C) – demonstrating that the aggregation of Swi1N-YFP, Swi1$_{1-38}$YFP and Swi1$_{1-32}$YFP is curable by Hsp104 deficiency.

[*SWI+*] maintained by small NH$_2$-terminal fragments of Swi1 can transmit the prion fold to full-length Swi1.

Next, we examined if small regions of Swi1 could propagate [*SWI+*] by transmitting a prion fold back to full-length Swi1. As illustrated by Fig 9A, [*SWI+*] cells of *swi1Δ/pSwi1$_{Trunc}$YFP* background were transformed

A

	[*SWI⁺*]			[*swi⁻*]		
	T	P	S	T	P	S

α-GFP

1-38

α-actin

1-32

α-GFP

B

Swi1N   1-38   1-32

vector control

overproduction of Hsp104ᴰᴺ

cells with aggregation (%)

■ Vector
▢ Hsp104DN

N   1-38   1-32

C

Swi1N   1-38   1-32

GdnHCl   GdnHCl   GdnHCl

(Figure legend on next page)

Figure 8. Prion-like features of Swi1 truncation mutants. (A) The insoluble fractions of Swi1$_{1-38}$ and Swi1$_{1-32}$ were seen in [SWI^+] samples but not observed in [swi^-] samples. [SWI^+] and [swi^-] cells of *swi1Δ/pSwi1$_{1-38}$YFP* or *swi1Δ/pSwi1$_{1-32}$YFP* background lacking Swi1 were lysed, cleared, and separated by high speed centrifugation (20,000 g) as described in the Materials and Methods. Cleared whole cell lysate (T), supernatant (S), and pellet (P) fractions were resolved by SDS-PAGE and probed with anti-GFP antibody by western blot. Blot was stripped and re-probed with an anti-actin antibody for a loading control. (B) The function of Hsp104 is required for [SWI^+]$_{TRUNC}$ propagation. [SWI^+] cells of *swi1Δ/pSwi1N-YFP, swi1Δ/pSwi1$_{1-38}$YFP,* or *swi1Δ/pSwi1$_{1-32}$YFP* background were transformed with an empty vector of *pRS316* or *pKT218,620* (Hsp104^{DN}). Aggregation of truncation mutants was assessed by fluorescence microscopy. Aggregation was averaged for six individual colonies grown in liquid media for Swi1N and Swi1$_{1-32}$, and three colonies for Swi1$_{1-38}$. Bars indicate standard error. (C) [SWI^+] cells of *swi1Δ/pSwi1NYFP, swi1Δ/pSwi1$_{1-38}$YFP,* or *swi1Δ/pSwi1$_{1-32}$YFP* background lacking Swi1 were streaked on media containing GdnHCl. Aggregation of truncation mutants was assessed by fluorescence microscopy.
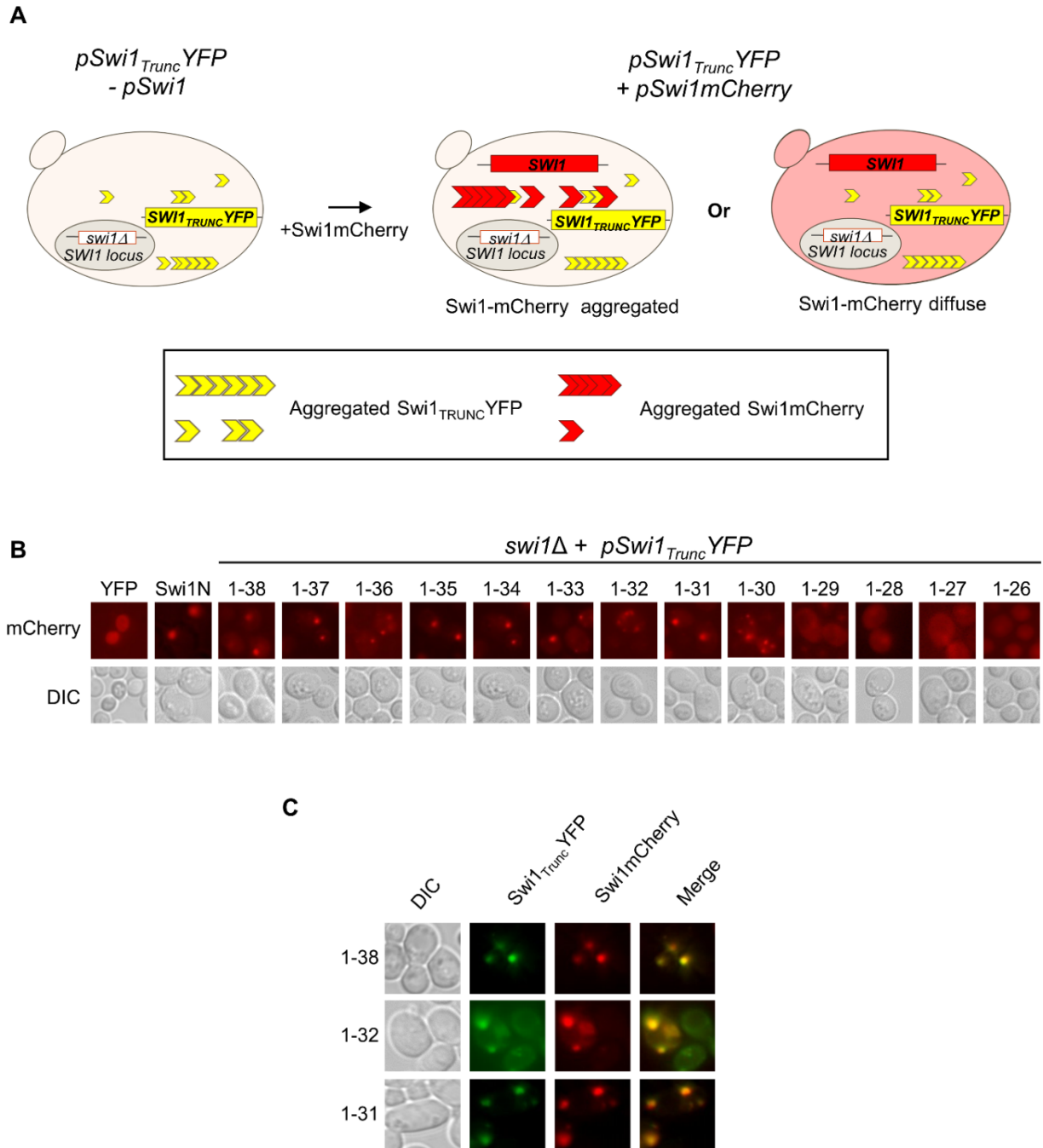
Figure 9. [*SWI*⁺] maintained by small NH₂-terminal fragments of Swi1 can transmit the prion fold to full-length Swi1. (A) A schematic of the experimental design. Individual *swi1Δ/pSwi1_TRUNC_YFP* colonies were transformed with full-length Swi1mCherry (*pSwi1mCherry*). If a Swi1 truncation mutant can transmit the prion fold to Swi1, we expect the appearance of Swi1mCherry foci, otherwise a diffuse mCherry signal is expected. (B) Fluorescence microscopy using mCherry-tagged Swi1. Six individual colonies from each truncation mutant were imaged and representative images are shown. (C) Colocalization of YFP-tagged truncation mutants and mCherry-tagged full-length Swi1 is shown by fluorescence microscopy.

with mCherry-tagged Swi1, *pSwi1mCherry,* and an aggregation assay was carried out to determine if the small *Swi1$_{Trunc}$* prion was able to transmit the prion fold to the Swi1mCherry. Consistent with our previous report, cells of *swi1Δ/pSwi1mCherry/pSwi1$_{1-38}$YFP* or *swi1Δ/pSwi1mCherry/pSwi1N-YFP* background were found to harbor punctate fluorescent foci when mCherry fluorescence was examined (Fig 9B), indicating that these two regions are able to transmit the prion fold back to Swi1 (128). Truncation mutants ranging from Swi1$_{1-37}$YFP to Swi1$_{1-31}$YFP were also able to transmit the prion fold back to full-length Swi1, as these cells exhibited punctate foci formed by Swi1mCherry (Fig 9B). Additionally, the aforementioned results showed that Swi1$_{1-30}$ is able to form prion aggregates and maintain [*SWI$^+$*] in the absence of full-length Swi1 but it was unstable. Such a prion fold, however, could be transmitted back to full-length Swi1 as Swi1mCherry foci were observed upon transformation (Fig 9B). Remarkably, most ring-shaped aggregates formed by Swi1$_{1-31}$YFP and Swi1$_{1-30}$YFP transition back into dot-like aggregates when cells are retransformed with full-length Swi1 (Fig 9B and 9C). Interestingly, Swi1$_{Trunc}$YFP aggregates were found to be colocalized with full-length Swi1mCherry in a portion of the cells that co-express both proteins, suggesting that small domains of Swi1 may cross-seed or decorate full-length Swi1 (Fig 9C).

Small NH$_2$-terminal region of Swi1 is a transferable PrD that supports prion *de novo* formation.

We next examined whether Swi1$_{1-38,}$ Swi1$_{1-32}$, and Swi1$_{1-31}$ could be transferable and could support *de novo* prion formation using a well-established Sup35 reporter assay (21, 25, 129).

As described in Chapter 1, the prion state of Sup35 can be easily assessed in a strain containing the *ade1-14* allele with a premature stop codon in the ORF of *ADE1* (37). While Sup35 is aggregated in prion cells, this allowing for read-through of the premature stop codon and a white colony color on YPD. In contrast, Sup35 is soluble in non-prion cells, allowing for efficient translational termination and red colony color on YPD. The N region of Sup35 was replaced with Swi1$_{1-38}$, Swi1$_{1-32}$, or Swi1$_{1-31}$ resulting in constructs expressing chimeric proteins, Swi1$_{1-38}$MC, Swi1$_{1-32}$MC, and Swi1$_{1-31}$MC (Swi1$_{TRUNC}$MC) under the control of *TEF1* promoter (Fig 10A). Next, these Swi1$_{TRUNC}$MC constructs were introduced into a W303 strain containing a chromosomal deletion of *SUP35* and expressing full-length Sup35 from a plasmid, *p316Sup35FL* (94). Given that the Sup35FL-expressing plasmid was under uracil selection, we were able
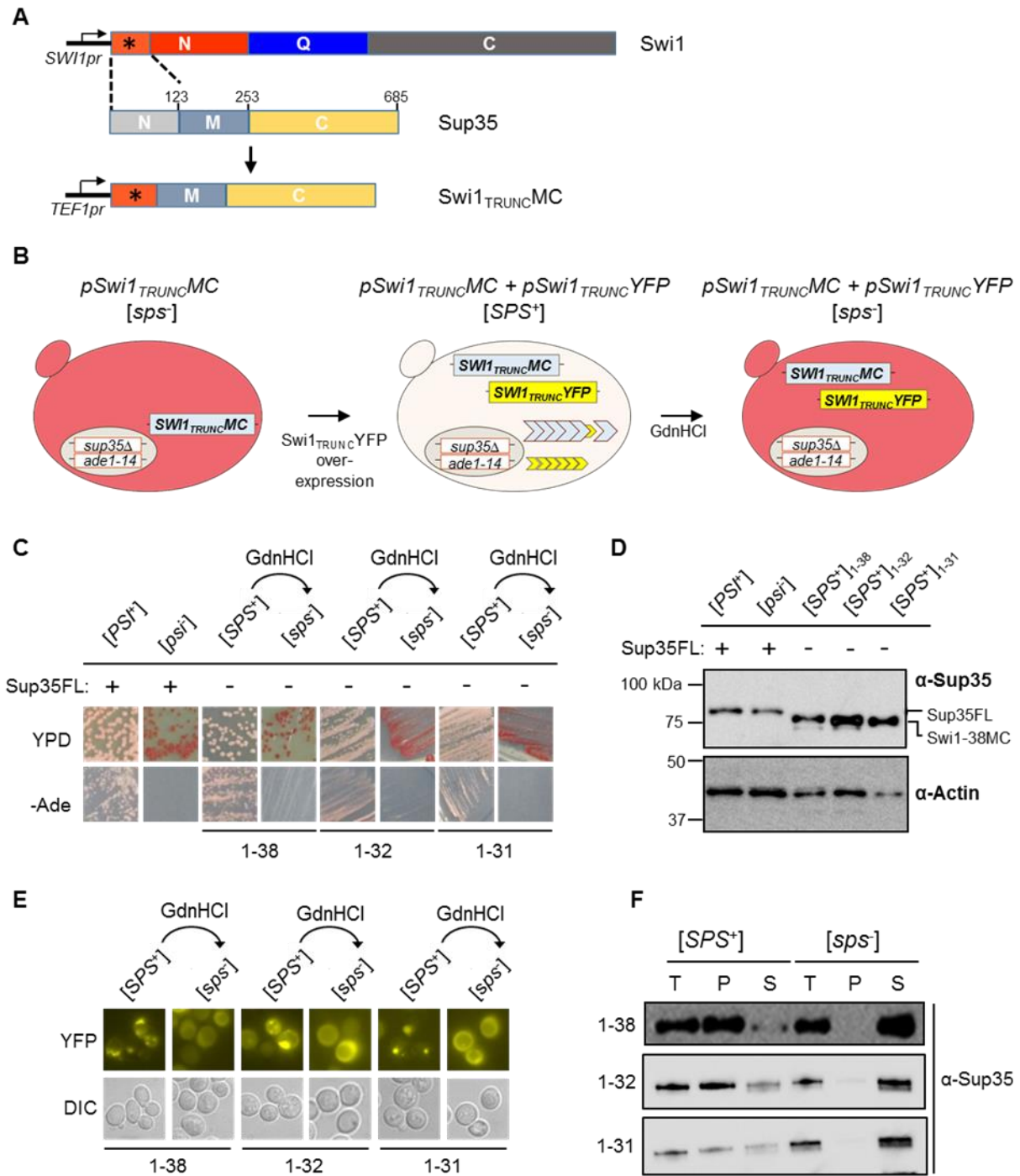
(Figure legend on next page)

Figure 10. Small NH$_2$-terminal regions of Swi1 are transferable and support prion *de novo* formation. (A) Diagram illustrating cloning scheme for Swi1$_{1-38}$MC, Swi1$_{1-32}$MC, and Swi1$_{1-31}$MC (Swi1$_{TRUNC}$MC) fusions. Swi1$_{TRUNC}$ was inserted in place of the NH$_2$-terminal (1-123) PrD of Sup35 resulting in Swi1$_{TRUNC}$MC fusions that were expressed under the control of the *TEF1* promoter. * denotes Swi1$_{TRUNC}$. (B) Experimental design. W303 *sup35Δ/pSwi1$_{TRUNC}$MC* [*psi*] strains with Ade$^-$ phenotype and red color on YPD were transformed with the corresponding *pSwi1$_{TRUNC}$YFP*. Transformants were grown and plated on -Ade plates to select for prion state (white on YPD, Ade$^+$, and aggregated Swi1$_{TRUNC}$YFP). Prion candidate isolates were treated by 5 mM GdnHCl. If this GdnHCl treatment resulted in red, Ade$^-$ isolates with diffuse Swi1$_{TRUNC}$YFP, the corresponding isolates were scored as a chimeric prion termed [*SPS$^+$*]. (C) Representative [*SPS$^+$*] isolates and their corresponding GdnHCl-treated [*sps$^-$*] cells were streaked onto YPD media and SC-ade plates to assess the color phenotype and growth ability. *sup35Δ/pSup35FL* [*PSI$^+$*] and [*psi*] strains were streaked simultaneously as controls. (D) Western blot showing the presence of either full-length Sup35 in *sup35Δ/p316Sup35FL* cells or Swi1$_{TRUNC}$MC fusion proteins in *sup35Δ/pSwi1$_{TRUNC}$MC/pSwi1$_{TRUNC}$YFP* [*SPS$^+$*] cells. Sup35FL and Swi1$_{TRUNC}$MC are expressed at different sizes when probed with C-domain-specific anti-Sup35 antibody. Blot was stripped and reprobed with anti-actin antibody. (E) Microscopy assay showing aggregation status of cells described in C. (F) [*SPS$^+$*]$_{1-38, 1-32}$ or $_{1-31}$ and [*sps$^-$*]$_{1-38, 1-32}$ or $_{1-31}$ cells of *sup35Δ/pSwi1$_{TRUNC}$MC/pSwi1$_{TRUNC}$YFP* background were subjected to centrifugation assay as described in the Materials and Methods. The cleared whole cell lysate (T), supernatant (S), and pellet (P) fractions were resolved by SDS-PAGE and presence of Swi1$_{TRUNC}$MC was detected by western blotting with anti-sup35 antibody.

to counter-select to remove this plasmid by growing cells in 5-FOA media. The resulting strains, which carried Swi1$_{1-38}$MC, Swi1$_{1-32}$MC, or Swi1$_{1-31}$MC as the only source of Sup35 function, produced red colonies on YPD media (Fig 10B left). As Sup35 function is required for cell survival and the red color of cell colonies is an indication of a functional Sup35, our results suggest that Swi1$_{TRUNC}$MC are functional fusion proteins that can provide cells with the essential function of Sup35.

Next, a second plasmid was introduced to overexpress Swi1$_{TRUNC}$YFP that corresponded to the Swi1$_{TRUNC}$MC in the cell, as this may increase the induction of the prion state of Swi1$_{TRUNC}$MC in non-prion cells (Fig 10B, middle). The Swi1$_{TRUNC}$MC fusion proteins were expressed at the expected size (Fig 10D). Given the low rate of prion appearance in the absence of positive selection, cells were plated on SC media lacking adenine to select for Ade$^+$ colonies. After Swi1$_{TRUNC}$YFP overexpression, cells that grew on SC-ade and were white on YPD were considered putative prion candidates and assayed further via examination of the aggregation state of Swi1$_{TRUNC}$YFP through fluorescence microscopy assays. As shown in Fig 10E, these candidate colonies contain punctate fluorescence foci and such aggregation could be stably inherited. Combined, our results demonstrated that Swi1$_{1-38}$MC, Swi1$_{1-32}$MC and Swi1$_{1-31}$MC support *de novo* prion formation that can be promoted by overproduction of the corresponding Swi1 truncation mutant. We termed the emerged chimeric prions [*SPS$^+$*]$_{1-38}$, [*SPS$^+$*]$_{1-32}$, and [*SPS$^+$*]$_{1-31}$ (stands for Swi1 conferred [*PSI$^+$*]).

The curability of [*SPS$^+$*]$_{1-38}$, [*SPS$^+$*]$_{1-32}$, and [*SPS$^+$*]$_{1-31}$ by 5 mM GdnHCl was then examined. Colonies became red in color on YPD after GdnHCl treatment, as would be expected if Swi1$_{1-38}$MC, Swi1$_{1-32}$MC and Swi1$_{1-31}$MC were soluble and functional (Fig 10B right and 10C). Further examination showed that GdnHCl-treated cells lacked growth on -Ade media and exhibited diffuse fluorescence of Swi1$_{TRUNC}$YFP, confirming that [*SPS$^+$*]$_{1-38}$, [*SPS$^+$*]$_{1-32}$, and [*SPS$^+$*]$_{1-31}$ are curable by GdnHCl, resulting in a non-prion state, [*sps$^-$*] (Fig 10C and 10E). While cured [*sps$^-$*] cells stably maintained their non-prion conformation after GdnHCl treatment, [*SPS$^+$*] cells did reappear at a rate of 1-2% for all three truncation mutants upon selection on media lacking adenine.

Next, the curability of [*SPS$^+$*]$_{1-32}$ and [*SPS$^+$*]$_{1-31}$ upon Hsp104 overexpression was examined. While overexpression of Hsp104 has been shown to result in curing of [*PSI$^+$*], such curing is not observed for

[*SWI*]. Therefore, [*SPS*$^+$]$_{1-38}$, [*SPS*$^+$]$_{1-32}$, and [*SPS*$^+$]$_{1-31}$ were transformed with either *p2HG*, a vector control or *p2HG-Hsp104*, which expresses Hsp104 from a 2 micron plasmid driven by a *GPD* promoter. Individual transformants were grown in selective media and spread on YPD. While [*SPS*$^+$]$_{1-32}$ cells generated 5.5% red colonies when transformed with *p2HG*, over expression of Hsp104 resulted in an appearance of red colonies of about 7.6%. Results were similar when the rate of curing was examined for [*SPS*$^+$]$_{1-31.}$ While [*SPS*$^+$]$_{1-31}$ cells generated 10.9% red colonies when transformed with *p2HG*, and over expression of Hsp104 resulted in an appearance of red colonies of 19.2%. Therefore, these results demonstrate that like [*SWI*], [*SPS*$^+$]$_{1-32\ or}$ [*SPS*$^+$]$_{1-31}$ are not significantly sensitive to Hsp104 overexpression, which differs [*PSI*$^+$].

Next, the solubility of the Swi1$_{TRUNC}$MC fusion protein was assessed in both [*SPS*$^+$] and [*sps*$^-$] cells by centrifugation assay. While the Swi1$_{1-38}$MC, Swi1$_{1-32}$MC and Swi1$_{1-31}$MC were mostly in the soluble supernatant fraction in [*sps*$^-$] cells, they were mostly found in the insoluble protein fraction in [*SPS*$^+$] cells, suggesting a prion-mediated change in solubility of the fusion proteins (Fig 10F). Thus, these results demonstrate that Swi1$_{1-38}$MC, Swi1$_{1-32}$MC and Swi1$_{1-31}$MC can exist in two heritable conformational states associated with distinct phenotypes.

Materials and methods

Yeast strains and media.

All yeast strains used in this study were grown and maintained according to methods outlined in ((128, 130))). Strains were propagated in rich (yeast extract, peptone, dextrose [YPD]) or synthetic complete (SC) media. Media was supplemented with 5 mM guanidine hydrochloride (GdnHCl) or 5 fluoroorotic acid (5-FOA) when indicated. Glucose was used as the carbon source unless otherwise indicated. For the raffinose phenotype assay, glucose was replaced with raffinose and supplemented with 0.5 µg/ml antimycin (Sigma-Aldrich, St. Louis, MO). Plates were incubated at 30°C for three days unless otherwise indicated. Agar plates were made as outlined in (33) Lysogeny broth (LB) supplemented with 100 µg/ml ampicillin was used to select for plasmids with corresponding selection markers in *Eschericia coli*.

The BY4741 [SWI^+][pin^-], and BY4741 $swi1\Delta$/$p416TEFSwi1$ [SWI^+] were described previously (128). The W303 $sup35\Delta$/$SUP35:TRP1$/$p316Sup35FL$ [PSI^+] $MAT\alpha$ strain was obtained from the Weissman laboratory (UC San Francisco).

Plasmids and Oligonucleotides.

Table 3 lists primers used for this study, and Table 4 shows plasmids used in this study. The $pRS316$ vector plasmid and $pKT218,620$ expressing dominant negative Hsp104 (Hsp104^{DN}) were gifted from the Chernoff lab (Georgia Institute of Technology). $p2HG$ vector control and $p2HGHsp104$ were previously described in (23). Plasmids $p416TEFSwi1_{1-38}YFP$, $p415TEFSwi1_{1-38}YFP$, $p416TEFYFP$, $p415TEFYFP$, $p416TEFSwiNYFP$, $p415TEFSwiNYFP$, $p416TEFSwi1mCherry$ were previously described in (128). To construct plasmid $p416SWI1-NYFP$, the $SWI1$ promoter was cut from $p416SWI1-NQYFP$ (33) through SacI/SpeI and used to replace to the $TEF1$ promoter of $p416TEFSwiNYFP$ (33). Our previous study investigated the aggregation of Swi1$_{1-37}$YFP and Swi1$_{1-31}$YFP. Subsequent sequencing determined that Swi1$_{1-37}$YFP is actually Swi1$_{1-38}$YFP and Swi1$_{1-31}$YFP is Swi1$_{1-32}$YFP. Plasmid $p416TEFNQYFP$ was previously described in (33). All YFP-tagged Swi1 truncation mutants in the $p416TEF$ vector were constructed by amplifying the Swi1 fragment from genomic DNA using a common forward primer (p415Swi1ForwardNEW) and unique reverse primers (Age1Swi1-37Rev, Age1Swi1-36Rev, Age1Swi1-35Rev, Age1Swi1-34Rev, Age1Swi1-33Rev, Age1Swi1-31Rev, Age1Swi1-30Rev, Age1Swi1-29Rev, Age1Swi1-28Rev, Age1Swi1-27Rev, Age1Swi1-26Rev) that contained an AgeI site. Swi1$_{1-37}$ to Swi1$_{1-33}$ were amplified from $p415TEFSwi1_{1-38}YFP$ template. Swi1$_{1-31}$, Swi1$_{1-27}$ and Swi1$_{1-26}$ were amplified from $p415TEFSwi1_{1-33}YFP$ template. $Swi1_{1-30}YFP$, $Swi1_{1-29}YFP$, $Swi1_{1-28}YFP$ were amplified from $p415TEFSwi1_{1-31}YFP$ template. Amplified Swi1$_{1-38}$ to Swi1$_{1-33}$ fragments were digested with SpeI and AgeI, purified, and ligated via SpeI and AgeI sites into p416TEFSwi1$_{1-38}$YFP, replacing Swi1$_{1-38}$ with the smaller truncated version. Amplified Swi1$_{1-31}$ to Swi1$_{1-26}$ fragments were digested with SpeI and AgeI, purified, and ligated via SpeI and AgeI sites into p416TEFSwi1$_{1-37}$YFP, replacing Swi1$_{1-37}$ with smaller truncated version.

To make YFP-tagged Swi1 truncation mutants in the $p415TEF$ vector, the ~850 bp fragments containing YFP-tagged Swi1 truncation mutants were digested from $p416TEFSwi1_{Trunc}YFP$ described above using SpeI and XhoI and ligated into $p415TEFSwiNYFP$ *via* SpeI *and* XhoI sites, replacing YFP-

Table 3. Primers used in study of Swi1 PrD

Primer name	Primer Sequence	Resulting Plasmid
p415Swi1ForwardNEW	5' CACTTTATGCTTCCGGCTCCT 3'	Carboxy terminal truncations
Age1Swi1-37Rev	5' GCGACCGGTGGATCATTATTATTATTATTAGT 3'	$p416TEFSwi1_{1-37}YFP$
Age1Swi1-36Rev	5' GCGACCGGTGGATCATTATTATTATTAGTATT 3'	$p416TEFSwi1_{1-36}YFP$
Age1Swi1-35Rev	5' GCGACCGGTGGATCATTATTATTAGTATTATT 3'	$p416TEFSwi1_{1-35}YFP$
Age1Swi1-34Rev	5' GCGACCGGTGGATCATTATTAGTATTATTATT 3'	$p416TEFSwi1_{1-34}YFP$
Age1Swi1-33Rev	5' GCGACCGGTGGATCATTAGTATTATTATTAGT 3'	$p416TEFSwi1_{1-33}YFP$
Age1Swi1-31Rev	5' GGCGACCGGTGGATCATTATTATTATTAGT 3'	$p416TEFSwi1_{1-31}YFP$
Age1Swi1-30Rev	5' GGCGACCGGTGGATCATTATTATTAGT 3'	$p416TEFSwi1_{1-30}YFP$
Age1Swi1-29Rev	5' GGCGACCGGTGGATCATTATTAGTATT 3'	$p416TEFSwi1_{1-29}YFP$
Age1Swi1-28Rev	5' GGCGACCGGTGGATCATTAGTATTATT 3'	$p416TEFSwi1_{1-28}YFP$
Age1Swi1-27Rev	5' GACCGGTGGATCAGTATTATTGTTATT 3'	$p416TEFSwi1_{1-27}YFP$
Age1Swi1-26Rev	5' GACCGGTGGATCATTATTGTTATTGGT 3'	$p416TEFSwi1_{1-26}YFP$
p415TEFSwiFor 4X HT	5' AAGACGATAGTTACCGGATAAGGCGCA 3'	Swi1MC fusion proteins
Swi1-38 +Linker Rev	5' ACCACCACCAGGACCACCCGGATTATTATTATTATTAGT 3'	$p415TEFSwi1_{1-38}Sup35MC$
Swi1-32 +Linker Rev	5' ACCACCACCAGGACCACCCGTATTATTATTATTAGTATTATTGTT 3'	$p415TEFSwi1_{1-32}Sup35MC$
Swi1-31 +Linker Rev	5' ACCACCACCAGGACCACCATTATTATTATTAGTATTATTGTT 3'	$p415TEFSwi1_{1-31}Sup35MC$
Linker + Sup35MC For	5' GGTGGTCCTGGTGGTGGTATGTCTTTGAACGACTTT 3'	Swi1MC fusion proteins
XhoI + Sup35MC	5' GCCCTCGAGTTACTCGGCAATTTTAACAATTTTACCAAT 3'	Swi1MC fusion proteins
Swi1 RT For	5' TCTTCGCGCCAGAGTTAGG 3'	
Swi1 RT Rev	5' CCGAGTATTGCCAAGGAGTC 3'	

Table 4. Plasmids used in study of Swi1 PrD

Plasmid Name	Marker	Replicon	Promotor	Used For	Source
p415TEFSwiNYFP	*LEU2*	*CEN6/ARSH4*	*TEF1*	Expression of Swi1-NYFP	(78)
p415TEFYFP	*LEU2*	*CEN6/ARSH4*	*TEF1*	Expression of YFP	This study
p415TEFSwi1$_{1-38}$YFP	*LEU2*	*CEN6/ARSH4*	*TEF1*	Expression of Swi1$_{1-38}$YFP	(128)
p415TEFSwi1$_{1-37}$YFP	*LEU2*	*CEN6/ARSH4*	*TEF1*	Expression of Swi1$_{1-37}$YFP	This study
p415TEFSwi1$_{1-36}$YFP	*LEU2*	*CEN6/ARSH4*	*TEF1*	Expression of Swi1$_{1-36}$YFP	This study
p415TEFSwi1$_{1-35}$YFP	*LEU2*	*CEN6/ARSH4*	*TEF1*	Expression of Swi1$_{1-35}$YFP	This study
p415TEFSwi1$_{1-34}$YFP	*LEU2*	*CEN6/ARSH4*	*TEF1*	Expression of Swi1$_{1-34}$YFP	This study
p415TEFSwi1$_{1-33}$YFP	*LEU2*	*CEN6/ARSH4*	*TEF1*	Expression of Swi1$_{1-33}$YFP	This study
p415TEFSwi1$_{1-32}$YFP	*LEU2*	*CEN6/ARSH4*	*TEF1*	Expression of Swi1$_{1-32}$YFP	(128)
p415TEFSwi1$_{1-31}$YFP	*LEU2*	*CEN6/ARSH4*	*TEF1*	Expression of Swi1$_{1-31}$YFP	This study
p415TEFSwi1$_{1-30}$YFP	*LEU2*	*CEN6/ARSH4*	*TEF1*	Expression of Swi1$_{1-30}$YFP	This study
p415TEFSwi1$_{1-29}$YFP	*LEU2*	*CEN6/ARSH4*	*TEF1*	Expression of Swi1$_{1-29}$YFP	This study
p415TEFSwi1$_{1-28}$YFP	*LEU2*	*CEN6/ARSH4*	*TEF1*	Expression of Swi1$_{1-28}$YFP	This study
p415TEFSwi1$_{1-27}$YFP	*LEU2*	*CEN6/ARSH4*	*TEF1*	Expression of Swi1$_{1-27}$YFP	This study
p415TEFSwi1$_{1-26}$YFP	*LEU2*	*CEN6/ARSH4*	*TEF1*	Expression of Swi1$_{1-26}$YFP	This study
p416SWI1-NYFP	*URA3*	*CEN6/ARSH4*	*SWI1*	Expression of Swi1-NYFP	This study
p416TEFSwiNYFP	*URA3*	*CEN6/ARSH4*	*TEF1*	Expression of Swi1-NYFP	(23)
p416TEFYFP	*URA3*	*CEN6/ARSH4*	*TEF1*	Expression of YFP	Lindquist lab
p416TEFSwi1$_{1-38}$YFP	*URA3*	*CEN6/ARSH4*	*TEF1*	Expression of Swi1$_{1-38}$YFP	(128)
p416TEFSwi1$_{1-37}$YFP	*URA3*	*CEN6/ARSH4*	*TEF1*	Expression of Swi1$_{1-37}$YFP	This study
p416TEFSwi1$_{1-36}$YFP	*URA3*	*CEN6/ARSH4*	*TEF1*	Expression of Swi1$_{1-36}$YFP	This study
p416TEFSwi1$_{1-35}$YFP	*URA3*	*CEN6/ARSH4*	*TEF1*	Expression of Swi1$_{1-35}$YFP	This study
p416TEFSwi1$_{1-34}$YFP	*URA3*	*CEN6/ARSH4*	*TEF1*	Expression of Swi1$_{1-34}$YFP	This study
p416TEFSwi1$_{1-33}$YFP	*URA3*	*CEN6/ARSH4*	*TEF1*	Expression of Swi1$_{1-33}$YFP	This study
p416TEFSwi1$_{1-32}$YFP	*URA3*	*CEN6/ARSH4*	*TEF1*	Expression of Swi1$_{1-32}$YFP	(128)
p416TEFSwi1$_{1-31}$YFP	*URA3*	*CEN6/ARSH4*	*TEF1*	Expression of Swi1$_{1-31}$YFP	This study
p416TEFSwi1$_{1-30}$YFP	*URA3*	*CEN6/ARSH4*	*TEF1*	Expression of Swi1$_{1-30}$YFP	This study
p416TEFSwi1$_{1-29}$YFP	*URA3*	*CEN6/ARSH4*	*TEF1*	Expression of Swi1$_{1-29}$YFP	This study
p416TEFSwi1$_{1-28}$YFP	*URA3*	*CEN6/ARSH4*	*TEF1*	Expression of Swi1$_{1-28}$YFP	This study
p416TEFSwi1$_{1-27}$YFP	*URA3*	*CEN6/ARSH4*	*TEF1*	Expression of Swi1$_{1-27}$YFP	This study
p416TEFSwi1$_{1-26}$YFP	*URA3*	*CEN6/ARSH4*	*TEF1*	Expression of Swi1$_{1-26}$YFP	This study
p416TEFSwi1mCherry	*URA3*	*CEN6/ARSH4*	*TEF1*	Expression of Swi1mCherry	(128)
p416TEFSwi1	*URA3*	*CEN6/ARSH4*	*TEF1*	Expression of Swi1	(23)
p316Sup35FL	*URA3*	*CEN6/ARSH4*	*SUP35*	Expression of Sup35FL	Weissman Lab
p415TEFSwi1$_{1-38}$MC	*LEU2*	*CEN6/ARSH4*	*TEF1*	Expression of Swi1$_{1-38}$MC	This study
p415TEFSwi1$_{1-32}$MC	*LEU2*	*CEN6/ARSH4*	*TEF1*	Expression of Swi1$_{1-32}$MC	This study
p415TEFSwi1$_{1-31}$MC	*LEU2*	*CEN6/ARSH4*	*TEF1*	Expression of Swi1$_{1-31}$MC	This study
p306Sup35SwiNMC	*URA3*		*SUP35*	Cloning of MC truncation mutants	This study
pRS316	*URA3*	*CEN6/ARSH4*	*T7*	Vector control for Hsp104[DN]	Chernoff Lab
pKT218,60	*URA3*	*CEN6/ARSH4*	*T7*	Expression of Hsp104[DN]	Chernoff Lab
p2HG	*HIS3*	*2 micron*	*GPD*	Vector control for Hsp104 over-expression	(23)
p2HG-Hsp104	*HIS3*	*2 micron*	*GPD*	Hsp104 over-expression	(23)

tagged SwiN with the YFP-tagged truncation mutant. The plasmids of *p415TEFSwi1$_{1-38}$MC, p415TEFSwi1$_{1-32}$MC, and p415TEFSwi1$_{1-31}$MC,* were constructed using a multistep PCR. First, Swi1$_{1-38}$, Swi1$_{1-32}$, and Swi1$_{1-31}$ were amplified using a forward primer (p415TEFSwiFor 4X HT) that binds upstream of the Swi1 ORF in *p415TEFSwi1$_{1-38}$YFP, p415TEFSwi1$_{1-32}$YFP,* and *p415TEFSwi1$_{1-31}$YFP* and a reverse primer containing a sequence encoding a GGPGGG linker (Swi1-38 +Linker Rev, Swi1-32 +Linker Rev, or Swi1-31 +Linker Rev). Next, Sup35MC was amplified from *p306Sup35SwiN-MC* using a forward primer containing a sequence encoding a GGPGGG linker (Linker + Sup35MC Forward) and a reverse primer containing an *Xho*I site (XhoI + Sup35MC). Products of the Swi1$_{TRUNC}$+Linker and Linker+ Sup35MC PCRs were then used as templates for a third PCR using forward primer (*p415TEFSwiFor 4X HT*) and reverse primer (XhoI + Sup35MC). The amplified products were digested using *Spe*I and *Xho*I, purified, and ligated into *p415TEFSwi1$_{1-38}$YFP* through *Spe*I and *Xho*I sites, replacing *Swi1$_{1-38}$YFP* with *Swi1$_{1-38}$MC, Swi1$_{1-32}$MC, or Swi1$_{1-31}$MC.* The correct insertion and sequence for all constructs were verified by sequencing.

Yeast transformations. Yeast cells were transformed according to a protocol adapted from (128). Alternatively, colony transformations were also adapted from a protocol provided with the S.c Easy Comp Transformation Kit (Thermo Fisher Scientific, Waltham, MA). Briefly, colonies were resuspended in 100 µl of Solution I. Cells were then collected by centrifugation at 2500 rpm for 3 minutes. Cell pellet was then resuspended in 10 µl of Solution II. The transformation system was completed by addition of 2 µl plasmid DNA, and 140 µl of Solution III to the 10 µl cell/ Solution II mixture. Transformation system was then briefly vortexed and incubated at 42˚C for 30 minutes. Transformation system was then placed on ice for a minimum of 3 minutes followed by spreading 50 µl onto selective media. Additionally, a high efficiency transformation was used as described in (131) with the following changes: Transformation mixture was set up by resuspending the cell pellet in 240 µl of 50% PEG followed by addition of 36 µl 1M LiAc, 20 µl single-stranded salmon sperm DNA (10 mg/ml), 4 µl plasmid, and 60 µl water.

Microscopy. Microscope images were taken with a Zeiss Axiovert 200 epifluoresnce microscope. Samples were viewed with a 100X objective and filters specific for DIC, YFP, mCherry, CFP, or DAPI. Images were captured using Axiovision AC (Zeiss, Oberkochen, Germany)

Immunoblotting. Samples for immunoblots were prepared using a protocol adapted from (128). Briefly, cells were grown overnight culture in selective media. $Swi1_{Trunc}YFP$ samples were normalized to 7.5 x 10^7 cells/mL. $Swi1_{TRUNC}MC$ samples (for figure 10D), as well as NYFP samples (for figure 6E) were normalized to 2.5 x 10^7 cells/mL in water. Cells were treated with 0.1 M NaOH and incubated for 5 minutes at room temperature. Cell lysates resuspended in 100 µl - 200 µl 2x Laemmli buffer (2% SDS for $Swi1_{TRUNC}MC$ and NYFP and 4% SDS for $Swi1_{TRUNC}YFP$), boiled for 5-10 minutes, and sonicated in 10 x 1-sec pulses. The lysates were spun down at 13,000 rpm to pellet debris. 5 µl of lysates were loaded for all samples. $Swi1_{TRUNC}MC$ cell lysates were loaded onto a 7.5% Tris-glycine gel, $Swi1_{Trunc}YFP$ cell lysates were loaded onto a 4-20% gradient Tris-glycine gel (Bio-Rad, Hercules, CA), and NYFP samples were loaded onto 12% Tris-glycine gel. The gels were transferred into polyvinylidene difluoride (PVDF) membrane and blotted with either 1:2500 α-GFP antibody (JL-8 antibody; Clontech, Mountain View, CA), 1:2500 α-Sup35 antibody (Gifted from Liebman laboratory- University of Nevada, Reno) or 1:5000 α-actin antibody (Chemicon, Temecula, CA) and 1:2500 horse radish peroxidase conjugated rat anti-mouse secondary antibody. The resulting chemiluminescence was detected using ECL Western blotting reagents (Bio-Rad). Blots were imaged using a Bio-Rad Chemidoc Imaging System.

Plasmid shuffle. A *swi1Δ/p416TEFSwi1* [*SWI+*] strain was transformed with YFP-tagged truncation mutants, *p415TEFSwi1_{TRUNC}YFP*. Three individual colonies were grown in selective media overnight at 30˚C. The three *swi1Δ/p416TEFSwi1/p415TEFSwi1_{TRUNC}YFP* [*SWI+*] colonies were spread onto SC-Leu media supplemented with 5-FOA and incubated for 3 days at 30˚C. Colonies from 5-FOA plate were then examined for *p416TEFSwi1* loss. Subsequently, two individual *swi1Δ/p415TEFSwi1_{TRUNC}YFP* colonies were transformed with *p416TEFSwi1mCherry*. At least three individual colonies were imaged at each step of the plasmid shuffle. For smaller fragments, $Swi1_{1-32}$ through $Swi1_{1-26}$, the experiment was repeated with an additional selection step. Aggregation was assessed on SC -Leu+5-FOA plates and cells were subsequently streaked on SC-Leu plates.

Raffinose assay. Cells from colonies were resuspended in 1 mL of water and counted. All samples were equalized to 1 x 10^6 cells/mL. 200 µl of cell mixture was pipetted into the first well of a 96 well plate. 140 µl of water was pipetted into rows 2 to 6 of plate. 40 µl of cells from the first well were pipetted into the second

well and serially diluted. Cells were then spotted onto YPD and raffinose + 0.5 µg/ml antimycin plates and incubated for 3-5 days at 30˚C.

RT-PCR. Total RNA was isolated using RNeasy Mini Kit (Qiagen, Hilden, Germany). The Superscript III First Strand DNA Synthesis Kit (Invitrogen, Cambridge, MA) was used to synthesize cDNA according to manufacturer's protocol. One microliter of cDNA was used as template for amplification with primers specific for the C-terminal region of Swi1, Swi1 RT fwd and Swi1 RT rev. The PCR products were run on a 1.8% agarose gel with 100 bp DNA ladder (New England Biolabs, Ipswitch, MA).

Centrifugation Assay. Isogenic BY4741 [*SWI⁺*] and [*swi⁻*] cells of *swi1Δ/p415TEFSwi1₁₋₃₈YFP* or *swi1Δ/p415TEFSwi1₁₋₃₂YFP* background and isogenic [*SPS⁺*]₁₋₃₈, ₁₋₃₂, or ₁₋₃₁ and [*sps⁻*]₁₋₃₈, ₁₋₃₂, or ₁₋₃₁ *sup35Δ/p415TEFSwi1_TRUNC_MC/p416TEFSwi1_TRUNC_YFP* cells were incubated in selective media overnight at 30˚C. Overnight cultures were diluted and grown to log-phase at 30˚C. Cells were resuspended in 0.1 M Tris buffer (pH 8) + 100 mM EDTA and 0.5% beta-mercaptoethanol and incubated at 30˚C for 45 minutes. Cells were subsequently washed with ST buffer (10mM Tris pH 7.5, 1M Sorbitol) and then resuspended in ST buffer supplemented with 10 µl of lyticase (Sigma-Aldrich; 10 U/ µl) and incubated 30˚C for 30 minutes. After centrifugation at 2000 rpm for 5 minutes, cell pellets were resuspended in 50 mM Tris (pH 7.5) + 50 mM NaCl supplemented with protease inhibitors (Roche Complete Mini Tablet (Roche, Mannheim, Germany) + Leupeptin (20 µg/ml), Pepstatin (20 µg/ml) and PMSF (10 mM)). Cells were sonicated for 5 x 1-sec pulses and lysates were cleared of debris with centrifugation at 100 x g for 5 minutes. The cleared lysate was transferred to a clean tube, 1/3 of cleared lysate saved as total (T) samples and remaining samples were spun at 20,000 x g for 20 minutes at 4 ˚C. After centrifugation, supernatant fraction (S) was transferred to a new tube and pellet fraction (P) was resuspended into a volume equal to that of the pellet fraction of 50 mM Tris (pH 7.5) + 50 mM NaCl supplemented with protease inhibitors. Samples were mixed with 2x Laemmli sample buffer (4% SDS) and boiled for 10 minutes. Samples resolved by SDS-PAGE on a 4-20% Tris-glycine gradient gel for YFP-tagged Swi1 samples and a 10% Tris-glycine for Swi1₁₋₃₈MC, Swi1₁₋₃₂MC, and Swi1₁₋₃₁MC. The gels were transferred onto polyvinylidene difluoride (PVDF) membrane and blotted with 1:2500 α-GFP antibody (JL-8 antibody; Clontech) or 1:2500 α-Sup35 antibody (for [*SPS⁺*] and [*sps⁻*] cells) and 1:2500 horse radish peroxidase conjugated rat anti-mouse secondary antibody. The

resulting chemiluminescence was detected using ECL Western blotting reagents (Bio-rad). Blots were imaged using a Bio-Rad Chemidoc Imaging System.

Prion curability with Hsp104^{DN}. [*SWI$^+$*] cells of *swi1Δ/p415TEFSwiNYFP, swi1Δ/p415TEFSwi1$_{1-38}$YFP, swi1Δ/p415TEFSwi1$_{1-32}$YFP* backgrounds were transformed with independently with *pRS316* or *pKT218,620* using a high efficiency yeast transformation protocol. Plates were incubated for three days at 30˚C. Three colonies from each plate were inoculated into selective media and were grown at 30˚C for 2 days. Cells were then imaged and aggregation was quantified.

Prion curability by Hsp104 over expression. [*SPS$^+$*]$_{1-38}$, $_{1-32}$, or $_{1-31}$ cells were transformed with either *p2HG* or *p2HG-Hsp104* and plated on selective media. Individual transformants were grown on selective media for 24 hours and subsequently spread on YPD. Plates were incubated at 30˚C for 3 days followed by 3 days of incubation at 4 ˚C to allow for color change. The number of completely cured cells (red) non-cured colonies were quantified.

Transferability of PrD. W303 *sup35Δ/p316Sup35FL* [*PSI$^+$*] strain was transformed with *p415TEFSwi1$_{1-38}$MC, p415TEFSwi1$_{1-32}$MC* or *p415TEFSw1$_{1-31}$MC*. Cells were plated on selective media. Transformants were then replica plated onto YPD to assess color change. Individual red colonies, whose pigmentation is caused by efficient termination of a premature nonsense stop codon in *ade1-14* mutant allele (37), from YPD plate were spread on -Leu plates supplemented with 5-FOA to select for colonies that had lost *p316Sup35FL*. Colonies were then grown on complete media (YPD) and SC plates lacking adenine (-Ade). *sup35Δ/p415TEFSwi1$_{1-38}$MC, sup35Δ/p415TEFSwi1$_{1-32}$MC* or *sup35Δ/p415TEFSwi1$_{1-31}$MC* [*psi$^-$*][*sps$^-$*] cells with Ade$^-$ growth phenotype and red color on YPD were then transformed with *p416TEFSwi1$_{1-38}$YFP, p416TEFSwi1$_{1-32}$YFP* or *p416TEFSwi1$_{1-31}$YFP*, respectively, and plated on selective media. Transformants were either replica plated into -Ade or colonies were spread onto -Ade media to select for Ade$^+$ cells. Ade$^+$ cells were then grown on YPD, YPD + 5mm GdnHCl, and SC-Ade plates. Colonies that were white on YPD, red on YPD after GdnHCl treatment, and showed a curable Ade$^+$ growth phenotype were considered [*SPS$^+$*] candidates. Aggregation status of Swi1$_{TRUNC}$YFP was assessed by fluorescence microscopy to further confirm presence or absence of [*SPS$^+$*]. Incubation of plates was done at 30 ˚C for three days for all steps. For color development, plates were incubated at 30˚C for 3 days followed by incubation at 4˚C for 3 days.

In order to determine the rate of reappearance of Ade$^+$ colonies of GdnHCl cured cells, [*sps*$^-$] cells were grown in selective media for 24 hours an equal number of cells were subsequently plated on SC-ura-leu medium as well as SC-ade and grown for 3 to 5 days. The number of Ade$^+$ colonies as well as the total number of cells plated were quantified.

CHAPTER THREE

Using Yeast for the Discovery of Chemical Probes for Prion Biology Research and Therapeutics for

Protein Misfolding-Based Diseases

Introduction

Prions are proteinaceous infectious particles responsible for a class of fatal mammalian neurodegenerative disorders known as transmissible spongiform encephalopathies (TSEs) (1, 132). TSEs are caused by conformational changes of a host protein called prion protein (PrP^C) whose pathogenic conformers (PrP^{Sc}) form protease-resistant amyloid inclusions in the central nerve system (CNS) (132). How PrP^C undergoes a conformational switch to PrP^{Sc} is not well understood, however, it is known that once PrP^{Sc} appears in a system, it can recruit and convert soluble PrP^C into the largely insoluble, β-sheet rich PrP^{Sc} conformers (132, 133). Recent research suggests that the general self-perpetuating aggregation seen in prion disease can be observed in other neurodegenerative disease-related proteins, including amyloid- beta (Aβ), α-synuclein, TAR DNA-binding protein 43 (TDP-43), and Fused in Sarcoma (FUS) (134-137). The prion-like propagation of various proteins indicates that the development of therapeutics for TSEs may also be beneficial in the treatment of other prion-like disorders.

Despite decades of research seeking to find treatment for the prion diseases, effective treatment for these neurodegenerative diseases is still lacking. Several difficulties have been encountered when searching for effective therapeutic approaches. First, the exact mechanisms underlying PrP misfolding and toxicity are still unclear, therefore finding defined targets has been challenging. Several approaches have included investigation of compounds that stabilize PrP^C, block PrP^C/PrP^{Sc} conversion, or increase degradation of PrP^{Sc}. Moreover, it is also possible that anti-prion compounds may affect non-PrP targets (138). Second, in order to be effective in the CNS, compounds must be able to cross the blood brain barrier. Unfortunately, a high number of small molecules do not cross the blood brain barrier, resulting in poor brain exposure and ultimately poor performance of these compounds in the clinical development process (139, 140). In addition to target-based approaches, phenotypic screenings, in which investigators start with a disease-relevant phenotype and screen for molecules that modulate that phenotype, have been performed.

One strong advantage of phenotypic approaches is that compounds discovered through this approach may have effects on multiple proteins or pathways, therefore elucidating multi-target mechanisms of action or new, unknown molecular targets.

Several systems have been used to investigate anti-prion compounds – including animal models, cell culture models, cell-free *in vitro* conversion assays, *in silico* strategies, and immunotherapeutic approaches (138, 141-145). While these animal models and cell-based models certainly have advantages – such as being able to work with the disease-relevant infectious protein and observe disease-relevant clinical pathology, they are often expensive, labor intensive, time consuming, and may not be readily amenable to high-throughput screening approaches (145). *In vitro* assays which aim to find compounds that inhibit accumulation of PrP^{Sc} are useful, however, such strategies may not elucidate compounds with non-PrP targets. Thus, despite intense search over the past few decades for anti-prion compounds using these models, no compounds that alter disease progression in human clinical trials have been discovered, suggesting the need for new screening strategies.

Bach et al. used a novel yeast-based approached to screen for anti-prion compounds (146). A growing number of prion proteins have been identified in the budding yeast *S. cerevisiae*, including [*SWI*+] (16, 17, 23). Like PrP, yeast prion proteins misfold into infectious conformers, resulting in the accumulation of β-sheet rich amyloid deposits. Furthermore, like PrP, which can exist in multiple distinct conformations (or strains) of PrP^{Sc}, some yeast prions have been demonstrated to have manifold variants that are stably transmitted by multiple, distinct protein conformations (16, 17, 51, 147). The similarities between the mammalian prion, PrP^{Sc}, and yeast prions and the genetic tractability of yeast, make it an ideal candidate for the examination of prion biology. Bach et al.'s screening system utilized the prion [*PSI*+]. As mentioned in the main introduction, the prion state of Sup35, the protein determinant of [*PSI*+], can be easily assessed in a strain containing the *ade1-14* allele with a premature stop codon in the ORF of *ADE1* (37). This strain allows for visualization of the prion state by assessment of colony color - prion cells are white and non-prion cells are red, therefore, white to red color change after treatment with compounds would be indicative of prion loss.

Bach et al. chose a strong [*PSI*+] strain which would allow for easier detection of prion status, due to the increased contrast in coloration of prion and non-prions cells. To increase permeability of the yeast cells, the *ERG6* gene was replaced with the *TRP1* auxotrophic marker. Deletion of the *ERG6* gene, which encodes an enzyme involved in ergosterol metabolism, results altered lipid composition and in the increased permeability of this strain - [*PSI*+]^S (STRg6) - from the 74-D694 background. In order to screen a chemically diverse library of 2,500 compounds, aliquots overnight cultures of [*PSI*+]^S (STRg6) were spread on petri dishes containing YPD agar medium supplemented with 200 µl GdnHCl, a sub-effective dose which increased the sensitivity of their screening method. Small filters were placed on the agar surfaces and individual compounds were applied to each filter (Fig 11). Cells were then incubated for 6 days to allow for cell growth and color change. Using this screening system, Bach et al. found 6 active compounds, including phenanthridine, which were active against the yeast prions [*PSI*+] (146). Several derivatives of phenanthridine, 6AP, 6A-8CP, and 6A-8tFP, were found to be more effective than all other molecules initially examined.

To examine whether the compounds that were active against [*PSI*+] were also active against another yeast prion, [URE3], Bach et al. used a reporter analogous to the [*PSI*+] reporter previously described. To this end, Bach et al. deleted the *ERG6* gene from a strain in which the *DAL5* gene was replaced with the *ADE2* gene so the *ADE2* gene was under the control of the *DAL5* promoter (146). In its soluble form Ure2 represses transcription at the *DAL5* promoter by binding transcription factors and inhibiting their translocation to the nucleus. Therefore, in this reporter strain, repression of the *DAL5* promoter results in a lack of adenine synthesis and red color. Conversely, [URE3] cells contain aggregated Ure2 and thus have no repression of transcription at the *DAL5* promoter. Therefore, [URE3] cells synthesize adenine and have white colony color when plated on YPD. As in the [*PSI*+] reporter system, conversion from white to red colony color is indicative of prion loss. Phenanthridine, 6AP, 6A-8CP, 6A-8tFP were all found to be active against [URE3]. Two compounds from the [*PSI*+]-based assay, KP1 and 6AP were found to induce a significant decrease in the accumulation of PrP^{Sc}. Bach et al. also treated yeast prion cells with compounds known to be active in the mammalian system. Interestingly, several examined compounds were
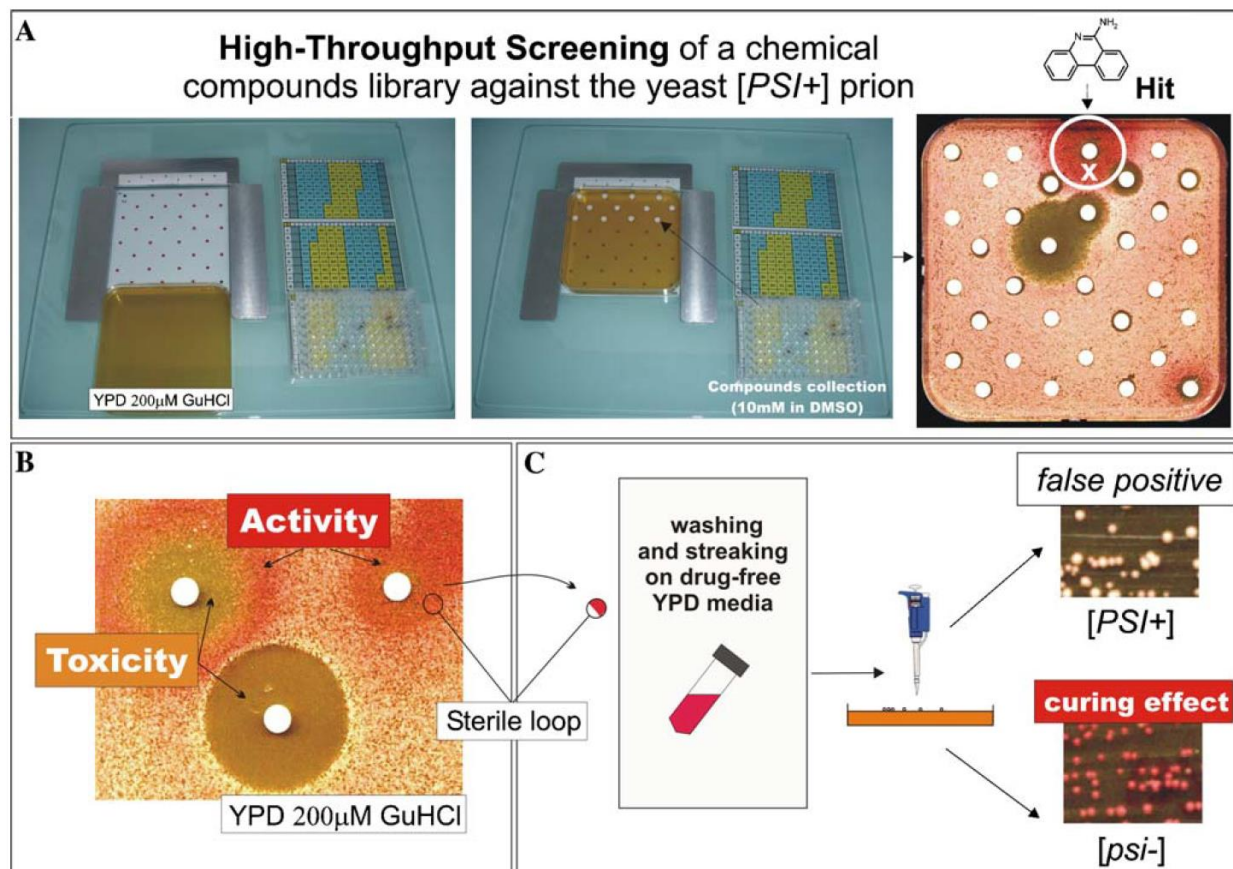
Figure 11. [*PSI*⁺]-based reporter system for screening for anti-prion compounds. [*PSI*⁺] cells were spread onto YPD plates and individual filters were placed on agar surface. Individual compounds, as well as controls, DMSO (- ; top left filter)) and GdnHCl (+ ; bottom right filter) were manually pipetted onto filters. Plates were incubated for three days at 25 °C, followed by 1–3 days at 4 °C. To eliminate false positives, red cells were grown in drug-free liquid media and subsequently plated on YPD. If cells were white, this would be indicative of false-positives that interfered with colorimetric reporter system. If cells were red, this would be indicative of curing effect by compound. Figure adapted from Tribouillard *et al. Biotechnol* (2006).

also effective in the [*PSI+*] based assay, further validating yeast-based assays as an effective screening strategy for the isolation of anti-mammalian prion compounds.

[*SWI+*]-based Reporter System

While the [*PSI+*]-based screening assay proved to be a useful method for the isolation of compounds that are effective against the mammalian prion, it required manual administration of individual compounds and at least 7 days are required to obtain hits. Therefore, Dr. Zhiqiang Du (Z.D.), an assistant research in our laboratory, made a novel reporter system that can faithfully report the prion status of Swi1 and allow for the automated screening of compound libraries in a high-throughput fashion. To this end, several steps of engineering were performed on the BY4741 strain: 1) the *FLO8* gene was restored, which allowed for filamentous growth, by integrating a wild-type copy of FLO8 at the *flo8* locus with a *HIS3* marker; 2) the *FLO1 ORF* was replaced with the *URA3 ORF*; 3) [*SWI+*] was transferred into the strain; and 4) the *ERG6* gene was disrupted by replacement with the *LEU2* coding sequence, which has been shown to result in increased cell permeability as noted earlier. The resulting strain – [*SWI+*]/*erg6Δ*::*LEU2/FLO1pr-URA3/FLO8-HIS3*, has *URA3* under the control of the *FLO1* promoter. Given the tight regulation of *FLO1* by [*SWI+*], we are able to distinguish between prion and non-prion cells using the *FLO1pr-URA3* reporter system. Specifically, when the cells are [*swi-*], Swi1 is in its soluble form and is therefore able to activate transcription at the *FLO1* promoter, a known target of the SWI/SNF chromatin remodeling complex. Therefore, [*swi-*] cells can grow on media lacking uracil, but are not able to grow on media containing 5-FOA (Fig 12). Conversely, [*SWI+*] cells, which contain aggregated and non-functional Swi1, do not have activation of the *FLO1* promoter and no uracil synthesis. Therefore, [*SWI+*] cells are unable to grow on media lacking uracil and able to grow on media containing 5-FOA. This screening system thus allows for us to select for or against [*SWI+*] and provides with a novel platform for searching for anti-prion compounds in a high-throughput fashion.

Results

Screening for Anti-[*SWI+*] Compounds Using the FLO1pr-URA3 Reporter System
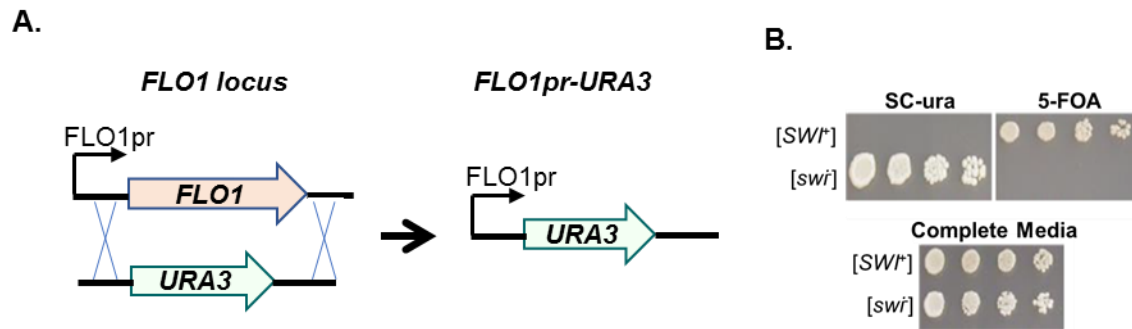
A.

B.

Figure 12. Gene replacement of *FLO1*. A. Reporter system for drug screening was created by replacing the *FLO1* ORF with the *URA3* open reading frame resulting in a stain in which *URA3* is under the control of the *FLO1* promoter. B. The SWI/SNF complex is required for expression of the *FLO1* gene, Therefore, [*SWI⁺*] cells, which have inactivation of the *FLO1* promoter, have no uracil synthesis and are unable to grow in media lacking uracil. [*SWI⁺*] cells are able to grow in media containing 5-FOA, which is toxic in cells that synthesize uracil. Conversely, [*swi*] are able to grow on media lacking uracil and are unable to grow on media supplemented with 5-FOA. Figure adapted from Du *et al., Cell Reports* (2015).

To establish the suitability of our reporter system for high-throughput screening, cells were first treated with 5 mM GdnHCl (positive control) and 2% DMSO (negative control) for 24 hours. Cells were subsequently transferred into medium lacking uracil followed by measurement of cell growth (A_{600}). The Z' $\left(Z' = 1 - \frac{3(\sigma_p + \sigma_n)}{|\mu_p - \mu_n|}\right)$, a measure of statistical effect size, for the high-throughput screens was determined to be 0.68, suggesting that our reporter system was indeed suitable for high-throughput screening (Fig 13)

Next, the *FLO1pr-URA3* reporter system was used to perform high-throughput screening of several compound libraries (done by Z.D.). First, high-throughput screens of four libraries (Table 5), which contain approximately ~12,500 compounds, were performed in a completely automated manner (Fig 14A). 84 hits were obtained with an assay Z' of 0.61 to 0.64 (Table 5). Interestingly, two of the hits from the NIH Clinical Collection were tacrine and amiridine, two compounds that were previously used for the treatment of Alzheimer's disease (Fig 15).

To confirm that the compounds that obtained from the initial screening were in fact positive, the 84 hit compounds were cherry picked and a confirmatory screen was performed. 37 of the 84 compounds were found to be effective at eliminating or inhibiting [*SWI*$^+$] (Supplemental table 1). Next, six of our hit compounds, which were both commercially available and economical, were purchased (Table 6). The ability of these compounds to inhibit or eliminate [*SWI*$^+$] was examined by treating [*SWI*$^+$]/*erg6Δ::LEU2/FLO1pr-URA3/FLO8-HIS3* cells with compounds at concentrations ranging from 0 µM to 1000 µM (Table 6 and Fig 16). As expected, treatment with DMSO, the negative control for the assay, did not result in elimination of [*SWI*$^+$]. Two compounds, nimustine and quinacrine, did not eliminate [*SWI*$^+$] at the concentrations examined, therefore, these compounds were not included in future studies. Tacrine and aminacrine, compounds previously found to eliminate [*PSI*$^+$] and previously examined for their ability to eliminate PrP^{Sc}, were found to be effective against [*SWI*$^+$] at the lowest concentration examined, 1 µM. Two other compounds, phloretin and pilocarpine, were found to be effective against [*SWI*$^+$] at a range of concentrations (Fig 16).

Given the effectiveness of phloretin and pilocarpine against [*SWI*$^+$] and the fact that these compounds have not, to our knowledge, been examined against other yeast prions or PrP, more in-depth
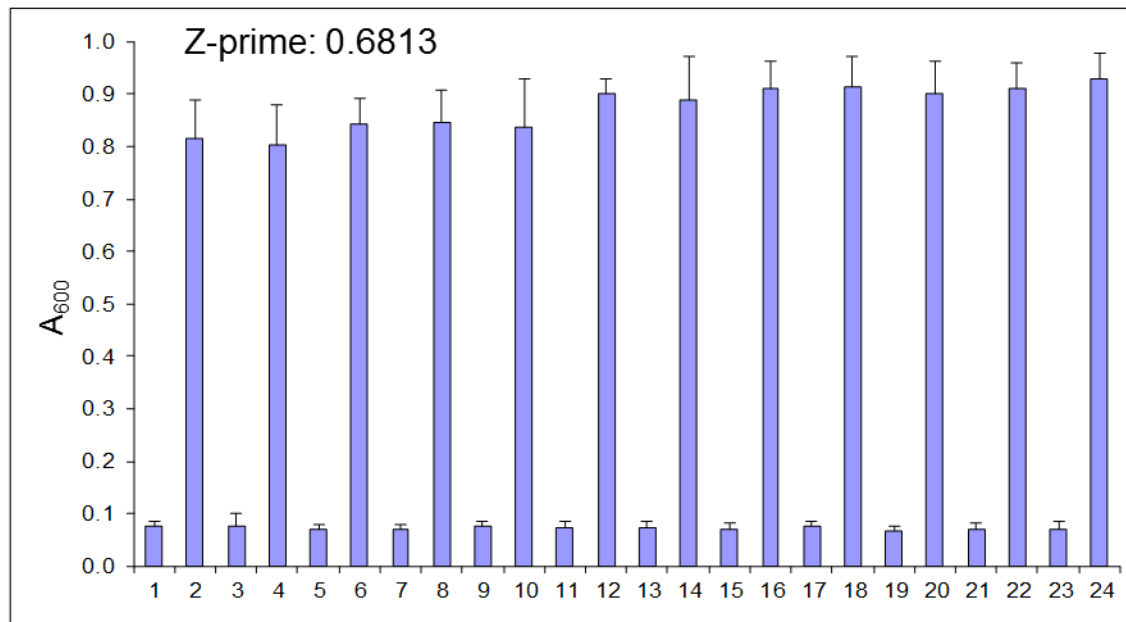
Figure 13. Measuring assay quality. Z' test. [*SWI⁺*]/*erg6Δ::LEU2*/*FLO1pr-URA3/FLO8-HIS3* were treated with 2% DMSO (odd numbered well), or 5 mM GdnHCl (even numbered wells) overnight. Cells were subsequently pinned into media lacking uracil, followed by reading at A_{600}. Z' value determined to be 0.6813. Performed by Zhiqiang Du (Z.D).

Table 5. Hits generated from anti-[*SWI*+] compound screen

Library	# of hits
NCC (~480 compounds)	2
Spectrum (~2000 compounds)	10
NCI/DTP (>3200 compounds)	20
ASDI (~6800 compounds)	52
Total	84
Z': 0.61-0.64	

Figure 14A Protocol for screening for anti-[*SWI*⁺] compound at NU-HTA :

1. Transfer compound (0.5 mM or 0.1 mM, as indicated), 5 mM GdnHCl (positive control), or 1% DMSO (negative control) into a 384-well plate
2. Dilute prion cells from 2.5×10^7 cells/ml stock 1000 fold into curing medium (SC-his, supplemented with 0.2 mM GdnHCl).
3. Add 50 µL of cell-containing curing medium to each well with multi-drop system.
4. Seal plates and grow for 24 h or 48 h at 30 ˚C with shaking.
5. Pin cells into 50 µL media lacking uracil (SC-his-ura), seal plates and grow for 24 h with shaking while measuring cell growth (A_{600}).

Figure 14B Protocol for confirmation of anti-prion activity in Li Laboratory:

1. Transfer compounds (at various concentrations), 5 mM GdnHCl (positive control), or DMSO or water (negative control) into a 96-well plate
2. Dilute prion cells from 5×10^7 cells/ml stock 1000 fold into curing medium (SC-his, supplemented with 0.2 mM GdnHCl).
3. Add 100 µL of cell-containing curing medium to each well.
4. Seal plates and grow for 24 h at 30 ˚C with shaking.
5. Transfer 3 µL cells into media lacking uracil (SC-his-leu-ura), seal plates and grow for 24 h with shaking while measuring cell growth (A_{600}.)
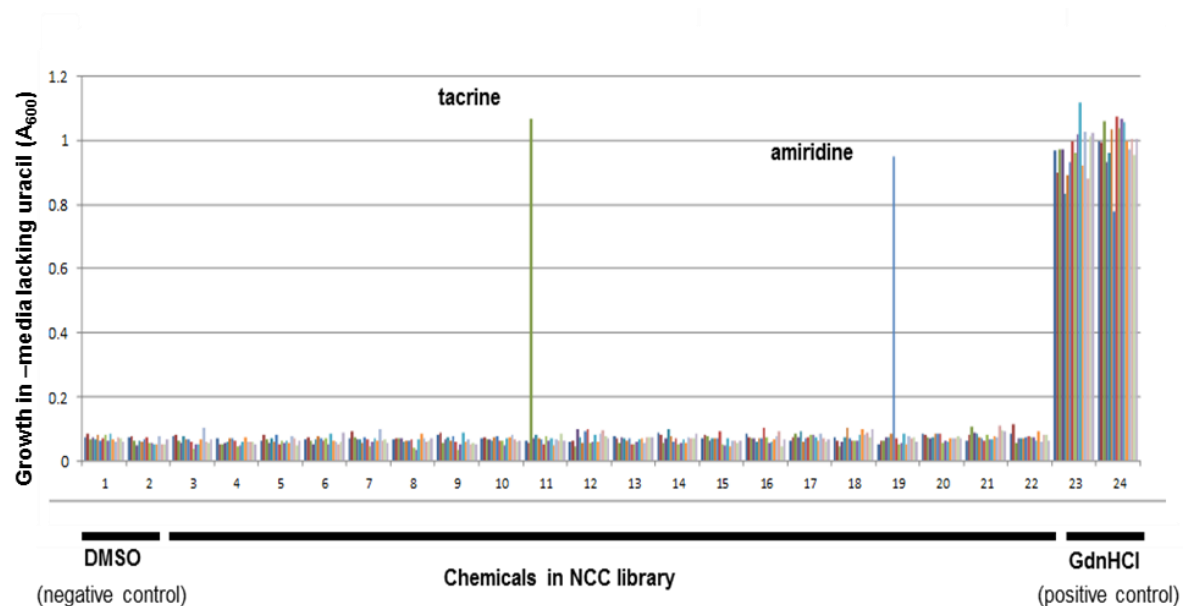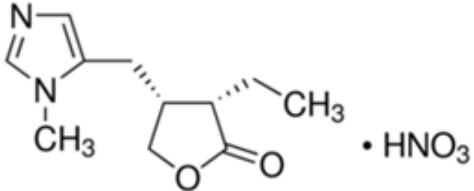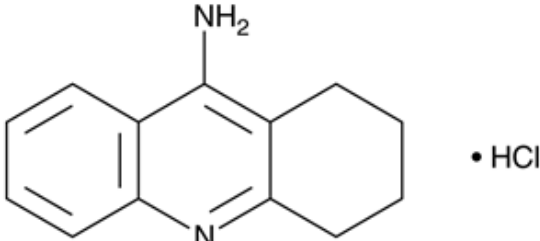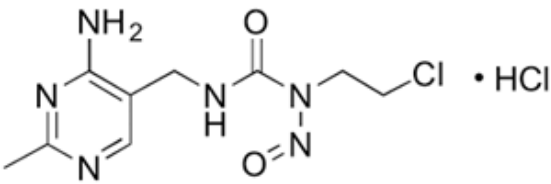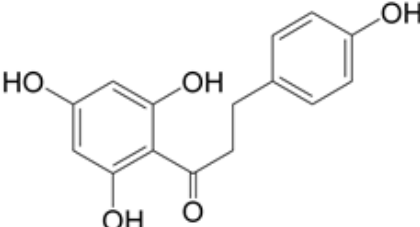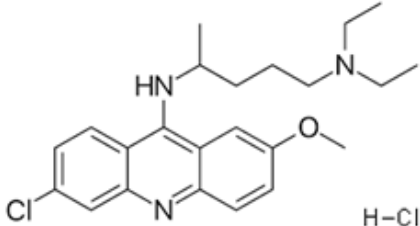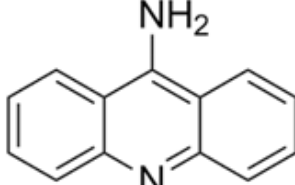
Figure 15. Results from screening of NIH Clinical Collection (NCC) Library. Results show lack of growth of DMSO treated wells, while GdnHCl treated cells resulted in growth in media lacking uracil. Two hits were obtained from our pilot screen of the NCC library, tacrine and amiridine. Performed by Z.D.

Table 6. Anti-prion compounds examined in the Li laboratory from pilot screen

Name	Structure
Pilocarpine Nitrate	• HNO₃
Tacrine Hydrochloride	• HCl
Nimustine Hydrochloride	• HCl
Phloretin	
Quinacrine Hydrochloride	
Aminacrine	
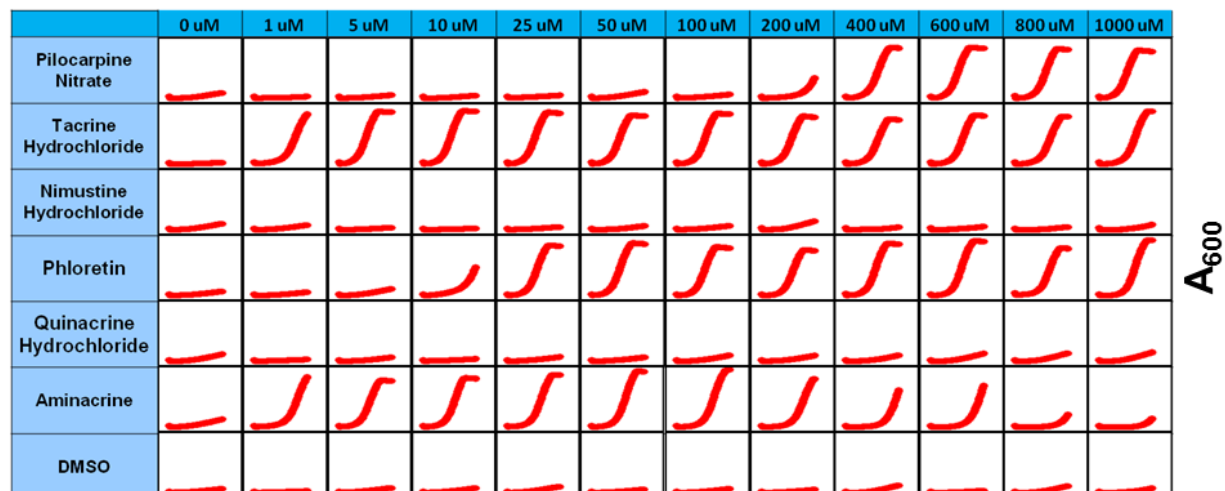
Figure 16. Confirmation of prion curing of compounds purchased in Li lab. 6 compounds were purchased for further examination in the Li laboratory. [*SWI*⁺] cells were treated with 6 compounds at concentrations ranging from 0 to 1000 µM for 24 hours. Cells were transferred into testing medium (SC-HLU) and growth was assessed (A_{600}). Cells growth, indicative of prion loss, was observed for 4 of the 6 compounds examined. Treatment with DMSO, our negative control, did not result in prion elimination.

analysis of these two compounds was performed in subsequent studies. Initial experiments demonstrated that phloretin eliminated [*SWI*] at low concentrations (below 5 µM), while pilocarpine required higher concentrations (>80 µM). Therefore, the effectiveness of the compounds at 0-5 µM and 0-400 µM for phloretin and pilocarpine, respectively, was examined. Cells were treated with indicated concentrations of compounds, as well as GdnHCl and DMSO, and cell growth was subsequently examined (A_{600}). As expected, no elimination of [*SWI*] was observed for our negative control, DMSO, while elimination was observed for cells treated with 5 mM GdnHCl. Approximately 50% of the [*SWI*] cells were cured when treated with ~2.5 µM for phloretin and ~300 µM for pilocarpine (Fig 17A and Table 8).

Secondary Assays Confirm Loss of [*SWI*]

Next, we wanted to confirm that the conversion from Ura$^-$ to Ura$^+$ in compound-treated cells was due to a loss of [*SWI*] and not due to mutations or interference with our reporter system. Therefore, confirmatory secondary assays were performed assessing the raffinose phenotype of cells after treatment with phloretin and pilocarpine (Fig 17B). As expected, cells treated with DMSO showed a phenotype of poor growth on raffinose media (Raf$^\pm$), suggesting that these cells are still [*SWI*]. Also in line with our previous report was the conversion of cells from Raf$^\pm$ to Raf$^+$ after treatment with 5 mM GdnHCl, which is indicative of prion loss. Cells treated with phloretin showed growth similar to that of [*swi*] cells (Raf$^+$), suggesting that the conversion from Ura$^-$ to Ura$^+$ was, in fact, due to [*SWI*] loss. Next, the aggregation status of Swi1 after treatment with our controls, DMSO and GdnHCl or with our compounds was examined (Fig 17C). To this end, [*SWI*] cells were transformed with Swi1-NQ-YFP driven by a galactose-inducible promoter. Cells were treated with our hit compounds or controls for 24 hours and subsequently spread on media lacking uracil. Expression of Swi1-NQ-YFP was induced with 2% galactose and aggregation of NQ-YFP was assessed by fluorescence microscopy. Prior to treatment, NQ-YFP was aggregated and formed distinct foci in [*SWI*] cells. Conversely, NQ-YFP was diffuse in [*swi*] cells. After treatment with 1.33% DMSO, NQ-YFP was found to be aggregated, demonstrating that DMSO itself did not alter the aggregation status of Swi1. Treatment with 1 mM pilocarpine, however, resulted in the loss of aggregation of Swi1. Combined, our
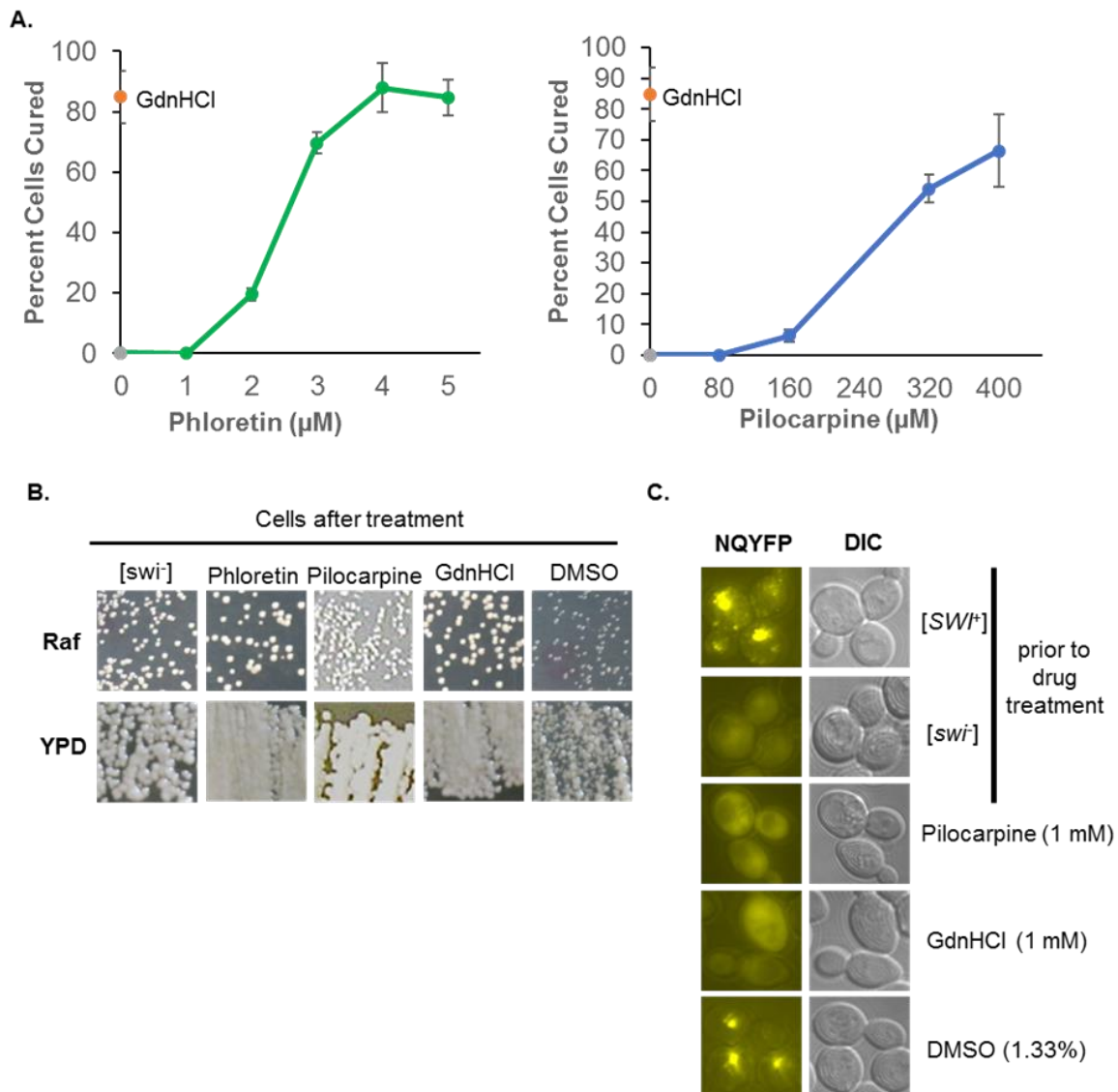
Figure 17. Assessing effectiveness of [*SWI*⁺] curing. A. [*SWI*⁺] cells were treated with phloretin (left) and pilocarpine (right) in triplicate at a range of concentrations. After 24 hours cells were spread onto SC-His and media lacking uracil (SC-HLU) media. Plates were incubated for 3 days and number of colonies were quantified. Dose response curves show percent of colonies observed on SC-HLU ([*swi*]) as a percent of total colonies numbers spread on SC-His. Error bars represent standard error. No curing observed for cells treated with DMSO (●), while curing is observed for cells treated with 5 mM GdnHCl (●). B. Ura⁺ isolates of [*SWI*⁺]/*erg6Δ::LEU2/FLO1pr-URA3/FLO8-HIS3* cells were reexamined for their growth on media containing raffinose as sole carbon source and YPD plates after treatment with the indicated hits or control chemicals (GdnHCl and DMSO as controls) to confirm effective curing of [*SWI*⁺]. C. In a second confirmatory assay, [*SWI*⁺] cells were transformed with a Swi1-NQYFP (driven by *GAL1* promoter) plasmid and aggregation of Ura⁺ isolates was examined after treatment with indicated hits and controls. Swi1 NQ-YFP aggregation was assessed by microscopy after 4 h induction with 2% galactose. Examination of raffinose phenotype was performed by S.V and Z.D. Assessment of aggregation was performed by Z.D.

results demonstrate that treatment with either phloretin or pilocarpine results in loss of [*SWI*] (Fig 17A, 17B and 17C).

Screening Chembrige DIVERset-CL library

Our first screen yielded hits that were previously shown to eliminate both yeast prions and/or PrP^{Sc}, suggesting our reporter system and screening strategy was ideal for searching for anti-prion compounds in a high-throughput manner. Therefore, another ~ 4,800 compounds from the Chembridge DIVERset-CL library were screened at a concentration of 100 μM. Thirty-one hits were obtained and 11 were shown to eliminate [*SWI*] upon re-examination in a cherry-picking experiment (Supplemental table 2). 6 of the most effective compounds (had the highest growth as compared to the GdnHCl control) were purchased (Table 7) and further examined their anti-prion properties. A preliminary experiment was performed to determine the effectiveness of [*SWI*] curing by compound 7-12 at 500 μM. While compounds 7-11 were found to effectively cure [*SWI*] at this concentration (>50% curing), treatment with 500 μM of compound 12 resulted in only ~50% curing of [*SWI*]. Next, [*SWI*] cells were treated with compounds 7-11 at concentrations ranging from 0-500 μM and with compound 12 at concentrations ranging from 0-1000 μM. All compounds were effective at eliminating [*SWI*], with 50% of cells being cured by all compounds at concentrations ranging from 100-250 μM (Fig 18A and Table 8).

Secondary Assays Confirm Loss of [*SWI*] Cells Treated with Chembridge DIVERset Compounds

Next, secondary assays were performed to confirm loss of [*SWI*] in cells treated with *Chembridge DIVERset* compounds. Cells were streaked onto raffinose media after treatment with either compounds 7-12, DMSO, or 5 mM GdnHCl (Fig 18B). As expected, cells treated with DMSO showed Raf$^{\pm}$ phenotype, suggesting that these cells were not cured by DMSO treatment. Conversely, treatment with 5 mM GdnHCl resulted in the conversion of cells from Raf$^{\pm}$ to Raf^{+}, demonstrating prion loss. Similarly, cells treated with compounds 7-12 had a Raf^{+} phenotype, suggesting that the conversion from Ura^{-} to Ura^{+} was, in fact, due to [*SWI*] loss.

Examination of Effectiveness of Phloretin and Pilocarpine on Other Yeast Prions

Table 7. Chembrige DIVERset-CL anti-prion compounds examined in the Li laboratory

Compound	Name	Structure
Compound 7	N-(2-isobutoxybenzyl)-N-methylisonicotinamide	
Compound 8	N~4~,N~4~,5-trimethyl-N~2~-(3-pyridin-4-ylpropyl)pyrimidine-2,4-diamine	
Compound 9	N-methyl-3-(1-methyl-1H-pyrrol-2-yl)-N-[(3-pyridin-4-ylisoxazol-5-yl)methyl]-1H-pyrazole-5-carboxamide	
Compound 10	4-[2-(trifluoromethyl)morpholin-4-yl]thieno[3,2-d]pyrimidine	
Compound 11	3-isopropyl-N,1-dimethyl-N-[(3-pyridin-4-ylisoxazol-5-yl)methyl]-1H-pyrazole-5-carboxamide	
Compound 12	5-{[[4-(2,6-dimethylpyridin-3-yl)pyrimidin-2-yl](methyl)amino]methyl}-2-methoxyphenol	

A.
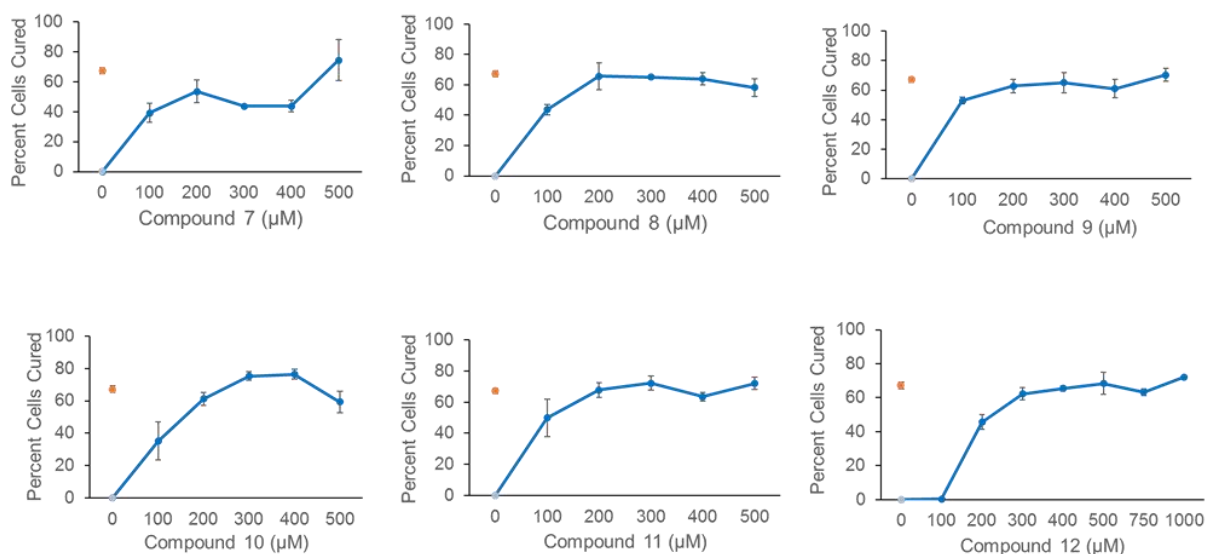
B.
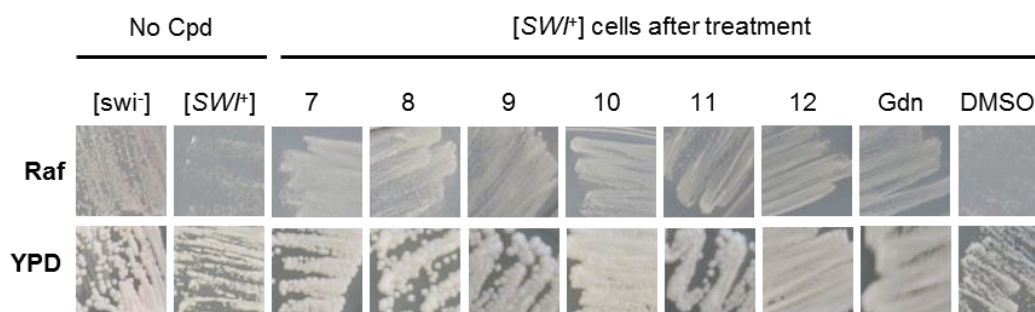
Figure 18. Assessing effectiveness of [*SWI+*] curing of hits from ChemBridge DIVERset-CL library. A. [*SWI+*] cells were treated with individual compounds in triplicate at a range of concentrations. After 24 hours cells were spread onto SC-His and SC-HLU media. Plates were incubated for 3 days and number of colonies were quantified. Dose response curves show percent of colonies observed on SC-HLU ([*swi-*]) as a percent of total colonies numbers spread on SC-His. Error bars represent standard error. No curing observed for cells treated with DMSO (⬤), while curing is observed for cells treated with 5 mM GdnHCl (⬤). B. Ura+ isolates of [*SWI+*]/*erg6Δ::LEU2/FLO1pr-URA3/FLO8-HIS3* cells were reexamined for their growth on media containing raffinose as sole carbon source and YPD plates after treatment with the indicated compounds or control chemicals (GdnHCl and DMSO as controls) to confirm effective curing of [*SWI+*].

Next, the ability of the hit compounds to eliminate other well-studied yeast prions including [*PSI*+], [URE3], and [*MOT3*+] was examined. Previous studies have shown that different prions have distinct sensitivities to various chaperones and therefore, their maintenance relies on distinct cellular networks. Therefore, examination of the effects of anti-[*SWI*+] compounds on other yeast prions may give us insight into their mechanisms of action. Additionally, examination into the anti-prion effects of distinct compounds may allow us to uncover previously unknown cellular components important for prion formation, maintenance, or propagation.

[*PSI*+]

To examine the ability of anti-[*SWI*+] compounds to eliminate [*PSI*+], two 74-D694 variants containing the *ade1-14* allele with a premature stop codon in the ORF of *ADE1*, [*PSI*+]^W and [*PSI*+]^S, were treated with phloretin and pilocarpine for 24 hours at multiple concentrations (Fig 19 and Fig 20). After treatment with the compounds, cells were plated on YPD and color change was assessed. Treatment with phloretin resulted in no appearance of red colonies, suggesting that there was no prion curing at a range of concentrations examined (Fig 19B). Prion curing was observed, however, when either strain is treated with pilocarpine at concentrations as low as 0.1 mM (Fig 20A and 20B). As expected, GdnHCl treatment resulted in [*PSI*+] curing, while treatment with DMSO did not result in prion curing. Restreaking of the red, cured cells resulted in the growth of red colonies, suggesting that cells were effectively cured by pilocarpine at all concentrations examined (Fig 20C).

Next, three [*PSI*+] variants ([*PSI*+]^W, [*PSI*+]$^M,$ and [*PSI*+]^S) with were treated with compounds 7-12 (Fig 23). These compounds at 0.5 mM in order to get an initial verification of their effectiveness on other non-[*SWI*+] yeast prions. Compound 7 was eliminated from further studies due to lack of prion curing. [*PSI*+]^W, [*PSI*+]^M, and [*PSI*+]^S cells were treated with the Chembridge compounds for 48 hours and subsequently plated on YPD. While four compounds, 8, 9, 10, and 12 were minimally or ineffective at eliminating [*PSI*+] at .5mM, compound 11 resulted in almost complete curing of [*PSI*+] in all three variants examined.

[URE3]

A.
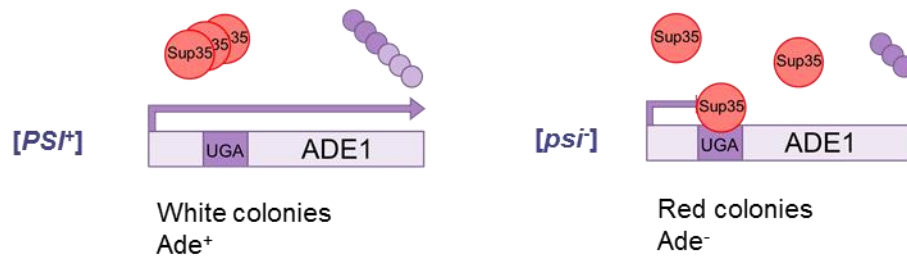
B.
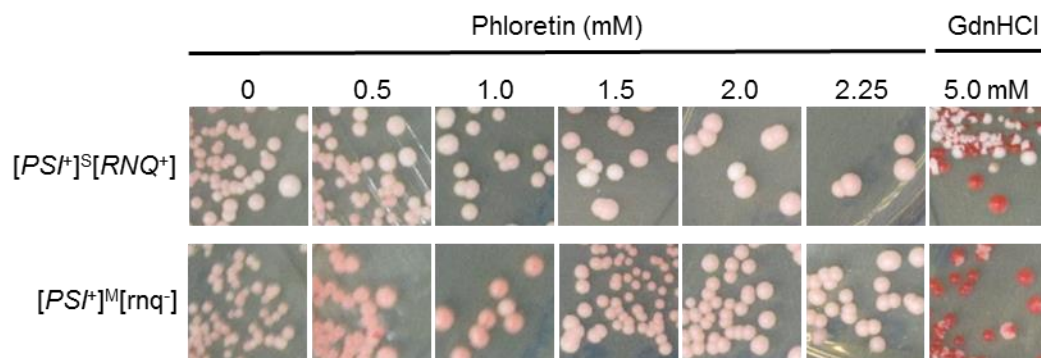
Figure 19. Treatment with phloretin does not eliminate [*PSI*]. A. The prion state of Sup35, the protein determinant of [*PSI*], was assessed in strains containing the *ade1-14* allele with a premature stop codon in the ORF of *ADE1*. In non-prion cells, [*psi*], functional Sup35 terminates translation at the premature stop codon, resulting in a lack of growth on media lacking adenine (-Ade) and red colonies on YPD media due to the blockage of the adenine biosynthesis pathway leading to pigment accumulation (right). In contrast, Sup35 is aggregated in [*PSI*] cells and its function of translation termination is compromised, resulting in the growth on -Ade media and pink/white colonies on YPD due to nonsense suppression (left) B. [*PSI*] cells were treated with a phloretin at a range on concentrations for 24 hours. After treatment, cells were spread onto YPD and color change was assessed after 3 days growth at 30°C followed by 3 day incubation at 4°C. While treatment with GdnHCl eliminates [*PSI*], resulting in red colonies, phloretin does not, resulting in the growth of white colonies.

A.

B.

C.
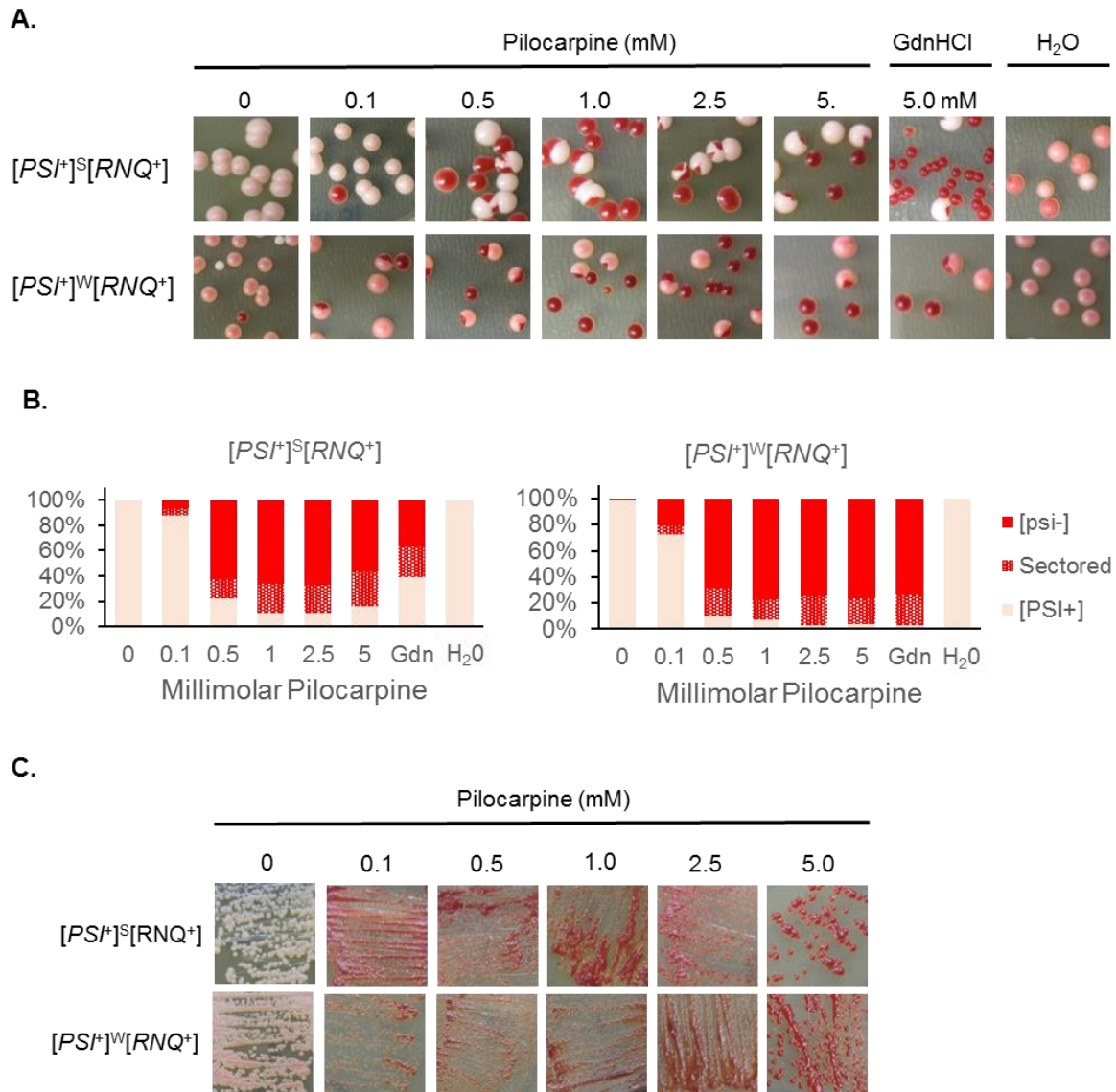
Figure 20. Pilocarpine eliminates two variants of [*PSI*]. A. The prion state of Sup35, was assessed in strains containing the *ade1-14* allele with a premature stop codon in the ORF of *ADE1*. [*PSI*] cells were treated in duplicate with various concentrations of phloretin and controls (5 mM GdnHCl or water) for 24 hours. After treatment, cells were spread onto YPD and color change was assessed after 3 days growth at 30°C followed by 3 day incubation at 4°C. B. The number of [*PSI*] (white) and [*psi*] (red) and sectored colonies quantified from two independent experiments (bottom panel). C. Colonies that were red ([*psi*]) after treatment with pilocarpine and white, untreated ([*PSI*]) were streaked onto YPD and color was assessed after 3 days growth at 30°C followed by 3 day incubation at 4°C.

Next, the ability of anti-[*SWI*] compounds to eliminate [URE3] was examined. The prion state of Ure2, the protein determinant of [URE3], can be easily assessed using a strain containing a *DAL5-ADE2* reporter, which is analogous to [*PSI*] red/white reporter described in the above section (Fig 21A). The Wickner group created this reporter system by replacing the endogenous *ADE2* promoter with the *DAL5* promoter, resulting in a strain in which *ADE2* is under the control of the *DAL5* promoter. In its soluble form, Ure2, a nitrogen catabolite transcriptional repressor, represses transcription of the *DAL5* gene by binding transcription factors and inhibiting their translocation to the nucleus. This repression results in a lack of adenine synthesis and red colony color. Conversely, [URE3] cells contain aggregated Ure2 and no repression of transcription at the *DAL5* promoter. Therefore, [URE3] synthesize adenine and have white colony color when plated on YPD. As in the [*PSI*] reporter system, conversion from white to red colony color is indicative of prion loss.

First, [URE3] cells were treated with pilocarpine and phloretin at concentrations ranging from 0-1.5 mM, as this range included concentration of compounds required to eliminate [*SWI*] and/or [PSI+]. No curing was observed at these concentrations (Fig 21B), therefore, [URE3] cells with pilocarpine and phloretin were treated at higher concentrations ranging from 0-6 mM (Fig 21C). While treatment with 5 mM GdnHCl resulted in the appearance of red colonies, indicative of prion loss, no such prion loss was observed at any concentration of pilocarpine and phloretin examined. Next, the ability of compounds 8-12 to eliminate [URE3] was examined by treating at a concentration of 0.5 mM (concentration used in our high-throughput screen) and examining colony color (Fig 23). While compounds 8, 9, and 12 were ineffective at eliminating [URE3], compound 11 was minimally effective at eliminating [URE3] (11% cells cured). Interestingly, while compound 10 was found to be largely ineffective in curing other yeast prions, approximately 40% of treated [URE3] cells were cured.

[*MOT3+*].

Next, the ability of anti-[*SWI*] compounds to cure [*MOT3+*] was examined. Mot3, the protein determinant of [*MOT3+*], is a transcriptional repressor (25). Our lab developed a novel [*MOT3+*] reporter system, by replacing the endogenous *ADE1* promoter with the *DAN1* promoter, resulting in a strain in which
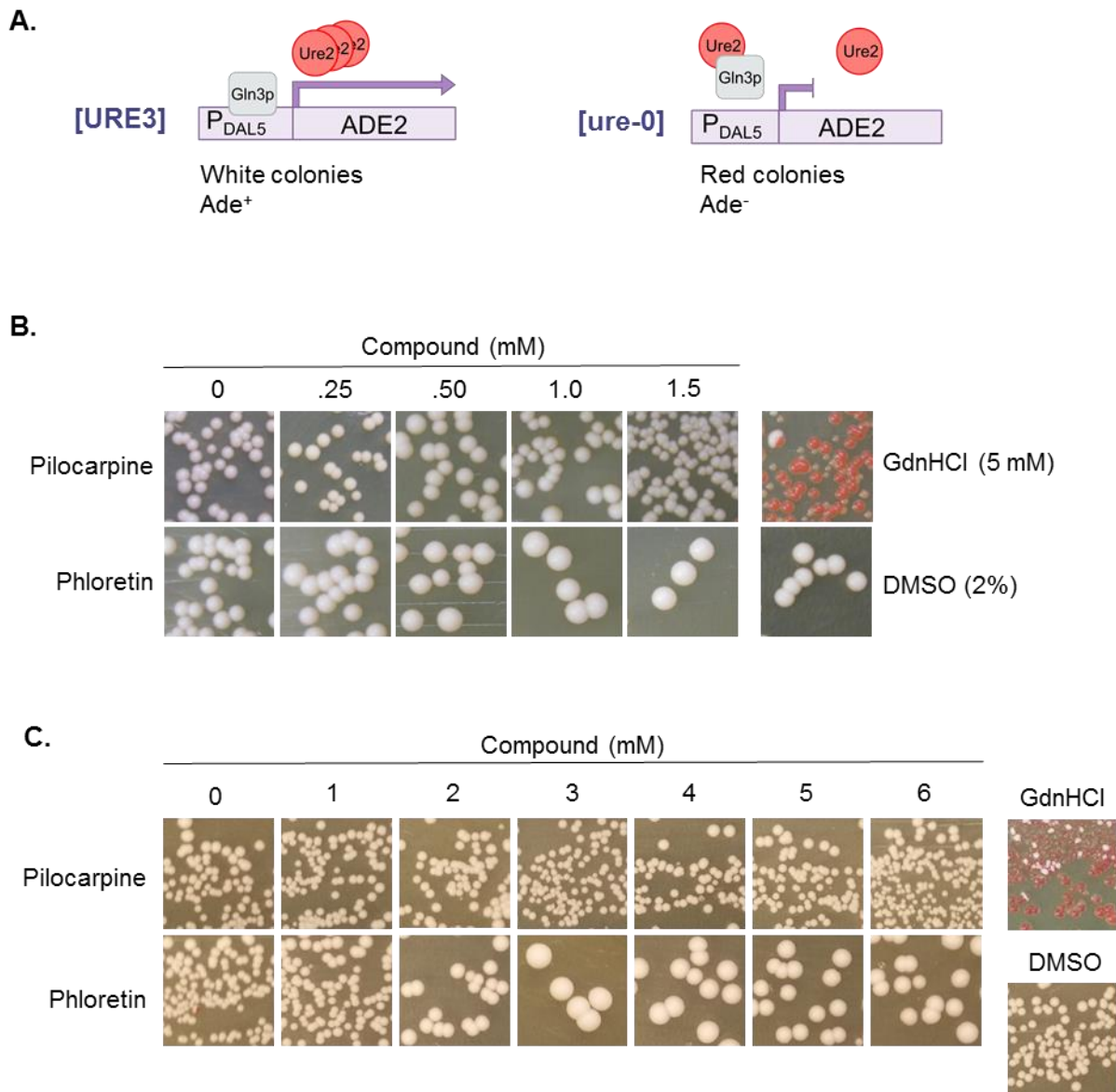
Figure 21. Reporter system for [URE3] detection. A. The prion state of Ure2, the protein determinant of [URE3] can be easily assessed using a strain containing a *pDAL5-ADE2* reporter, in which the ADE2 gene is under the control of the *DAL5* promoter. In [ure-0] cells, Ure2, a nitrogen catabolite transcriptional repressor, is soluble and represses transcription at the *DAL5* promoter, resulting in a lack of adenine synthesis and red color (right). Conversely, [URE3] cells contain aggregated Ure2 and no repression of transcription at the DAL5 promoter. Therefore, [URE3] cells synthesize adenine and display white colony color when plated on YPD (left). B. *pDAL5-ADE2* [URE3] cells were treated in duplicate with pilocarpine and phloretin at concentrations ranging from 0- 1.5 mM. C. *pDAL5-ADE2* [URE3] cells were treated in duplicate with pilocarpine and phloretin at concentrations ranging from 0- 6 mM. In both experiments cells were treated for 24 hours. After treatment ~500 cells were spread on YPD. Plated were incubated at 30˚C for 3 days followed by 3 day incubation at 4˚C to allow for color change.

A.

[*MOT3*⁺]   P_DAN1   ADE1

White colonies
Ade⁺

[*mot3*⁻]   P_DAN1   ADE1

Red colonies
Ade⁻

B.

No Cpd

Pilocarpine

Phloretin

C.

Compound	Percent Cells Cured
Pilocarpine	34%
Phloretin	0%
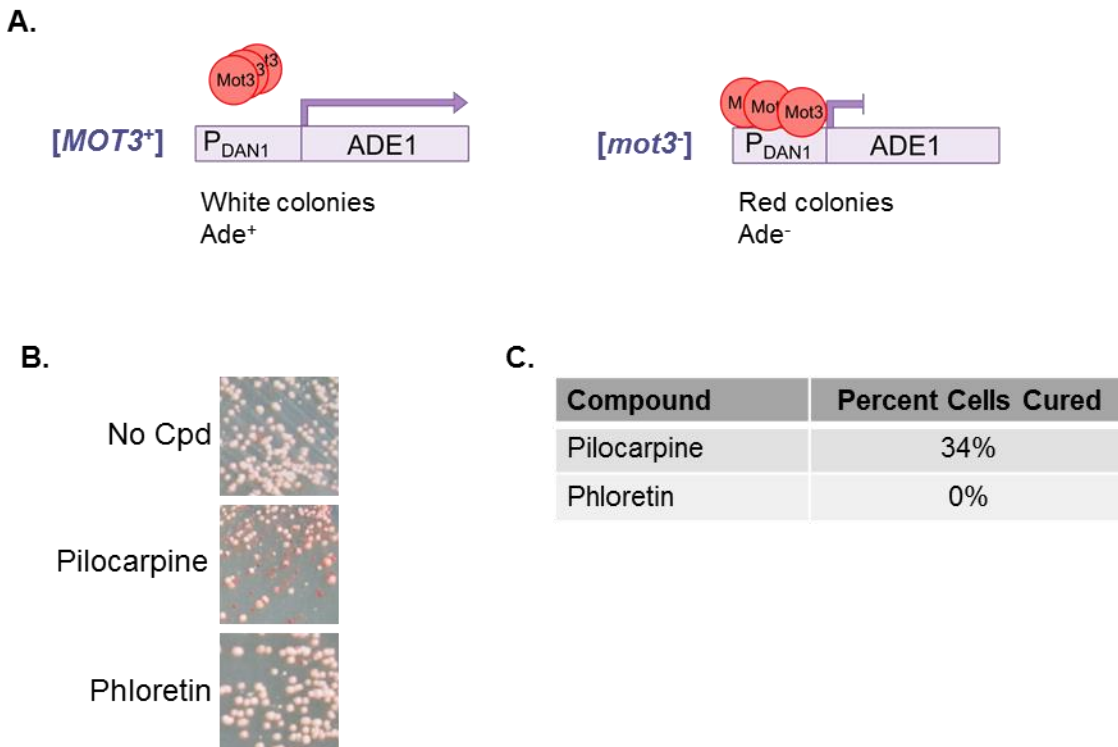
Figure 22. [*MOT3*⁺] eliminated by pilocarpine but not phloretin. A. The prion status of Mot3, a transcriptional repressor can be easily assessed in cells containing *pDAN1-ADE1* reporter. In [*mot*] cells, mot3, a transcriptional repressor, represses transcription of *DAN1*, therefore resulting in a lack of adenine synthesis and red colony color on YPD (right). Conversely, in [*MOT3*⁺], Mot3 is aggregated and therefore does not repress transcription at DAN1 promoter, resulting in adenine synthesis and white colony color on YPD (left). B. *pDAN1-ADE1* [*MOT3*⁺] cells were treated in duplicate with pilocarpine and phloretin at 0.5 mM for 48 hours. After treatment, cells were streaked on YPD. Plated were incubated at 30°C for 3 days followed by 3 day incubation at 4°C to allow for color change C. Percent of red ([*mot3*]) and white ([*MOT3*⁺]) cells were quantified and percentages were normalized to untreated control. Performed by Luzivette Robles (L.R.).
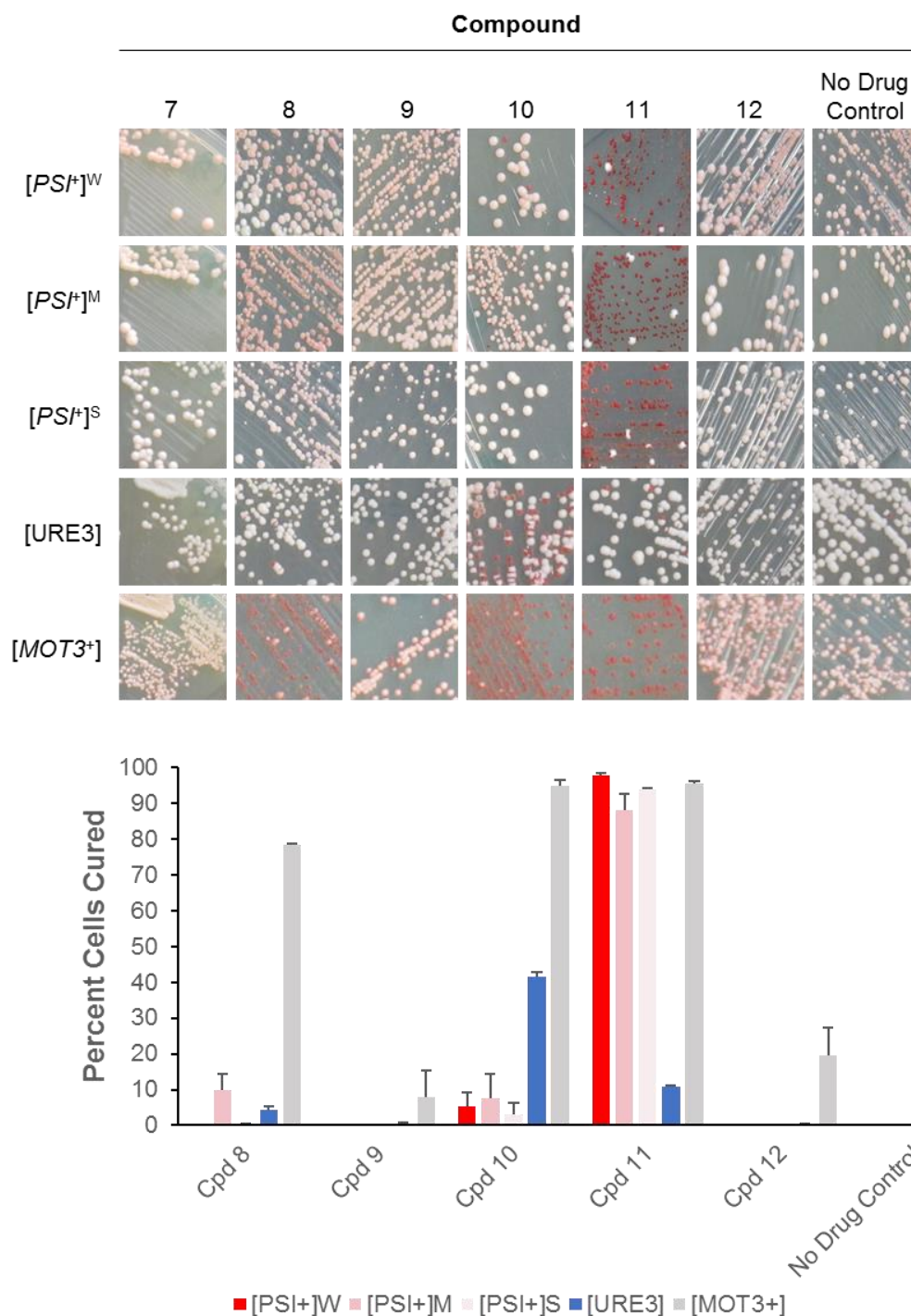
Figure 23. Chembridge DIVERset-CL compounds differentially cure yeast prions. Three [*PSI+*] variants, [URE3], and [*MOT3+*] cells were treated with hits 8-12 (.5mM) from the Chembridge DIVERset-CL library for 48 hours. After treatment, cells were streaked onto YPD. Plates were incubated at 30˚C for 3 days followed by 3 day incubation at 4˚C to allow for color change. C. Percent of red ([*psi-*], [ure-0], or [*mot3-*]) and white ([*PSI+*], [URE3], or [*MOT3+*]) cells were quantified and percentages were normalized to untreated control. Error bars indicate standard deviation. Performed by L.R.

Table 8. Summary table of prion curing

	Phloretin	Pilocarpine	7	8	9	10	11	12
[SWI⁺]	2.5 µM	300 µM	200 µM	125 µM	100 µM	150 µM	100 µM	250 µM
[PSI⁺]^S	-	100-500 µM	-	-	-	500 µM (3%)	500 µM (94%)	-
[PSI⁺]^M	N/A	N/A	-	500 µM (10%)	-	500 µM (8%)	500 µM (88%)	-
[PSI⁺]^W	1500 µM (20%)	100-500 µM	-	-	-	500 µM (5%)	500 µM (98%)	-
[URE3]	-	-	-	500 µM (4%)	-	-	500 µM (11%)	-
[MOT3⁺]	N/A	500 µM (35%)	-	500 µM (78%)	500 µM (8%)	500 µM (95%)	500 µM (20%)	500 µM (96%)

Note: Blue denotes concentrations at which 50% cells are cured. If EC_{50} is not shown, dose response experiments were not performed.

ADE1 is under the control of the *DAN1* promoter (Fig 22A). This novel reporter system, developed by Dr. Zhiqiang Du, *pDAN1-ADE1*, can therefore report the prion status of Mot3 in a simple red/white color assay analogous to the [*PSI+*] and [URE3] previously described. In non-prion cells ([*mot3-*]), Mot3 is soluble and therefore able to repress transcription at the *DAN1* promoter, resulting in a lack of adenine synthesis and red colony color on a YPD plate. Conversely, Mot3 is aggregated in [*MOT3+*] cells, resulting in a lack of repression of the *DAN1* promoter, adenine synthesis and white colony color on YPD.

[*MOT3+*] cells were treated with 0.5 mM pilocarpine, phloretin, and compounds 8-12 for 48 hours and quantified the number of red cells that appeared compared to untreated [*MOT3+*] cells, which are not stably white. While treatment with pilocarpine resulted in increase in the appearance of red colonies compared to the untreated control, treatment with phloretin did not result in curing of [*MOT3+*] (Fig 22B and 22C). Interestingly, treatment with compounds 8-12 resulted in the increased appearance of red colonies, and thus demonstrating that treatment with these compounds results in prion curing (Fig 23).

Materials and Methods

Chemical Libraries. The following chemical libraries were used in these studies: *ADSI* – a library of 6,800 compounds of diverse chemical structure that meet the Lipinski guidelines for drug-likeness; *NIH Clinical Collection -* A small library of 450 molecules with a history of use in human clinical trials; *NCI Plate Sets from the Open Chemical Repository Collection -* A total of 3,000 compounds made available through the NCI's Developmental Therapeutics Program. The collection consists of ~2,000 structurally diverse compounds, ~880 mechanistically diverse anti-cancer compounds, and 120 natural products. Spectrum: a library of ~2000 (i) drugs that have been introduced in the US, Europe and Japan and have known pharmacological profiles, (ii) natural products with unknown biological properties and (iii) other bioactive compounds such as non-drug enzyme inhibitors, receptor blockers, membrane active compounds, and cellular toxins ; *ChemBridge DIVERSet-CL -* A collection of 50,000 small molecules with enhanced potential for therapeutic development. >90% of compounds pass a rigorous set of drug-like filters including Lipinski and Veber rules, and Pipeline Pilot SMARTS liability filtering. Approximately 4800 molecules were screened from this library. All compounds from pilot screen were solubilized in DMSO and stored at the

Northwestern's High Throughput Analysis Lab (Evanston, Il). Compounds for subsequent experiments were solubilized in DMSO or water. Compounds used in the Li laboratory experiments were purchased from Sigma-Aldrich, St. Louis, MO (Quinacrine Hydrochloride), Santa Cruz Biotechnology, Dallas, Texas (phloretin, nimustine hydrochloride, pilocarpine nitrate, tacrine hydrochloride and aminacrine), and Chembridge Corporation, San Diego, CA (Chembridge compound ID numbers: 91109249 (cpd 7), 74610971 (cpd8), 71326175 (cpd 9), 66861843 (cpd 10), 63161364 (cpd 11), 47774380 (cpd12)).

Yeast strains and media. All yeast strains used in this study were grown and maintained according to methods outlined in (128, 130). Strains were propagated in rich (yeast extract, peptone, dextrose (YPD)) or synthetic complete (SC) media. Media was supplemented with 5 mM guanidine hydrochloride (GdnHCl) when indicated. Glucose was used as the carbon source unless otherwise indicated. For the raffinose phenotype assay, glucose was replaced with raffinose and supplemented with 0.5 µg/ml antimycin (Sigma-Aldrich, St. Louis, MO). Plates were incubated at 30˚C for three days unless otherwise indicated. Agar plates were made as outlined in (33).

[*SWI⁺*]/*erg6Δ*::*LEU2/FLO1pr-URA3/FLO8-HIS3* strain was constructed by replacing the *ERG6* gene with *LEU2* from the [*SWI⁺*]/*FLO1pr-URA3/FLO8-HIS3* described in (148). The [*MOT3⁺*] reporter, BY4741 *FLO8* (*MET15*) flo1::*FLO1pr-URA3 DAN1pr-ADE1*, was created by replacing endogenous ADE1 promoter with the *DAN1* promoter. The 74-D694 [*PSI⁺*] cells containing the *ade1-14* allele with a premature stop codon in the ORF of *ADE1* was previously described in (37). The BY241 [URE3] cells (*MAT*a *leu2 trp1 ura3* P$_{DAL5}$:*ADE2* P$_{DAL5}$:*CAN1 kar1)* were obtained from the Wickner laboratory and descried previously in (32).

Screening protocol for anti-[*SWI⁺*] compounds at Northwestern University's High Throughput Analysis Lab. Compounds (0.5 µl stock; 0.5 mM final for first screen, 0.1 mM for Chembridge Diverset-CL), 5 mM GdnHCl (positive control), or 1% DMSO (negative control) were transferred into a 384-well plate using Echo 550 Acoustic Liquid Transfer System. [*SWI⁺*]/*erg6Δ*::*LEU2/FLO1pr-URA3/FLO8-HIS3* cells were diluted 1000-fold from 2.5×10^7 cells/ml stock into curing medium (SC-his, supplemented with 0.2 mM GdnHCl). 50 µL of cell-containing curing medium were added to each well with multi-drop system. Plates

were sealed and grown for 24 h or 48 h at 30 °C with shaking. Cells were then pinned into 50 μL media

lacking uracil (SC-his-ura), seal plates and grow for 24 h with shaking while measuring cell growth at A_{600}.

[*SWI⁺*] screening protocol in Li laboratory. Compounds, 5 mM GdnHCl (positive control), DMSO or water

(negative control) were transferred into a 96-well plate. [*SWI⁺*]/*erg6Δ*::*LEU2/FLO1pr-URA3/FLO8-HIS3*

were diluted 1000-fold from $5X10^7$ cells/ml stock into curing medium (SC-his, supplemented with 0.2 mM

GdnHCl). 100 μL of cell-containing curing medium were added to each well. Volume was adjusted to 150

μL final volume with curing medium. Plated were sealed and grown for 24 h at 30 °C with shaking. 3 μL cell

suspension was transferred into media lacking uracil (SC-his-leu-ura; SC-HLU), and plates were sealed

and grown for 24 h with shaking while measuring cell growth at A_{600}.

For quantification of curing, cells were treated in triplicate with individual compounds or controls as

described above. Cells were then spread on SC-his and SC-HLU media. Plated were incubated for 3 days

at 30 °C. Colonies were counted and percent cells cured was calculated - #Ura⁺ colonies/#total colonies on

SC-His.

Assessment of raffinose utilization. After treatment with compounds, individual Ura⁺ colonies were

streaked onto YPD and raffinose + 0.5 μg/ml antimycin media. Untreated [*swi*] cells and DMSO treated

cells, as well as cells treated with 5 mM GdnHCl, were streaked as negative and positive controls,

respectively. Plated were incubated for 3 days at 30 °C.

Assessment of aggregation status of Swi1NQ-YFP. BY4741 *FLO8*(*MET15*) *flo1*::*URA3* [*SWI⁺*] cells

were transformed with a pGal1-Swi1-NQYFP plasmid (description of transformation protocol in chapter 2).

Cells were treated with indicated hits and controls for 24 hours. Cells were spread on SC-his and SC-HLU

media and plates were incubated for 3 days at 30 °C. Swi1 NQ-YFP expression was induced with 2%

galactose and aggregation of Ura⁺ isolates was assessed by fluorescence microscopy.

Treatment of [*PSI⁺*], [URE3], [*MOT3⁺*] with hit compounds. Compounds, 5 mM GdnHCl (positive

control), DMSO or water (negative controls) were transferred into a 96-well plate. [*PSI⁺*] and [URE3] reporter

cells were diluted 1000-fold from $5X10^7$ cells/ml stock into curing medium (YPD, supplemented with 0.2

mM GdnHCl). 100 μL of cell-containing curing medium were added to each well. Volume was adjusted to

150 µL final volume with curing medium. Plated were sealed and grown for 24 h at 30 ˚C with shaking. Cells were treated in duplicate or triplicate, as noted in figure legends. Compound or control treated cells were subsequently spread onto YPD media. Plated were incubated for 3 days at 30 ˚C followed by a 3-day incubation at 4 ˚C to allow for color change. The number of red, sectored or white colonies counted. When indicated, red colonies were subsequently streaked onto YPD and plated were incubated for 3 days at 30 ˚C followed by a 3-day incubation at 4 ˚C.

Alternatively, 0.5 mM compounds, 5 mM GdnHCl (positive control), DMSO or water (negative controls) were transferred into a 96-well plate. [*PSI*]^W, [*PSI*]^M, [*PSI*]^S, [URE3] and [*MOT3*] cell stocks were diluted in curing medium (YPD, supplemented with 0.2 mM GdnHCl) to a final concentration of 1x10^5 cells/mL. Plated were sealed and grown at 30 ˚C with shaking. After 2 days of treatment, 5 µL of cells were transferred and spread onto YPD plates. Plates were incubated at 30 ˚C for 3 days followed by 3-day incubation at 4 ˚C. Counted colonies from both sets of plates and the number of red and white/pink colonies were quantified.

Supplemental Table 1. List of hit compounds from high-throughput screen of four libraries

Hit No.	Library	Synonym	CID/CAS/NCS	Cherry Picking Result
1	NCC	Amiridine	604519	+
2	NCC	Tacrine hydrochloride	2723754	+
3	Spectrum	guanabenz acetate	23256-50-0	+
4	Spectrum	pilocarpine nitrate	148-72-1	+
5	Spectrum	quinacrine hydrochloride	69-05-6	+
6	Spectrum	aminacrine	90-45-9	+
7	Spectrum	desloratidine	100643-71-8	-
8	Spectrum	tacrine hydrochloride	1684-40-8	+
9	Spectrum	lobendazole	6306-71-4	+
10	Spectrum	hydroxytacrine maleate	118909-22-1	+
11	Spectrum	phloretin	60-82-2	+
12	Spectrum	nimustine	42471-28-3	+
13	NCI/DTP	1-(2-chloro-6-fluorophenyl)-1,3-dihydro-[1,3]thiazolo[3,4-a]benzimidazole	625483	+
14	NCI/DTP	thiazolobenzimidazole	625487	+
15	NCI/DTP	4-methyl-2-quinazolinamine	110275	+
16	NCI/DTP	2-(6-methoxyquinolin-4-yl)sulfanylacetic acid	13581	+
17	NCI/DTP	2-methyl-2-(quinazolin-4-ylamino)propane-1,3-diol	14179	+
18	NCI/DTP	2-(4,5-dimethylimidazol-1-yl)phenol	42069	+
19	NCI/DTP	3-(quinazolin-4-ylamino)propane-1,2-diol	13220	+
20	NCI/DTP	[(E)-(4-methoxyphenyl)methylideneamino]carbamic acid	47652	+
21	NCI/DTP	(2Z)-2-hydroxyimino-3-quinolin-4-ylpropanoic acid	85359	+
22	NCI/DTP	2-amino-5-(3-anilinopropyl)-6-methyl-1H-pyrimidine-4-thione	85069	+
23	NCI/DTP	1-(diaminomethylidene)-2-(2,3,4,5,6-pentafluorophenyl)guanidine;hydrochloride	274902	+
24	NCI/DTP	3-phenyl-4,13b-dihydro-1H-[1,2,4]triazino[4,3-f]phenanthridine	153625	+
25	NCI/DTP	(1E)-1-[amino-(phenanthren-9-ylamino)methylidene]-2-methylguanidine;chloride	401366	+
26	NCI/DTP	4-[3-[(4-hydroxyphenyl)methyl]-1H-benzimidazol-2-ylidene]cyclohexa-2,5-dien-1-one	648927	+
27	NCI/DTP	1-(2-((3,3,5-trimethyl-1-phenylcyclohexyl)oxy)ethyl)piperidine	96255	+
28	NCI/DTP	(5-methyl-2,3,4,6,7,12b-hexahydro-1H-indolo[2,3-a]quinolizin-5-ium-7a-yl)acetate;iodide	112671	-
29	NCI/DTP	Naphthylazoxine	148354	-

30	NCI/DTP	[(3S,8S,9S,10R,13S,14S,17S)-17-[1-acetyl-5-(trifluoromethyl)pyrazol-3-yl]-10,13-dimethyl-2,3,4,7,8,9,11,12,14,15,16,17-dodecahydro-1H-cyclopenta[a]phenanthren-3-yl] acetat	82803	-
31	NCI/DTP	3',6'-dihydroxy-4,5,6,7-tetraphenylspiro[2-benzofuran-3,9'-xanthene]-1-one	119886	-
32	NCI/DTP	17-(2-amino-1,3-thiazol-4-yl)-11-hydroxy-10,13-dimethyl-1,2,6,7,8,9,11,12,14,15,16,17-dodecahydrocyclopenta[a]phenanthren-3-one;4-bromobenzenesulfonic acid	93355	-
33	ASDI	N-[2-(1H-indol-3-yl)ethyl]-4-methylbenzenesulfonamide	2737722	-
34	ASDI	AQ-13	9820475	+
35	ASDI	9-phenylphenanthridine	5148150	-
36	ASDI	AC1Q5GUV	44724445	-
37	ASDI	1-(4-ethylphenyl)-2-[(5-pyridin-4-yl-1H-1,2,4-triazol-3-yl)sulfanyl]ethanone	715374	-
38	ASDI	N-(7-methoxy-1,2,3,4-tetrahydroacridin-9-yl)benzamide	4050302	+
39	ASDI	Data Unavailable		+
40	ASDI	Data Unavailable		+
41	ASDI	4-(2-thiophen-2-ylquinolin-4-yl)morpholine	2729704	-
42	ASDI	1-(benzenesulfonyl)naphthalene	4189459	-
43	ASDI	Data Unavailable		+
44	ASDI	N-(5-ethyl-1,3,4-thiadiazol-2-yl)-2-methoxybenzamide	902966	-
45	ASDI	3-{[benzyl(methyl)amino]methyl}-2-methylquinolin-4-ol	710601	+
46	ASDI	N-[2-(dimethylamino)quinolin-4-yl]-3-phenylpropanamide	2725904	+
47	ASDI	5-Ethoxy-2-ethylsulfanyl-1H-benzoimidazole	5344707	+
48	ASDI	6-bromo-n-isobutylquinazolin-4-amine	710708	+
49	ASDI	3-(4-chlorobenzyl)quinazolin-4(3H)-one	677888	-
50	ASDI	1-benzyl-4-[(3-phenyl-1H-pyrazol-4-yl)methyl]piperazine	2812589	-
51	ASDI	ZINC00405673	854264	-
52	ASDI	6-amino-3-methyl-4-(2-thienyl)-1,4-dihydropyrano[2,3-c]pyrazole-5-carbonitrile	2814547	-
53	ASDI	N-(5-benzyl-1,3-thiazol-2-yl)pentanamide	1567629	-
54	ASDI	N-(2,6-dimethylphenyl)-2-ethoxybenzamide	902976	-
55	ASDI	Ethyl 2-(methanesulfonamido)-6-methyl-4,5,6,7-tetrahydro-1-benzothiophene-3-carboxylate	3127949	-
56	ASDI	ZINC00126731	722617	-
57	ASDI	ST50913746	1219681	-
58	ASDI	MLS000109398	3127949	-
59	ASDI	AC1MSASV	3581394	+
60	ASDI	ST50199012	693952	-

61	ASDI	BAS 05988845	1081740	-
62	ASDI	BAS 04037980	1071850	-
63	ASDI	(4-Hydroxy-2-oxo-1,2-dihydro-quinolin-3-yl)-acetic acid propyl ester	54687731	-
64	ASDI	ZINC02379288	1987633	-
65	ASDI	ZINC00530023	936160	-
66	ASDI	4-tert-butylphenyl 4-bromobenzoate	788585	-
67	ASDI	ZINC00146661	2810950	-
68	ASDI	N-{4-[(3,4-dimethyl-1,2-oxazol-5-yl)sulfamoyl]phenyl}-2,2-dimethylpropanamide	987761	-
69	ASDI	ZINC00147867	2811597	-
70	ASDI	1-(azepan-1-yl)-2-ethyl-3-methylpyrido[1,2-a]benzimidazole-4-carbonitrile	680836	-
71	ASDI	ZINC00116689	2808903	+
72	ASDI	AC1MWXW7	3781665	-
73	ASDI	3-chloro-N-(quinolin-8-yl)-1-benzothiophene-2-carboxamide	679715	-
74	ASDI	2-(1,3-benzodioxol-5-yl)-7-ethylimidazo[1,2-a]pyridine	2812756	-
75	ASDI	2-{[4-ethyl-5-(2-methoxyphenyl)-4H-1,2,4-triazol-3-yl]sulfanyl}-N-(4-ethylphenyl)acetamide	4006963	-
76	ASDI	SMR000048490	667163	-
77	ASDI	ST50131963	6469842	-
78	ASDI	ZINC04784027	3993473	-
79	ASDI	ST50413295	2038578	-
80	ASDI	Nylidrin hydrochloride	5702098	-
81	ASDI	Data Unavailable		-
82	ASDI	Data Unavailable		-
83	ASDI	Data Unavailable		-
84	ASDI	Data Unavailable		-

Note: N/A indicates that the NCS number is not available for compound.

Supplemental Table 2. List of hit compounds from Chembridge DIVERset CL High-throughput Screen

Hit No.	Names	Synonyms	Cherry Picking Result
1	N-(2-isobutoxybenzyl)-N-methylisonicotinamide	DCL_91109249	Positive
2	8-[3-(4-methyl-1,3-thiazol-5-yl)propanoyl]hexahydro-2H-pyrazino[1,2-a]pyrazin-1(6H)-one	DCL_89793178	Negative
3	N,N-dimethyl-2'-(5-methyl-1,3,4-thiadiazol-2-yl)biphenyl-4-carboxamide	DCL_78494806	Negative
4	N-[5-(1,2,3,4-tetrahydroisoquinolin-5-yl)pyridin-2-yl]cyclopropanecarboxamide	DCL_78156175	Negative
5	N-{[4-(2-phenylethyl)-4H-1,2,4-triazol-3-yl]methyl}-3-azaspiro[5.5]undecan-9-amine	DCL_76126193	Positive (D2)
6	N~4~,N~4~,5-trimethyl-N~2~-(3-pyridin-4-ylpropyl)pyrimidine-2,4-diamine	DCL_74610971	Positive
7	3-(2-phenoxyethyl)-1-pyrimidin-2-ylpiperidine-3-carboxylic acid	DCL_73630002	Negative
8	N-methyl-3-(1-methyl-1H-pyrrol-2-yl)-N-[(3-pyridin-4-ylisoxazol-5-yl)methyl]-1H-pyrazole-5-carboxamide	DCL_71326175	Positive
9	2-{2-[(3-methoxy-1,3-dimethylbutyl)amino]ethyl}phthalazin-1(2H)-one	DCL_69592360	Negative
10	4-[2-(trifluoromethyl)morpholin-4-yl]thieno[3,2-d]pyrimidine	DCL_66861843	Positive
11	6-methoxy-N-[2-(2-pyridin-4-yl-1,3-thiazol-4-yl)ethyl]pyrimidin-4-amine	DCL_63330616	Positive (D2)
12	5-{[[4-(2,6-dimethylpyridin-3-yl)pyrimidin-2-yl](methyl)amino]methyl}-2-methoxyphenol	DCL_63161364	Positive
13	2-(3,4-dichlorophenyl)-4-(2-propoxyethyl)morpholine	DCL_62167167	Positive
14	(3R*,3aR*,7aR*)-3-phenyl-1-(pyrazolo[1,5-a]pyrimidin-2-ylcarbonyl)octahydro-4,7-ethanopyrrolo[3,2-b]pyridine	DCL_59978768	Negative
15	4-methyl-2-({methyl[(1-methyl-1H-benzimidazol-2-yl)methyl]amino}methyl)phenol	DCL_59388686	Negative
16	(2S)-N-{[3-(2-thienylmethyl)-1,2,4-oxadiazol-5-yl]methyl}piperidine-2-carboxamide	DCL_57227047	Negative
17	5-{[1-(3,4-dimethylphenyl)-1H-pyrazol-4-yl]methyl}-4-pyridin-4-yl-4,5,6,7-tetrahydro-1H-imidazo[4,5-c]pyridine	DCL_54384959	Negative
18	3-isopropyl-N,1-dimethyl-N-[(3-pyridin-4-ylisoxazol-5-yl)methyl]-1H-pyrazole-5-carboxamide	DCL_47874380	Positive
19	1-{3-[4-(2,3-dihydro-1,4-benzodioxin-6-yl)-1H-1,2,3-triazol-1-yl]propyl}-6-methylpyridin-2(1H)-one	DCL_47727234	Negative
20	4-[3-(2,2,2-trifluoroethoxy)benzoyl]piperazine-2-carboxylic acid	DCL_43381440	Negative
21	{5-[4-(ethylamino)pyrimidin-2-yl]-2-fluorophenyl}methanol	DCL_40149589	Negative
22	8-{5-methyl-6-[(2-methyl-3-pyridinyl)oxy]-4-pyrimidinyl}-1-oxa-8-azaspiro[4.5]decane	DCL_35902178	Positive (D2)
23	8-methoxy-N-{[2-(4-methylpiperazin-1-yl)pyridin-3-yl]methyl}chromane-3-carboxamide	DCL_34140216	Negative
24	(4S)-N-ethyl-4-(4-pyridin-3-yl-1H-1,2,3-triazol-1-yl)-L-prolinamide	DCL_25572199	Negative

25	(3S*,4S*)-1-[(3-ethylisoxazol-5-yl)methyl]-4-(2-naphthyl)piperidin-3-ol	DCL_25270617	Positive (D2)
26	({4-[(4-ethyl-3,3-dimethylpiperazin-1-yl)carbonyl]-1,3-thiazol-2-yl}methyl)dimethylamine	DCL_25070930	Negative
27	2-[4-(2-ethoxyethyl)piperazin-1-yl]-4-(3,3,3-trifluoropropyl)pyrimidine	DCL_20142800	Negative
28	7-[(2,5-dimethyl-1,3-thiazol-4-yl)acetyl]-3-(2-phenylethyl)-6,7,8,9-tetrahydro-5H-[1,2,4]triazolo[4,3-d][1,4]diazepine	DCL_18358878	Negative
29	1,6-dimethyl-N-[1-phenyl-2-(1H-pyrazol-1-yl)ethyl]-1H-pyrazolo[3,4-d]pyrimidin-4-amine	DCL_13551672	Negative
30	2-{1-[1-methyl-3-(1H-pyrazol-1-yl)propyl]-1H-imidazol-2-yl}benzoic acid	DCL_11137790	Negative
31	1-(cyclopropylmethyl)-4-[2-(trifluoromethyl)benzyl]piperidine-4-carboxylic acid	DCL_10549378	Negative

Note: 31 hits were found in initial screen. All were cherry-picked and several were positive upon cherry picking (+). D2 indicates that there was growth in media lacking uracil after 2 day treatment with compound.

CHAPTER 4

Discussion

Small regions of Swi1 confer prion formation, maintenance and transmission

A prion domain is a limited portion of a prion protein that is necessary and sufficient for prion formation and propagation. In this study we find that a small region containing the first 32 amino acids of Swi1 is able to decorate [*SWI*+] aggregates and maintain the prion fold in the absence of full-length Swi1 (Fig 6 and 7). In addition, when a region consisting of the first 31 amino acids of Swi1 was fused to Sup35MC, the resulting fusion was able to form [*PSI*+]-like nonsense suppression prion ([*SPS*+]) *de novo* (Fig 10). The Swi1-PrD is unique in some respects. First, its size, ~30 amino acids. The PrD of Cyc8 is defined as amino acids 465-966 (24). Previous *in vivo* research has described the Ure2 PrD as the first 65 amino acids of the protein (89). To our knowledge, the Swi1 PrD is the smallest PrD currently identified that supports *de novo* prion formation and propagation *in vivo*. Second, the composition of this small Swi1 PrD is also unique; being highly rich in asparagine and threonine, it is distinguishable from most other PrDs which are also enriched in glutamine.

In general, the prevalence of glutamine/asparagine-rich regions in the proteomic sequences of different organisms may be an evolutionary selection for eukaryotic proteins as a means to regulate protein-protein interactions (76). The enrichment of glutamine and asparagine residues in PrDs, however, is not an absolute requirement, as some prion proteins, namely PrP in mammals, Mod5 and several newly identified prions in *S. cerevisiae* (26, 97), and HET-s in *P. anserine* (149), lack an enrichment in these residues. Swi1 has a PrD that is uniquely glutamine-free and asparagine-rich. Research into the contributions of both glutamine and asparagine residues to prion formation and propagation have yielded interesting results that may give us some insight into the ability of these small regions of Swi1 to propagate [*SWI*+]. While the two amino acids only differ subtly, with glutamine having one additional methylene group in the side chain relative to asparagine, Halfmann *et al* found that they have opposing effects on prion and amyloid formation (150). Examination of glutamine and asparagine replacement variants (all glutamines in the Sup35 PrD were replaced with asparagines (Sup35^N) and vice versa, (Sup35^Q)) showed that while the Sup35^N variant

promoted self-templating amyloidogenesis and prion formation, the Sup35^Q variant promoted the formation of non-amyloid aggregates and thus inhibited prionogenesis. Asparagine and glutamine substitution variants were also made for other prion proteins and the prion promoting effects of asparagine and the prion inhibiting effect of glutamine was also observed- suggesting that prion promotion or inhibition are not protein specific, but rather general properties of these amino acids (150). Additionally, examination of the thermodynamic properties of regions composed of 30 asparagines (N_{30}) or 30 glutamines (Q_{30}) found that the poly-asparagine molecule had a higher propensity to form β-sheets and a lower disorderedness compared to the poly-glutamine molecule (150). Combined, these studies demonstrate that glutamine and asparagine residues have dramatic and disparate effects on prion formation. It is proposed that the smaller side chains found in asparagine allow for stronger hydrogen binding compared to glutamine, which in turn allows for the formation of β-sheets and a decreased amount of non-specific interactions – preventing formation of non-amyloid pathway aggregates (off-pathway) (150). The unusually high asparagine content of extreme N-terminus of Swi1 is likely an important factor contributing to its ability to form and propagate [*SWI*+]. However, it was reported that while poly-asparagine molecules 21 residues in length were highly disordered and had high amyloidogenic propensity compared to poly-glutamine sequences, these residues alone did not endorse prionogenicity (110) – suggesting that being asparagine-rich is not the sole factor determining PrD properties and other residues are likely required for prionogenesis. Moreover, a longer poly-asparagine peptide consisting of 104-asparagines did not demonstrate prion-like heritability, suggesting that simply increasing the size of this moderately amyloidogenic residue is not enough to cause prion formation (151).

While Q/N-rich regions are common in the yeast proteome, analysis of the frequency of N repeats in mammals revealed a complete lack of repeats longer than eight consecutive Ns (152). In SWISS-PORT, one entry was found to contain eight consecutive Ns and two entries with five eight consecutive Ns. Analysis of repeats of other residues revealed asparagine is the only amino acid in which there is a significant difference between proteins from all organisms and those from mammals (152). The aforementioned studies demonstrated that asparagine residues are more prionogenic than glutamine residues (150). Another recent study demonstrated that N-peptides has faster self-assembly and more rapid conversion

into amyloid fibers compared to Q-peptides (153). Given these findings it is not surprising that mammals would lack asparagine repeats. It is known that at least nine neurodegenerative diseases are caused abnormal expansion of Q-repeat domains and that prion-like domains with compositional similarity to yeast prions domains are present in several disease-associated proteins, including ataxin1, ataxin2, TDP-43, FUS, hnRNP1 and hnRNP2, therefore, the presence of these either Q or Q/N rich regions seems to be detrimental to mammals. Proteins containing N-repeats, which form amyloid more rapidly and are more prionogenic, may be expected to be more deleterious to mammals than Q-repeat proteins. Therefore, while N-rich proteins may have been selected for in yeast to provide cells with a mechanism for adaptive inheritance, N-repeat proteins may be evolutionarily selected against in mammals to protect against aggregation prone proteins.

The study described in this thesis illustrates the importance of protein levels on the varying ability of small regions of Swi1 to form prion aggregates and to maintain and propagate [*SWI*$^+$]. While Swi1$_{1-31}$ and Swi1$_{1-30}$ were not able to form aggregates in WT [*SWI*$^+$] cells, they do so when Swi1 protein levels are higher. Swi1$_{1-30}$ was also capable of not only adopting the prion fold in *swi1*Δ/*pSwi1* [*SWI*$^+$] cells, which express Swi1 at higher level than in WT cells, but also propagating the acquired prion fold in the absence of full-length Swi1. Previous research has shown that over-expression of a prion protein or its PrD results in a significant increase in *de novo* prion formation (16). Results described in this thesis show that the length requirement for a region that constitutes the Swi1 PrD is strongly influenced by the expression level of full-length Swi1. Increased levels of Swi1 may enable previously non-prionogenic fragments that are on the edge of aggregation to form prion aggregates. Increased levels of Swi1 in *swi1*Δ/*pSwi1* [*SWI*$^+$] cells may also explain the increased level of aggregation of Swi1$_{TRUNC}$YFP in general that we observed in these cells compared to WT cells. Increased levels of Swi1 in the cells may results in an increased amount of prion seeds that are available for cross-seeding or decoration, this resulting in the increased levels of aggregation that we observed upon over-expression of our Swi1 truncation mutants.

Another interesting finding in this study was the change of aggregation morphology of Swi1$_{1-30}$ and Swi1$_{1-31}$ in *swi1*Δ/Swi1$_{Trunc}$YFP [*SWI*$^+$] cells upon removal of the full-length Swi1. The presence of ring/rod-

shaped (hereafter referred to as ring-shaped) aggregates is usually observed in pre-mature [*PSI*+], [*PIN*+] and [*SWI*+] cells (70, 148). Although combined results from various studies have shown that these pre-mature aggregates are processed into dot-shaped aggregates, and this processing is often linked to the transition of premature prion aggregation to mature, stable prion conformations (68, 70, 154-156), a recent study suggest that the *de novo* formation of [*PSI*+] can involve multiple pathways and both ring- and dot-shaped Sup35 aggregation are prionogenic (157). My study shows that in the presence of full-length Swi1, Swi1$_{1-30}$ and Swi1$_{1-31}$ formed punctate aggregates, some of which transitioned into ring-shaped aggregates when the full-length protein was lost. Remarkably, most of these ring-shaped aggregates transition back into punctate dots when cells are retransformed with full-length Swi1, where the truncation mutant and full-length protein co-localize (Fig 4C). It is possible that full-length Swi1 provides stability to the [*SWI*+] formed by Swi1$_{1-30}$ or Swi1$_{1-31}$ through interaction of the full-length protein and Swi1 truncation mutants. In the absence of full-length Swi1, the morphological changes in the aggregates are perhaps due to interaction with the insoluble protein deposit (IPOD), an ancient quality control compartment and/or with the actin cytoskeleton, as shown for Sup35 ring structures (75, 155).

Ganusova et al. found that Sup35 interacted with several components of the actin cytoskeleton, including Lsb2, Sla1, Sla2, End3, Arp2, and Arp3 (75, 155). In future studies, it would be of interest to elucidate the cellular components with which Swi1 interacts. A two-hybrid assay can be used to determine if full-length Swi1 or smaller regions of Swi1, including Swi1$_{1-31}$, interact with the cytoskeleton components that Sup35 interacts with and if there are differences in the interactions observed between cells containing punctate foci and those containing rings. Additionally, individual components of the actin cytoskeleton can be tagged and colocalization of either Swi1 or Swi1$_{1-31}$YFP and individual components can be assessed. To determine if any components of the actin cytoskeleton are required for [*SWI*+] formation, maintenance and propagation, strains containing deletions of individual components of the actin cytoskeleton can be utilized to examine the ability of Swi1 to aggregate, and maintain and propagate [*SWI*+]. Lack of prion formation, maintenance or propagation would indicate that the deleted component may be critical for Swi1 prion behavior.

Examination of Swi1 localization to the IPOD can be done by assessing colocalization of Swi1 with Hsp42, a small heat shock protein and IPOD marker (158). Carrying out these experiments in cells containing ring or dot structures may elucidate the role of IPOD as well as other cellular components with which Swi1 is interacting with and provide additional information as to how broadly the actin cytoskeleton in is involved in prion formation (i.e Is its involvement specific to Sup35).

Taken together, results from my thesis study show that a small NH_2-terminal region of ~30 amino acids contains all necessary information for *in vivo* prion formation, maintenance, and transmission and *de novo* prion formation. My thesis research thus sheds light on the determinants that contribute to protein misfolding, aggregation, amyloid formation, and prionization and their significance in biology. Its small size and transferability may also allow us to tag a protein-of-interest to subject it to prion-mediated functional modulation.

Discovery of Chemical Probes for Prion Biology Research and Therapeutics for Protein Misfolding-Based Diseases

Despite significant effort, efficient treatment for prion diseases is still lacking. Bach et al. created a yeast-based reporter system using [*PSI+*] (146). Several compounds found to be effective against [*PSI+*] were found to induce a significant decrease in the accumulation of PrP^{Sc}, demonstrating that yeast is a suitable model organism for the screening of anti-prion compounds. The [*PSI+*]-based reporter system was effective, however, it was also time-consuming and labor intensive.

Based on the need for the development of therapeutics for protein misfolding diseases and the need for chemical probes for the study of prion biology, our laboratory developed a novel [*SWI+*]-based approach for the isolation of anti-prion compounds. Based on our previous findings of the tight regulation of *FLO1* by Swi1 and [*SWI+*] (Fig 5), a novel reporter system that faithfully reported the prion status of Swi1 (Fig 12) was designed and used in high-throughput screens of several compound libraries.

There are several benefits to the screening strategy described in this thesis. First, the use of yeast for the screening has been validated by several studies (146, 159), therefore, while this approach is novel

in its use of [*SWI*+] and in the automated thigh-throughput strategy used, the use of yeast in screening assays has demonstrated effectiveness. Second, this yeast-based approach yields results in 2 days, a significantly shorter period than the [*PSI*+]-based approach and other *in vivo* non-yeast-based approaches. Third, our novel reporter system strategy allows for completely automated high-throughput screening, which significantly reduces the amount of time and labor associated with carrying out these screens. This straightforward screening strategy allows us to screen 1000's of compounds in a short period of time (days). The narrowed list of compounds can then be tested in other model systems, some of which require higher biosafety levels. Fourth, as with other phenotype-based approaches, we are not limiting ourselves to one potential target, therefore, elucidation of the mechanism of action of our hit compounds may allow us to find novel target(s).

Using the novel *FLO1pr-URA3* reporter system, several compounds libraries were screened in a high-throughput fashion and 115 hits were obtained (Table 5 and Supplemental tables 1 and 2). Several of the compounds, including quinacrine, guanabenz, and tacrine were previously found to be active in the [*PSI*+]-based screen (146, 159). Several hit compounds were also previously examined for their effectiveness against PrP^{Sc} and found to be effective against PrP^{Sc}, demonstrating that the yeast-based screening strategy is an effective approach for high-throughput screening of anti-prion molecules (159-161). Interestingly, our hits also included tacrine (Cognex) and amiridine, two compounds previously used for the treatment of Alzheimer's disease. Tacrine was previously shown to have activity against [*PSI*+], however, further studies demonstrated that it did not have activity against PrP^{Sc} (159).

Several of the hit compounds were purchased for further examination in our laboratory (Tables 6 and 7). Some of the compounds were effective at eliminating [*SWI*+] at a range of concentrations (17A and 18A). As with any other reporter system, it was important to demonstrate that phenotype observed was not unrelated to prion loss. Confirmatory secondary assays were carried out and demonstrated that treatment of [*SWI*+] with pilocarpine or phloretin resulted in a loss of aggregation of Swi1 (NQ-YFP) and in a transition from Raf± to Raf+, observed phenotypes were not due to interference with our reporter system, but rather prion loss (Fig 17B, 17C and 18B).

The ability of several compounds to eliminate other yeast prions, including [*PSI*+], [URE3], and [*MOT3*+] were also examined and found differential curing among the non-[*SWI*+] yeast (Figs. 19-23). The well-established [*PSI*+] and [URE3] reporter systems, where colony color is tightly associated with prion status, were used. A series of secondary assays were performed to confirm prion loss, including assessment of aggregation using fluorescence microscopy or assessment of growth on media lacking adenine. The adenine-based Mot3 reporter system is novel, however, [*MOT3*+]-curing experiments by the described compounds were carefully designed and contained the appropriate controls, therefore, I am confident in the validity and reproducibility of the obtained Mot3 data. Additionally, another Mot3 reporter has been used effectively in previous study (47), further validating the use of this reporter system in studying anti-prion compounds. Secondary assays, however, can also be performed as described for the [*PSI*+] and [URE3] reporter systems.

The efficacy of hit compounds at eliminating yeast prions was examined at a range of concentrations. One compound, phloretin, was effective at eliminating [*SWI*+] at concentrations in the low micromolar range, while other required a higher dosage to eliminate the examined yeast prions. It is important take into consideration, however, that our yeast cells contain a cell wall- albeit it a more permeable one. We would expect that lower effective concentrations may be obtained if examined in models systems that do not contain cell walls, which would make effective concentrations more suitable when considering these compounds in the development of therapeutics.

None of the compounds examined eliminated all the four prions tested – [*SWI*+], [*PSI*+], [URE3], and [*MOT3*+]. GdnHCl, the positive control for all assays, inhibits Hsp104, and therefore cures all four prions. The lack of universal curing of the yeast prions examined suggest that Hsp104 is not the target of the compounds studied. Therefore, additional studies can be performed to elucidate the mechanism of action of our hit compounds (Fig 24). It is possible that the compounds act through two main mechanisms – 1) through the interaction with the protein of interest, either in its native conformation or its prion form or 2) through interfering with the activity of factors required for prion propagation or maintenance. Due to the nature of our assay, which is a phenotypic assay, compounds could target anything from protein synthesis,

amyloid formation, seed formation, chaperone activity, etc. Compound 7 was [*SWI⁺*]-specific and did not demonstrate activity against any of the other yeast prions. Given the sensitivity of [*SWI⁺*] to alterations in the Hsp70 chaperone system, one future direction may be the examination compound 7 and possible alterations in the Hsp70 chaperone system. [*SWI⁺*] is the only yeast prion known to date known to require Ydj1, therefore, it may be of interest to examine the levels of Ydj1 before and after treatment with compound 7. Interestingly, [*MOT3⁺*] was cured by many of the anti-[*SWI⁺*] compounds. Conversely, [URE3] was relatively resistant to curing by the anti-[*SWI⁺*] compounds examined. Alterations in other chaperones can also be assessed before and after treatment with compounds. Given the distinct sensitivities to alterations in certain chaperones by individual prions, changes in levels or function may underlay differential curing.

Future experiments may also be performed to determine if our hit compounds inhibit Swi1 amyloid formation, as our laboratory has established protocols for purification of Swi1N protein and amyloid fiber assembly. Assembly reactions can also be performed with other purified yeast prion proteins using previously published protocols. Addition of compounds to different times of the amyloid assembly process may give us insight into the step in amyloid assembly process that the compound may be targeting. Additionally, direct interaction of compound with prion proteins can be assessed using surface plasmon resonance. It is possible that the compounds interact with certain yeast prion proteins and not others, either stabilizing the native conformation or preventing interaction with the misfolded conformer. Such experiments may give us insight into the possible compound-protein interactions and differences that may explain differential curing.

In addition to examining interaction between compounds and yeast prions, future experiments can be performed to determine if the hit compounds have an effect on PrP^C to PrP^{Sc} conversion. In collaboration with Dr. Claudio Soto (UTHealth), we can perform Protein Misfolding Cyclic Amplification (PMCA), a method analogous to PCR, which results in rapid conversion of a large excess of PrP^C in the presence of minute amounts PrP^{Sc} (162). The hit compounds can be added the PMCA reaction and followed by examination of the presence or absence of PrP^{Sc}, thus giving us insight into our compounds ability to prevent PrP^C to PrP^{Sc} conversion. There are conflicting reports on the effect of one compound, phloretin, in studies involving

Aβ. One study, however, found that Aβ oligomers and oligomer associated toxicity was prevented with phloretin (163), therefore it would be interesting to determine if this compound works in a similar fashion with PrP or yeast prion proteins.

If compounds are not found to directly interact with yeast or mammalian prion proteins, we can use a variety of established protocols for the investigation of non-prion protein targets. Affinity chromatography using immobilized drugs on sepharose beads, followed by mass spectroscopy, was used previously to find elucidate the targets of anti-prions compounds. Therefore, this well-established assay may allow us to determine our hit compounds' targets (164). It is still possible, however, that targets may be missed due to interference by the bead and linker attached to the bead. Alternatively, we can use other yeast-based approaches, including haploinsufficiency profiling, synthetic lethality screens, or genome wide overexpression screens, each of which has been previously used to identify drug targets (165).

Future directions also include performing structure activity relationship studies on our most interesting hit compounds (Fig 24). These studies may give us insight into the active group(s) within the compounds and uncover possible modifications that may enhance the anti-prion activity of each molecule. Using a structural activity approach, Bach et al. synthesized several derivatives of one of some of their anti-[*PSI*+] hit compounds. One derivative, 6AP, was subsequently found to be effective against PrP^{Sc} in cellular assays (146). Therefore, structural activity relationships studies of our compounds may yield compounds that are not only more effective against yeast prions but also increasingly effective against mammalian prions.

As previously mentioned, two of our hit compounds, tacrine and amiridine, were previously used compounds for the treatment of Alzheimer's disease. Therefore, it is of interest to determine if any of our anti-prion compounds also have anti-Aβ properties. To this end, future studies can be performed in collaboration with Dr. Ferreira to investigate if our anti-[*SWI*+] can reduce toxicity associated with Aβ in cultured hippocampal neurons. Compounds found to reduce Aβ-associated toxicity may be of interest as chemical probes to further understand the mechanisms underlying Alzheimer's disease.
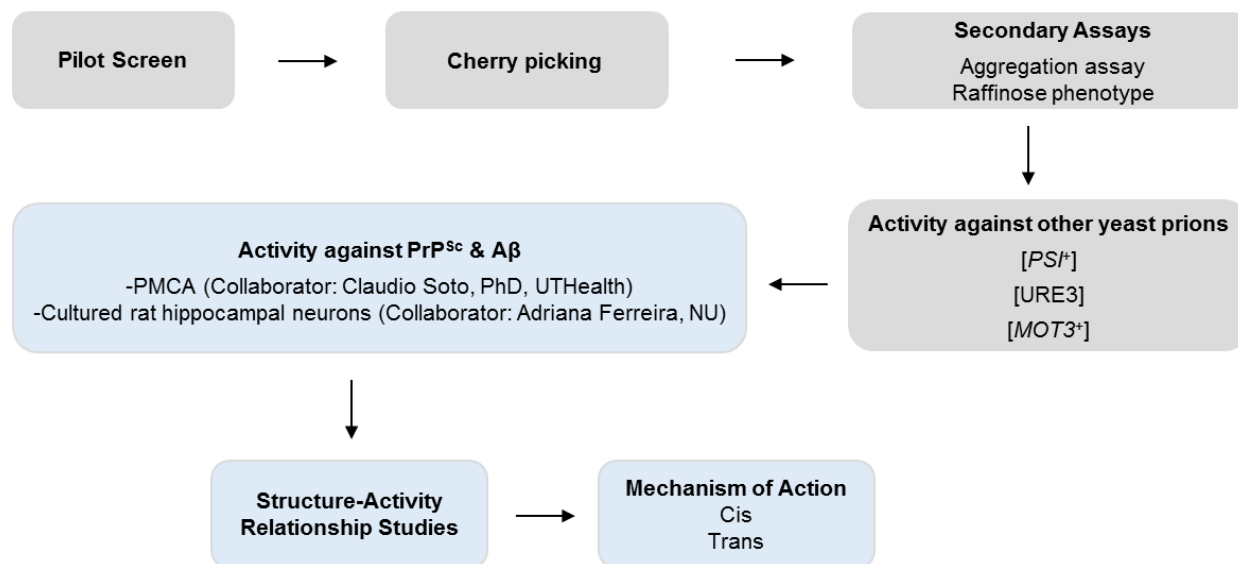
Figure 24. Flow chart of work and future approaches. Several steps, including pilot screening, cherry-picking, secondary assays, and examination of activity against other yeast prions have already been completed. Future work includes investigation of compound activity against PrP^{Sc} and Aβ, structure activity relationship studies and investigation into our hit compounds mechanisms of actions.

.

In conclusion, we have developed a novel and effective yeast-based system for the isolation of anti-prion compounds which we have used to screen several compound libraries. Several of our hit compounds have been further investigated. Given the amyloid based nature of prion disease and the prion-like behavior of several neurodegenerative disease-associated proteins, insights gained through the discovery of compounds effective against yeast and mammalian prions may also be invaluable to our understanding of the mechanisms underlying protein misfolding-based diseases. Further work is required to determine the mechanism of action of these compounds and determine their efficacy against PrP and Aβ.

REFERENCES

1. **Prusiner SB.** 1982. Novel proteinaceous infectious particles cause scrapie. Science **216:**136-144.

2. **Pan KM, Baldwin M, Nguyen J, Gasset M, Serban A, Groth D, Mehlhorn I, Huang Z, Fletterick RJ, Cohen FE, et al.** 1993. Conversion of alpha-helices into beta-sheets features in the formation of the scrapie prion proteins. Proc Natl Acad Sci U S A **90:**10962-10966.

3. **Colby DW, Prusiner SB.** 2011. Prions. Cold Spring Harb Perspect Biol **3:**a006833.

4. **Soto C, Estrada LD.** 2008. Protein misfolding and neurodegeneration. Arch Neurol **65:**184-189.

5. **Stohr J, Watts JC, Mensinger ZL, Oehler A, Grillo SK, DeArmond SJ, Prusiner SB, Giles K.** 2012. Purified and synthetic Alzheimer's amyloid beta (Abeta) prions. Proc Natl Acad Sci U S A **109:**11025-11030.

6. **Watts JC, Condello C, Stohr J, Oehler A, Lee J, DeArmond SJ, Lannfelt L, Ingelsson M, Giles K, Prusiner SB.** 2014. Serial propagation of distinct strains of Abeta prions from Alzheimer's disease patients. Proc Natl Acad Sci U S A **111:**10323-10328.

7. **Sanders DW, Kaufman SK, DeVos SL, Sharma AM, Mirbaha H, Li A, Barker SJ, Foley AC, Thorpe JR, Serpell LC, Miller TM, Grinberg LT, Seeley WW, Diamond MI.** 2014. Distinct tau prion strains propagate in cells and mice and define different tauopathies. Neuron **82:**1271-1288.

8. **Li JY, Englund E, Holton JL, Soulet D, Hagell P, Lees AJ, Lashley T, Quinn NP, Rehncrona S, Bjorklund A, Widner H, Revesz T, Lindvall O, Brundin P.** 2008. Lewy bodies in grafted neurons in subjects with Parkinson's disease suggest host-to-graft disease propagation. Nat Med **14:**501-503.

9. **Desplats P, Lee HJ, Bae EJ, Patrick C, Rockenstein E, Crews L, Spencer B, Masliah E, Lee SJ.** 2009. Inclusion formation and neuronal cell death through neuron-to-neuron transmission of alpha-synuclein. Proc Natl Acad Sci U S A **106:**13010-13015.

10. **Kordower JH, Chu Y, Hauser RA, Freeman TB, Olanow CW.** 2008. Lewy body-like pathology in long-term embryonic nigral transplants in Parkinson's disease. Nat Med **14:**504-506.

11. **Pearce MM, Spartz EJ, Hong W, Luo L, Kopito RR.** 2015. Prion-like transmission of neuronal huntingtin aggregates to phagocytic glia in the Drosophila brain. Nat Commun **6:**6768.

12. **Prusiner SB.** 2013. Biology and genetics of prions causing neurodegeneration. Annu Rev Genet **47:**601-623.

13. **Brundin P, Melki R, Kopito R.** 2010. Prion-like transmission of protein aggregates in neurodegenerative diseases. Nat Rev Mol Cell Biol **11:**301-307.

14. **Peggion C, Sorgato MC, Bertoli A.** 2014. Prions and prion-like pathogens in neurodegenerative disorders. Pathogens **3:**149-163.

15. **Lee S, Kim HJ.** 2015. Prion-like Mechanism in Amyotrophic Lateral Sclerosis: are Protein Aggregates the Key? Exp Neurobiol **24:**1-7.

16. **Liebman SW, Chernoff YO.** 2012. Prions in yeast. Genetics **191:**1041-1072.

17. **Wickner RB.** 2016. Yeast and Fungal Prions. Cold Spring Harb Perspect Biol **8**.

18. **Cox B.** 1965. [*PSI*], a cytoplasmic suppressor of super-suppression in yeast. Heredity **20:**505-521.

19. **Lacroute F.** 1971. Non-Mendelian mutation allowing ureidosuccinic acid uptake in yeast. J Bacteriol **206:**519-522.

20. **Wickner RB.** 1994. [*URE3*] as an altered Ure2 protein: evidence for a prion analog in *Saccharomyces cerevisiae*. Science **264:**566-569.

21. **Sondheimer N, Lindquist S.** 2000. Rnq1: an epigenetic modifier of protein function in yeast. Mol Cell **5:**163-172.

22. **Derkatch IL, Bradley ME, Zhou P, Chernoff YO, Liebman SW.** 1997. Genetic and environmental factors affecting the *de novo* appearance of the [*PSI+*] prion in *Saccharomyces cerevisiae*. Genetics **147:**507-519.

23. **Du Z, Park KW, Yu H, Fan Q, Li L.** 2008. Newly identified prion linked to the chromatin-remodeling factor Swi1 in Saccharomyces cerevisiae. Nat Genet **40:**460-465.

24. **Patel BK, Gavin-Smyth J, Liebman SW.** 2009. The yeast global transcriptional co-repressor protein Cyc8 can propagate as a prion. Nat Cell Biol **11:**344-349.

25. **Alberti S, Halfmann R, King O, Kapila A, Lindquist S.** 2009. A systematic survey identifies prions and illuminates sequence features of prionogenic proteins. Cell **137:**146-158.

26. **Suzuki G, Shimazu N, Tanaka M.** 2012. A yeast prion, Mod5, promotes acquired drug resistance and cell survival under environmental stress. Science **336:**355-359.

27. **Halfmann R, Wright JR, Alberti S, Lindquist S, Rexach M.** 2012. Prion formation by a yeast GLFG nucleoporin. Prion **6:**391-399.

28. **Chernova T.A. K, D.A., Romanyuk A.V., Shanks J.R., Laur O5, Ali M., Ghosh A., Kim D., Yang Z., Mang M., Chernoff Y.O., Wilkinson K.D.** 2017. Yeast Short-Lived Actin-Associated Protein Forms a Metastable Prion in Response to Thermal Stress. Cell Reports**:**751-761.

29. **Tuite MF, Marchante R, Kushnirov VV.** 2011. Fungal Prions: Structure, Function and Propagation. Top Curr Chem **305:**257-298.

30. **King CY, Diaz-Avalos R.** 2004. Protein-only transmission of three yeast prion strains. Nature **428:**319-323.

31. **Tanaka M, Chien P, Naber N, Cooke R, Weissman JS.** 2004. Conformational variations in an infectious protein determine prion strain differences. Nature **428:**323-328.

32. **Brachmann A, Baxa U, Wickner RB.** 2005. Prion generation in vitro: amyloid of Ure2p is infectious. Embo J **24:**3082-3092.

33. **Du Z, Crow ET, Kang HS, Li L.** 2010. Distinct subregions of Swi1 manifest striking differences in prion transmission and SWI/SNF function. Mol Cell Biol **30:**4644-4655.

34. **Sparrer HE, Santoso A, Szoka FC, Jr., Weissman JS.** 2000. Evidence for the prion hypothesis: induction of the yeast [*PSI*+] factor by *in vitro-* converted Sup35 protein. Science **289:**595-599.

35. **Ross ED, Minton A, Wickner RB.** 2005. Prion domains: sequences, structures and interactions. Nat Cell Biol **7:**1039-1044.

36. **Toombs JA, Petri M, Paul KR, Kan GY, Ben-Hur A, Ross ED.** 2012. De novo design of synthetic prion domains. Proc Natl Acad Sci U S A **109:**6519-6524.

37. **Chernoff YO, Lindquist SL, Ono B, Inge-Vechtomov SG, Liebman SW.** 1995. Role of the chaperone protein Hsp104 in propagation of the yeast prion-like factor [*PSI*+]. Science **268:**880-884.

38. **Moriyama H, Edskes HK, Wickner RB.** 2000. [*URE3*] prion propagation in *Saccharomyces cerevisiae*: requirement for chaperone Hsp104 and curing by overexpressed chaperone Ydj1p. Mol Cell Biol **20:**8916-8922.

39. **Kushnirov VV, Ter-Avanesyan MD.** 1998. Structure and replication of yeast prions. Cell **94:**13-16.

40. **Romanova NV, Chernoff YO.** 2009. Hsp104 and prion propagation. Protein Pept Lett **16:**598-605.

41. **Paushkin SV, Kushnirov VV, Smirnov VN, Ter-Avanesyan MD.** 1996. Propagation of the yeast prion-like [*PSI*+] determinant is mediated by oligomerization of the *SUP35*-encoded polypeptide chain release factor. EMBO J **15:**3127-3134.

42. **Wegrzyn RD, Bapat K, Newnam GP, Zink AD, Chernoff YO.** 2001. Mechanism of prion loss after Hsp104 inactivation in yeast. Mol Cell Biol **21:**4656-4669.

43. **Satpute-Krishnan P., Langseth SX, Serio TR.** 2007. Hsp104-dependent remodeling of prion complexes mediates protein-only inheritance. PLoS Biol **5**.

44. **Kryndushkin DS, Alexandrov IM, Ter-Avanesyan MD, Kushnirov VV.** 2003. Yeast [PSI+] prion aggregates are formed by small Sup35 polymers fragmented by Hsp104. J Biol Chem **278:**49636-49643.

45. **Tuite MF, Mundy CR, Cox BS.** 1981. Agents that cause a high frequency of genetic change from [*PSI*+] to [*psi*-] in *Saccharomyces cerevisiae*. Genetics **98:**691-711.

46. **Eaglestone SS, Ruddock LW, Cox BS, Tuite MF.** 2000. Guanidine hydrochloride blocks a critical step in the propagation of the prion-like determinant [*PSI*+] of *Saccharomyces cerevisiae*. Proc Natl Acad Sci U S A **97:**240-244.

47. **Holmes DL, Lancaster AK, Lindquist S, Halfmann R.** 2013. Heritable remodeling of yeast multicellularity by an environmentally responsive prion. Cell **153:**153-165.

48. **Ferreira PC, Ness F, Edwards SR, Cox BS, Tuite MF.** 2001. The elimination of the yeast [*PSI*[^+]] prion by guanidine hydrochloride is the result of Hsp104 inactivation. Mol Microbiol **40:**1357-1369.

49. **Jung G, Masison DC.** 2001. Guanidine hydrochloride inhibits Hsp104 activity *in vivo*: a possible explanation for its effect in curing yeast prions. Curr Microbiol **43:**7-10.

50. **Chernova T.A., Wilkinson K.D., Y.O. C.** 2017. Prions, Chaperones and Proteostasis in Yeast. Cold Spring Harb Perspect Biol **9**.

51. **Wickner RB, Shewmaker FP, Bateman DA, Edskes HK, Gorkovskiy A, Dayani Y, Bezsonov EE.** 2015. Yeast prions: structure, biology, and prion-handling systems. Microbiol Mol Biol Rev **79:**1-17.

52. **Reidy M, Masison D.** 2011. Modulation and elimination of yeast prions by protein chaperones and co-chaperones. Prion **5:**245-249.

53. **Jung G, Jones G, Wegrzyn RD, Masison DC.** 2000. A role for cytosolic Hsp70 in yeast [*PSI*[^+]] prion propagation and [*PSI*[^+]] as a cellular stress. Genetics **156:**559-570.

54. **Kushnirov VV, Kryndushkin DS, Boguta M, Smirnov VN, Ter-Avanesyan MD.** 2000. Chaperones that cure yeast artificial [*PSI*[^+]] and their prion-specific effects. Curr Biol **10:**1443-1446.

55. **Sondheimer N, Lopez N, Craig EA, Lindquist S.** 2001. The role of Sis1 in the maintenance of the [*RNQ*[^+]] prion. EMBO J **20:**2435-2442.

56. **Schwimmer C, Masison DC.** 2002. Antagonistic interactions between yeast [PSI(+)] and [URE3] prions and curing of [URE3] by Hsp70 protein chaperone Ssa1p but not by Ssa2p. Mol Cell Biol **22:**3590-3598.

57. **Higurashi T, Hines JK, Sahi C, Aron R, Craig EA.** 2008. Specificity of the J-protein Sis1 in the propagation of 3 yeast prions. Proc Natl Acad Sci U S A **105:**16596-16601.

58. **Hines JK, Li X, Du Z, Higurashi T, Li L, Craig EA.** 2011. [SWI], the prion formed by the chromatin remodeling factor Swi1, is highly sensitive to alterations in Hsp70 chaperone system activity. PLoS Genet **7:**e1001309.

59. **Ter-Avanesyan MD, Kushnirov VV, Dagkesamanskaya AR, Didichenko SA, Chernoff YO, Inge-Vechtomov SG, Smirnov VN.** 1993. Deletion analysis of the *SUP35* gene of the yeast *Saccharomyces cerevisiae* reveals two non-overlapping functional regions in the encoded protein. Mol Microbiol **7:**683-692.

60. **Patino MM, Liu JJ, Glover JR, Lindquist S.** 1996. Support for the prion hypothesis for inheritance of a phenotypic trait in yeast. Science **273:**622-626.

61. **Tessier PM, Lindquist S.** 2009. Unraveling infectious structures, strain variants and species barriers for the yeast prion [PSI+]. Nat Struct Mol Biol **16:**598-605.

62. **Derkatch IL, Chernoff YO, Kushnirov VV, Inge-Vechtomov SG, Liebman SW.** 1996. Genesis and variability of [*PSI*] prion factors in *Saccharomyces cerevisiae*. Genetics **144:**1375-1386.

63. **Krishnan R, Lindquist SL.** 2005. Structural insights into a yeast prion illuminate nucleation and strain diversity. Nature **435:**765-772.

64. **McGlinchey RP, Kryndushkin D, Wickner RB.** 2011. Suicidal [PSI+] is a lethal yeast prion. Proc Natl Acad Sci U S A **108:**5337-5341.

65. **Toyama BH, Kelly MJ, Gross JD, Weissman JS.** 2007. The structural basis of yeast prion strain variants. Nature **449:**233-237.

66. **Uptain SM, Sawicki GJ, Caughey B, Lindquist S.** 2001. Strains of [*PSI*+] are distinguished by their efficiencies of prion-mediated conformational conversion. EMBO J **20:**6236-6245.

67. **Schlumpberger M, Prusiner SB, Herskowitz I.** 2001. Induction of distinct [*URE3*] yeast prion strains. Mol Cell Biol **21:**7035-7046.

68. **Derkatch IL, Bradley ME, Hong JY, Liebman SW.** 2001. Prions affect the appearance of other prions: the story of [*PIN*+]. Cell **106:**171-182.

69. **Bradley ME, Edskes HK, Hong JY, Wickner RB, Liebman SW.** 2002. Interactions among prions and prion "strains" in yeast. Proc Natl Acad Sci U S A **99 Suppl 4:**16392-16399.

70. **Du Z, Li L.** 2014. Investigating the interactions of yeast prions: [SWI+], [PSI+], and [PIN+]. Genetics **197:**685-700.

71.   **Stein KC, True HL.** 2014. Prion strains and amyloid polymorphism influence phenotypic variation. PLoS Pathog **10:**e1004328.

72.   **Huang VJ, Stein KC, True HL.** 2013. Spontaneous variants of the [RNQ+] prion in yeast demonstrate the extensive conformational diversity possible with prion proteins. PLoS One **8:**e79582.

73.   **Kalastavadi T, True HL.** 2010. Analysis of the [RNQ+] Prion Reveals Stability of Amyloid Fibers as the Key Determinant of Yeast Prion Variant Propagation. J Biol Chem **285:**20748–20755.

74.   **Green SR, Johnson AD.** 2004. Promoter-dependent roles for the Srb10 cyclin-dependent kinase, and the Hda1 deacetylasse in Tup1-mediated repression in Saccaharomyces cerevisiae. Mol Bio Cell **15:**4191-4202.

75.   **Chernova TA, Romanyuk AV, Karpova TS, Shanks JR, Ali M, Moffatt N, Howie RL, O'Dell A, McNally JG, Liebman SW, Chernoff YO, Wilkinson KD.** 2011. Prion induction by the short-lived, stress-induced protein Lsb2 is regulated by ubiquitination and association with the actin cytoskeleton. Mol Cell **43:**242-252.

76.   **Michelitsch MD, Weissman JS.** 2000. A census of glutamine/asparagine-rich regions: implications for their conserved function and the prediction of novel prions. Proc Natl Acad Sci U S A **97:**11910-11915.

77.   **Sudarsanam P, Iyer VR, Brown PO, Winston F.** 2000. Whole-genome expression analysis of snf/swi mutants of Saccharomyces cerevisiae. Proc Natl Acad Sci U S A **97:**3364-3369.

78.   **Du Z, Zhang Y, Li L.** 2015. The Yeast Prion [SWI(+)] Abolishes Multicellular Growth by Triggering Conformational Changes of Multiple Regulators Required for Flocculin Gene Expression. Cell Rep **13:**2865-2878.

79.   **Du Z, Goncharoff DK, Cheng X, Li L.** 2017. Analysis of [SWI+] formation and propagation events. Molecular Microbiology **104**.

80.   **De Las Penas A, Pan SJ, Castano I, Alder J, Cregg R, Cormack BP.** 2003. Virulence-related surface glycoproteins in the yeast pathogen Candida glabrata are encoded in subtelomeric

clusters and subject to RAP1- and SIR-dependent transcriptional silencing. Genes Dev **17:**2245-2258.

81. **Dranginis AM, Rauceo JM, Coronado JE, Lipke PN.** 2007. A biochemical guide to yeast adhesins: glycoproteins for social and antisocial occasions. Microbiol Mol Biol Rev **71:**282-294.

82. **Guo B, Styles CA, Feng Q, Fink GR.** 2000. A Saccharomyces gene family involved in invasive growth, cell-cell adhesion, and mating. Proc Natl Acad Sci U S A **97:**12158-12163.

83. **Hahn MW, De Bie T, Stajich JE, Nguyen C, Cristianini N.** 2005. Estimating the tempo and mode of gene family evolution from comparative genomic data. Genome Res **15:**1153-1160.

84. **Nizhnikov A.A., Ryzhova .T.A, Volkov K.V., Zadorsky S.P., Sopova J.V., S.G. I-V, Galkin AP.** 2016. Interaction of Prions Causes Heritable Traitsin Saccharomyces cerevisiae. Plos Genetics **12**.

85. **Cascarina SM, Ross ED.** 2014. Yeast prions and human prion-like proteins: sequence features and prediction methods. Cell Mol Life Sci **71:**2047-2063.

86. **Edskes HK, Gray VT, Wickner RB.** 1999. The [*URE3*] prion is an aggregated form of Ure2p that can be cured by overexpression of Ure2p fragments. Proc Natl Acad Sci U S A **96:**1498-1503.

87. **Maddelein ML, Wickner RB.** 1999. Two prion-inducing regions of Ure2p are nonoverlapping. Mol Cell Biol **19:**4516-4524.

88. **Masison DC, Wickner RB.** 1995. Prion-inducing domain of yeast Ure2p and protease resistance of Ure2p in prion-containing cells. Science **270:**93-95.

89. **Masison DC, Maddelein ML, Wickner RB.** 1997. The prion model for [*URE3*] of yeast: spontaneous generation and requirements for propagation. Proc Natl Acad Sci U S A **94:**12503-12508.

90. **Doel SM, McCready SJ, Nierras CR, Cox BS.** 1994. The dominant *PNM2*- mutation which eliminates the [*PSI*] factor of *Saccharomyces cerevisiae* is the result of a missense mutation in the *SUP35* gene. Genetics **137:**659-670.

91. **Osherovich LZ, Cox BS, Tuite MF, Weissman JS.** 2004. Dissection and design of yeast prions. PLoS Biol **2:**E86.

92.   **Parham SN, Resende CG, Tuite MF.** 2001. Oligopeptide repeats in the yeast protein Sup35p stabilize intermolecular prion interactions. EMBO J **20:**2111-2119.

93.   **Shkundina IS, Kushnirov VV, Tuite MF, Ter-Avanesyan MD.** 2006. The role of the N-terminal oligopeptide repeats of the yeast Sup35 prion protein in propagation and transmission of prion variants. Genetics **172:**827-835.

94.   **DePace AH, Santoso A, Hillner P, Weissman JS.** 1998. A critical role for amino-terminal glutamine/asparagine repeats in the formation and propagation of a yeast prion. Cell **93:**1241-1252.

95.   **Ross ED, Edskes HK, Terry MJ, Wickner RB.** 2005. Primary sequence independence for prion formation. Proc Natl Acad Sci U S A **102:**12825-12830.

96.   **Ross ED, Baxa U, Wickner RB.** 2004. Scrambled prion domains form prions and amyloid. Molecular & Cellular Biology **24:**7206-7213.

97.   **Chakrabortee S, Byers JS, Jones S, Garcia DM, Bhullar B, Chang A, She R, Lee L, Fremin B, Lindquist S, Jarosz DF.** 2016. Intrinsically Disordered Proteins Drive Emergence and Inheritance of Biological Traits. Cell **167:**369-381 e312.

98.   **Brown JC, Lindquist S.** 2009. A heritable switch in carbon source utilization driven by an unusual yeast prion. Genes Dev **23:**2320-2332.

99.   **Toombs JA, McCarty BR, Ross ED.** 2010. Compositional determinants of prion formation in yeast. Mol Cell Biol **30:**319-332.

100.   **Harrison PM, Gerstein M.** 2003. A method to assess compositional bias in biological sequences and its application to prion-like glutamine/asparagine-rich domains in eukaryotic proteomes. Genome Biol **4:**R40.

101.   **Ross ED, Toombs JA.** 2010. The effect of amino acid composition on yeast prion formation and prion domain interactions. Prion **4:**60-65.

102.   **Du Z.** 2011. The complexity and implications of yeast prion domains. Prion **5:**311-316.

103.   **Bryan AW, Jr, Menke M, Cowen LJ, Lindquist S, Berger B.** 2009. BETASCAN: probable beta-amyloids identified by pairwise probabilistic analysis. PLoS Comput Biol **5**.

104. **Bryan AW, Jr, O'donnell CW, Menke M, Cowen LJ, Lindquist S, berger B.** 2011. STITCHER: Dynamic assembly of likely amyloid and prion β-structures from secondary structure predictions. **80:**410-420.

105. **Tartaglia GG, Vendruscolo M.** 2008. The Zyggregator method for predicting protein aggregation propensities. Chem Soc Rev **37:**1395-1401.

106. **Goldschmidt L, Teng PK, Riek R, Eisenberg D.** 2010. Identification of the amylome, proteins capable of forming amyloid-like fibrils. Proc Natl Acad Sci U S A **107:**3487-3492.

107. **Fernandez-Escamillla AM, Rousseau F, Schymkowitz J, Serrano L.** 2004. Prediction of sequence-dependent and mutational effects on the aggregation of peptides and proteins. Nat Biotechnol **22:**1302-1306.

108. **Zibaee S, Makin OS, Goedert M, Serpell L.** 2007. A simple algorithm locates beta-strands in the amyloid fibril core of alpha-synuclein, Abeta, and tau using the amino acid sequence alone. Protein Sci **16:**906-918.

109. **Trovato A, Seno F, Tosatto SC.** 2007. The PASTA server for protein aggregation prediction. Protein Eng Des Sel **20:**521-523.

110. **Sabate R, Rousseau F, Schymkowitz J, Ventura S.** 2015. What makes a protein sequence a prion? PLoS Comput Biol **11:**e1004013.

111. **Lancaster AK, Nutter-Upham A, Lindquist S, King OD.** 2014. PLAAC: a web and command-line application to identify proteins with prion-like amino acid composition. Bioinformatics **30:**2501-2502.

112. **Zambrano R, Conchillo-Sole O, Iglesias V, Illa R, Rousseau F, Schymkowitz J, Sabate R, Daura X, Ventura S.** 2015. PrionW: a server to identify proteins containing glutamine/asparagine rich prion-like domains and their amyloid cores. Nucleic Acids Res **43:**W331-337.

113. **Afsar Minhas F, Ross ED, Ben-Hur A.** 2017. Amino acid composition predicts prion activity. PLoS Comput Biol **13**.

114. **Patel BK, Liebman SW.** 2007. "Prion-proof" for [PIN+]: infection with in vitro-made amyloid aggregates of Rnq1p-(132-405) induces [PIN+]. J Mol Biol **365:**773-782.

115.   **Shewmaker F, Wickner RB, Tycko R.** 2006. Amyloid of the prion domain of Sup35p has an in-register parallel β-sheet structure. Proc Natl Acad Sci U S A **103:**19754-19759.

116.   **Baxa U, Wickner RB, Steven AC, Andersen D, Marekov L, Yau W-M, Tycko R.** 2007. Characterization of β-sheet structure in Ure2p1-89 yeast prion fibrils by solid state nuclear magnetic resonance. Biochemistry **46:**13149–13162.

117.   **Wickner RB, Dyda F, Tycko R.** 2008. Amyloid of Rnq1p, the basis of the [PIN+] prion, has a parallel in-register beta-sheet structure. Proc Natl Acad Sci U S A **105:**2403-2408.

118.   **Luckgei N, Schutz AK, Bousset L, Habenstein B, Souigues Y, Gardiennet C, Meier BH, Melki R, Bockmann A.** 2013. The conformation of the prion domain of Sup35p in isolation and in the full-length protein. Angew Chem Int Ed Engl **52:**12741–12744.

119.   **Chan JC, Oyler NA, Yau WM, Tycko R.** 2005. Parallel beta-sheets and polar zippers in amyloid fibrils formed by residues 10-39 of the yeast prion protein Ure2p. Biochemistry **44:**10669-10680.

120.   **Tanaka M, Chien P, Yonekura K, Weissman JS.** 2005. Mechanism of cross-species prion transmission: an infectious conformation compatible with two highly divergent yeast prion proteins. Cell **121:**49-62.

121.   **King CY, Tittmann P, Gross H, Gebert R, Aebi M, Wuthrich K.** 1997. Prion-inducing domain 2-114 of yeast Sup35 protein transforms *in vitro* into amyloid-like filaments. Proc Natl Acad Sci U S A **94:**6618-6622.

122.   **Glover JR, Kowal AS, Schirmer EC, Patino MM, Liu JJ, Lindquist S.** 1997. Self-seeded fibers formed by Sup35, the protein determinant of [*PSI*+], a heritable prion-like factor of *S. cerevisiae*. Cell **89:**811-819.

123.   **Baxa U, Cheng N, Winkler DC, Chiu TK, Davies DR, Sharma D, Inouye H, Kirschner DA, Wickner RB, Steven AC.** 2005. Filaments of the Ure2p prion protein have a cross-beta core structure. J Struct Biol **150:**170-179.

124.   **True HL, Lindquist SL.** 2000. A yeast prion provides a mechanism for genetic variation and phenotypic diversity. Nature **407:**477-483.

125. **Tyedmers J, Madariaga ML, Lindquist S.** 2008. Prion switching in response to environmental stress. PLoS Biol **6:**e294.

126. **Chernova TA, Wilkinson KD, Chernoff YO.** 2014. Physiological and environmental control of yeast prions. FEMS Microbiol Rev **38:**326-344.

127. **Halfmann R, Lindquist S.** 2010. Epigenetics in the extreme: prions and the inheritance of environmentally acquired traits. Science **330:**629-632.

128. **Crow ET, Du Z, Li L.** 2011. A small, glutamine-free domain propagates the [SWI(+)] prion in budding yeast. Mol Cell Biol **31:**3436-3444.

129. **Halfmann R, Jarosz DF, Jones SK, Chang A, Lancaster AK, Lindquist S.** 2012. Prions are a common mechanism for phenotypic inheritance in wild yeasts. Nature **482:**363-368.

130. **Sambrook J, Russell DW.** 2000. Molecular Cloning: A laboratory manual vol 3. Cold Spring Harbor Laboratory Press.

131. **Gietz RD, Schiestl RH.** 2007. High-efficiency yeast transformation using the LiAc/SS carrier DNA/PEG method. Nat Protoc **2:**31-34.

132. **Prusiner SB.** 1998. Prions. Proc Natl Acad Sci U S A **95:**13363-13383.

133. **Legname G, Baskakov, I.V., Nguyen, H.O., Riesner,D., Cohen, F.E., DeArmond, S.J. and Prusiner, S.B.** 2004. Synthetic mammalian prions. Science **305:**673-676.

134. **Eraña H, Venegas V, Moreno J, Castilla J.** 2017. Prion-like disorders and Transmissible Spongiform Encephalopathies: An overview of the mechanistic features that are shared by the various disease-related misfolded proteins. Biochem Biophys Res Commun **483:**1125–1136.

135. **Soto C.** 2012. Transmissible proteins: expanding the prion heresy. Cell **149:**968-977.

136. **Prusiner SB.** 2012. Cell biology. A unifying role for prions in neurodegenerative diseases. Science **336:**1511-1513.

137. **Eisenberg D, Jucker M.** 2012. The amyloid state of proteins in human diseases. Cell **148:**1188-1203.

138. **Bolognesi MLaL, G.** 2015. Approaches for discvering anti-prion compounds: lessons learend and challenges ahead. Expert Opin Drug Discov **10:**389-397.

139. **Ghose AK, Herbertz T, Hudkins RL, Dorsey BD, Mallamo JP.** 2012. Knowledge-Based, Central Nervous System (CNS) Lead Selection and Lead Optimization for CNS Drug Discovery. ACS Chem Neurosci, **3:**50-68.

140. **Abbott NJ.** 2013. Blood-brain barrier structure and function and the challeneges of CNS drug discovery. J Inherit Metab Dis **36:**437-449.

141. **Brazier MW, Mot AI, White AR, Collins SJ.** 2013. Immunotherapeutic approaches in prion disease: progress, challenges and potential directions Ther Deliv **4:**615-628.

142. **Rovis TLaL, G.** 2014. Prion Protein-specific Antibody Development, Modes of Action and Therapeutic Applications. Viruses **6:**3719-3737.

143. **Trevitt. C.R. and Collinge J.** 2006. A systematic review of prion therapeutics in experimental models. Brain **129:**2241-2265.

144. **Pagadala NS, Syed K, Bhat R.** 2017. In silico strategies n prion pathogenic conversion and inhibition from PrPC-PrPSc. Expert Opinion on Drug Discovery **12:**241-248.

145. **Cordeiro YaF, N.C.** 2015. New approaches for the selection and evaluation of anti-prion organic compounds. Mini Rev Med Chem **15:**84-92.

146. **Bach S, Talarek N, Andrieu T, Vierfond JM, Mettey Y, Galons H, Dormont D, Meijer L, Cullin C, Blondel M.** 2003. Isolation of drugs active against mammalian prions using a yeast-based screening assay. Nat Biotechnol **21:**1075-1081.

147. **Wickner RB, Kelly AC.** 2016. Prions are affected by evolution at two levels. Cell Mol Life Sci **73:**1131-1144.

148. **Du Z, Goncharoff DK, Cheng X, Li L.** 2016. Analysis of [SWI+] formation and propagation events. Mol Microbiol doi:10.1111/mmi.13616.

149. **Coustou V, Deleu C, Saupe S, Begueret J.** 1997. The protein product of the *het-s* heterokaryon incompatibility gene of the fungus *Podospora anserina* behaves as a prion analog. Proc Natl Acad Sci U S A **94:**9773-9778.

150. **Halfmann R, Alberti S, Krishnan R, Lyle N, O'Donnell CW, King OD, Berger B, Pappu RV, Lindquist S.** 2011. Opposing effects of glutamine and asparagine govern prion formation by intrinsically disordered proteins. Mol Cell **43:**72-84.

151. **Peters TW, Huang M.** 2007. Protein aggregation and polyasparagine-mediated cellular toxicity in Saccharomyces cerevisiae. Prion **1:**144-153.

152. **Kreil DP KG.** 2000. Asparagine repeats are rare in mammalian proteins. Trends Biochem Sci **25:**270-271.

153. **Lu X, Murphy RM.** 2015. Asparagine repeat peptides: Aggregation kinetics and comparaison with glutamine repeats. Biochemistry **54:**4784-4794.

154. **Zhou P, Derkatch IL, Liebman SW.** 2001. The relationship between visible intracellular aggregates that appear after overexpression of Sup35 and the yeast prion-like elements [*PSI*[+]] and [*PIN*[+]]. Mol Microbiol **39:**37-46.

155. **Ganusova EE, Ozolins LN, Bhagat S, Newnam GP, Wegrzyn RD, Sherman MY, Chernoff YO.** 2006. Modulation of prion formation, aggregation, and toxicity by the actin cytoskeleton in yeast. Mol Cell Biol **26:**617-629.

156. **Tyedmers J, Treusch S, Dong J, McCaffery JM, Bevis B, Lindquist S.** 2010. Prion induction involves an ancient system for the sequestration of aggregated proteins and heritable changes in prion fragmentation. Proc Natl Acad Sci U S A **107:**8633-8638.

157. **Sharma J, Wisniewski BT, Paulson E, Obaoye JO, Merrill SJ, Manogaran AL.** 2017. De novo [PSI +] prion formation involves multiple pathways to form infectious oligomers. Sci Rep **7:**76.

158. **Specht S, Miller SB, Mogk A, Bukau B.** 2011. Hsp42 is required for sequestration of protein aggregates into deposition sites in Saccaromyces cerevisiae. J Cell Biol **195:**617-629.

159. **Tribouillard-Tanvier D, Beringue V, Desban N, Gug F, Bach S, Voisset C, Galons H, Laude H, Vilette D, Blondel M.** 2008. Antihypertensive drug guanabenz is active in vivo against both yeast and mammalian prions. PLoS One **3:**e1981.

160. **Korth C, May BC, Cohen FE, Prusiner SB.** 2001. Acridine and phenothiazine derivatives as pharmacotherapeutics for prion disease. Proc Natl Acad Sci U S A **98:**9836-9841.

161. **Doh-Ura K, Iwaki T, Caughey B.** 2000. Lysosomotropic agents and cysteine protease inhibitors inhibit scrapie-associated prion protein accumulation. J Virol **74:**4894-4897.

162. **Saborio GP, Permanne B, Soto C.** 2001. Sensitive detection of pathological prion protein by cyclic amplification of protein misfolding. Nature **411:**810-813.

163. **Ladiwala ARA, Mora-Pale M, Lin JC, Bale SS, Fishman ZS, Dordick JS, Tessier PM.** 2011. Polyphenolic Glycosides and Aglycones Utilize Opposing Pathways To Selectively Remodel and Inactivate Toxic Oligomers of Amyloid β. Chembiochem **12**.

164. **Tribouillard D, Gug F, Galons H, Bach S, Saupe SJ, Blondel M.** 2007. Antiprion drugs as chemical tools to uncover mechanisms of prion propagation. Prion **1:**48-52.

165. **Sturgeon CM, Kemmer D, Anderson HJ, Roberge M.** 2006. Yeast as a tool to uncover the cellular targets of drugs. Biotechnol J **1:**289-298.